RECONSTITUTION OF MOUSE INNER EAR SENSORY DEVELOPMENT FROM PLURIPOTENT STEM CELLS

Karl R. Koehler

Submitted to the faculty of the University Graduate School
in partial fulfillment of the requirements
for the degree
Doctor of Philosophy
in the Medical Neuroscience Program
Indiana University

January 2014

Accepted by the Graduate Faculty, Indiana University, in partial fulfillment of the requirements for the degree of Doctor of Philosophy.

Gerry S. Oxford, Ph.D., Chair

Theodore R. Cummins, Ph.D.

Doctoral Committee

Eri Hashino, Ph.D.

December 16, 2013

Jason S. Meyer, Ph.D.

Xin Zhang, Ph.D.

DEDICATION

This work is dedicated to my parents Kathryn and Stephen Koehler who always encouraged me to have ambitious goals, my sisters Emily Koehler and Maggie Clifford for continually being a source of guidance and wisdom, and my wife Beth Koehler for supporting me through the many failures that led to this dissertation.

ACKNOWLEDGMENTS

First and foremost, I would like to thank my mentor Dr. Eri Hashino for the incredible support she has given me throughout my time at IUSM. She has been extremely trusting to allow me to develop my own research plan and for that I am very thankful. I would also like to thank my research committee members Drs. Gerry Oxford, Xin Zhang, Ted Cummins, and Jason Meyer for their guidance and expert advice throughout my graduate journey.

Among my coworkers, I especially want to thank Takako Kondo for displaying extraordinary patience as she trained me to be an adequate experimentalist. Her initial guidance and mentorship when I first joined the Hashino lab was absolutely invaluable for my future success. I would like to thank the many students and technicians that have filtered through the Hashino Lab during my tenure. Each of them has challenged me to be a more engaging mentor and educator. In this regard, I owe thanks to Joe McSoley, Riddhi Trevedi, Emily Beans, Alyssa Burton, Cristiano Prion, Yohance Allete, James Hamilton, Sreeparna Majumdar, and Alex Malone. A special thanks goes to Andrew Mikosz who has been a superb undergraduate trainee and collaborator during the most productive years of my graduate career. I would still be doing experiments without him. In addition, I am thankful to have worked with three fantastic post-doctoral researchers, Atsushi Shimomura, Dharmeshkumar Patel, and Andrei Molosh, who were always willing to impart their wisdom and advice.

I would not have my sanity without my fellow graduate students, Rena Meadows, Gregg Wagner, Chandler Walker, Melissa Walker, Lengxiao Deng, Nicole

Ashpole and Polina Feldman. Thank you for always being up for a chat. Likewise I owe a debt of gratitude to current and past SNRI staff members, Nastassia Belton, Miriam Barr, and Alexandra Miller, for keeping me enrolled and making sure my grants were submitted on time and in top form.

My close friends and family have been extremely supportive. I would like to thank my friends Cory Westerfield and Craig Callahan; my family members, Kathryn Koehler, Stephen Koehler, Emily Koehler, Maggie Clifford, Adam Clifford; and my wife Beth Koehler. I would also like to thank Benicio, Bernard, Ozzy and Neko for the many therapy sessions they endured during the preparation of this dissertation.

KARL R. KOEHLER

RECONSTITUTION OF MOUSE INNER EAR SENSORY DEVELOPMENT FROM PLURIPOTENT STEM CELLS

The inner ear contains specialized sensory epithelia that detect head movements, gravity and sound. Hearing loss and imbalance are primarily caused by degeneration of the mechanosensitive hair cells in sensory epithelia or the sensory neurons that connect the inner ear to the brain. The controlled derivation of inner ear sensory epithelia and neurons from pluripotent stem cells will be essential for generating *in vitro* models of inner ear disorders or developing cell-based therapies. Despite some recent success in deriving hair cells from mouse embryonic stem (ES) cells, it is currently unclear how to derive inner ear sensory cells in a fully defined and reproducible manner. Progress has likely been hindered by what is known about induction of the nonneural and preplacodal ectoderm, two critical precursors during inner ear development. The studies presented here report the step-wise differentiation of inner ear sensory epithelia from mouse ES cells in three-dimensional culture. We show that nonneural, preplacodal and pre-otic epithelia can be generated from ES cell aggregates by precise temporal control of BMP, TGFβ and FGF signaling, mimicking *in vivo* development. Later, in a self-guided process, vesicles containing supporting cells emerge from the presumptive otic epithelium and give rise to hair cells with stereocilia bundles and kinocilium. Remarkably, the vesicles developed into large cysts with sensory epithelia reminiscent of vestibular sense organs (i.e. the utricle, saccule and crista), which sense head movements and gravity in the animal. We have designated these stem cell-derived structures *inner*

ear organoids. In addition, we discovered that sensory-like neurons develop alongside the organoids and form putative synapses with hair cells in a similar fashion to the hair cell-to-neuron circuit that forms in the developing embryo. Our data thus establish a novel *in vitro* model of inner ear organogenesis that can be used to gain deeper insight into inner ear development and disorder.

Gerry S. Oxford, Ph.D., Chair

TABLE OF CONTENTS

LIST OF TABLES

LIST OF FIGURES

LIST OF ABBREVIATIONS

PSC	Pluripotent stem cell or PS cell
ESC	Embryonic stem cell or ES cell
iPSC	Induced pluripotent stem cell or iPS cell
DE	Definitive ectoderm
NNE	Nonneural ectoderm
PPE	Preplacodal ectoderm
PPR	Preplacodal region
ME	Mesendoderm (i.e. general term referring to both the mesoderm and endoderm germ lineages)
NE	Neural ectoderm, Neuroectoderm, or Neuroepithelia
OEPD	Otic-epibranchial placode domain
SGN	Spiral ganglion neurons
VGN	Vestibular ganglion neurons
SNHL	Sensorineural hearing loss
FGF	Fibroblast growth factor (e.g. FGF signaling of FGF2 protein)
BMP	Bone morphogenetic protein (e.g. BMP signaling or BMP4 protein)
IGF	Insulin-like growth factor (e.g. IGF signaling or IGF1 protein)
TGFβ	Transforming growth factor-beta (e.g. TGFβ signaling)
SB	SB-431542 (a small molecule inhibitor of activin receptor-like kinase receptors ALK4, ALK5 and ALK7)
LDN	LDN-193189 (a small molecule inhibitor of BMP type I receptors ALK2 and ALK3)
SFEBq	Serum-free culture of embryoid body aggregates with quick aggregation

"What I cannot create, I do not understand."

Richard P. Feynman
Physicist

CHAPTER 1: INTRODUCTION

The mammalian inner ear is essential for interpreting verbal communication and maintaining proper balance and orientation in an environment. The inner ear contains two sensory apparatuses for the vestibular and auditory senses. The vestibular apparatuses—the utricle, saccule and the semicircular canals with three cristae—comprise a series of fluid filled chambers. Each chamber is equipped with sensory epithelia containing a cluster of mechanosensitive hair cells that can detect linear acceleration and gravity. The auditory apparatus, by contrast, is a conch-shaped organ containing three fluid-filled tubes surrounding a sensory epithelium known as the organ of Corti. The organ of Corti contains four rows of hair cells that detect different sound frequencies depending on their coordinates along the basal-to-apical spiral of cochlea. Importantly, each vestibular and cochlear hair cell is contacted by one or more sensory neurons that transmit information to the central nervous system for interpretation.

Like other sensory systems in the body, the inner ear is susceptible to genetic mutations and environmental insults leading to dysfunction. Hearing loss is one of the most prevalent sensory impairments and is estimated to occur in over 500 million individuals worldwide (Stevens et al., 2011). Current treatment strategies focus on sound amplification using conventional hearing aids, bone-anchored hearing aids, and in the most severe cases, cochlear implantation (Sprinzl and Riechelmann, 2010). These devices provide immense benefit to those with hearing loss, but are only able to amplify acoustic signals and cannot cure deafness. Additionally, hearing aids and cochlear implants are unable to treat hearing loss that

occurs due to pathology aside from to the sensory hair cells (e.g. acoustic neuromas damage the auditory nerve). There is some hope that these pathologies could be treated with auditory brainstem implants, but currently available data have shown great variability in subject response, with only limited improvement in speech comprehension (Lim et al., 2009). In addition, vestibular impairment can cause individuals to become dizzy and fall; accidental falls are the leading cause of injury related death in adults over the age of 65 in the United States, with 30% of this population experiencing at least one fall annually (Hausdorff et al., 2001). There are no existing treatments to amplify vestibular signals similar to a hearing aid, but vestibular prostheses are currently being studied (Davidovics et al., 2013). However, these prostheses only improve the semicircular canal function and it is unknown whether prostheses could be made to repair otolith malfunction. Both semicircular canal and otolith function are necessary for proper balance.

Compounding these issues is the fact that sensory hair cells and primary afferent neurons in the mammalian inner ear do not regenerate to any clinically relevant degree; therefore, most forms of hearing loss and balance disorders do not improve over time (Brigande and Heller, 2009; Groves, 2010; Shi and Edge, 2013). Stem cells have been proposed as a possible source of cells to replace lost or damaged hair cells and neurons. Specifically, pluripotent stem (PS) cells are defined by their unique ability to self-renew and differentiate into cells from all three germ layers (Hanna et al., 2010). The use of PS cells, such as embryonic stem (ES) cells or induced pluripotent stem (iPS) cells, could provide a means to circumvent the difficulty of obtaining native inner ear cells for investigation. Genetically modified

animal models have been used to study inner ear disorders; however, these animal models recapitulate some, but not all, phenotypes of human genetic disorders. Thus, a human PS stem cell model of inner ear development has the potential to be a powerful complement to *in vivo* studies. In particular, the development of an efficient and accurate method to produce inner ear sensory cells from human PS cells would enable *in vitro* studies of the exact onset and mechanism of various disease processes within the human inner ear and could be readily accessible testing ground for novel therapeutics that could prevent or treat hearing loss and improve imbalance (Brigande and Heller, 2009; Groves, 2010; Han et al., 2011). In this chapter I will discuss the state of stem cell research as it relates to the inner ear and identify critical gaps in knowledge addressed by the work described in **Chapters 2, 3**, **4**, and **5** of this dissertation.

INNER EAR DEVELOPMENT: IN VIVO AND IN VITRO

The development of an efficient method to derive inner ear hair cells or sensory neurons *in vitro* from stem cells has been the subject of intense investigation over the past decade (Brigande and Heller, 2009; Groves, 2010). Despite this effort, progress has been modest relative to similar work aimed at deriving other ectodermal tissues, such as the cortex, retina, spinal cord and epidermis, or tissues originating in other germ layers (Han et al., 2011; Hansen et al., 2011; Williams et al., 2012). In this section I will outline the key developmental checkpoints (see Figure 1) leading to normal inner ear induction as well as the techniques employed by researchers to guide stem cells to an inner ear fate *in vitro*.

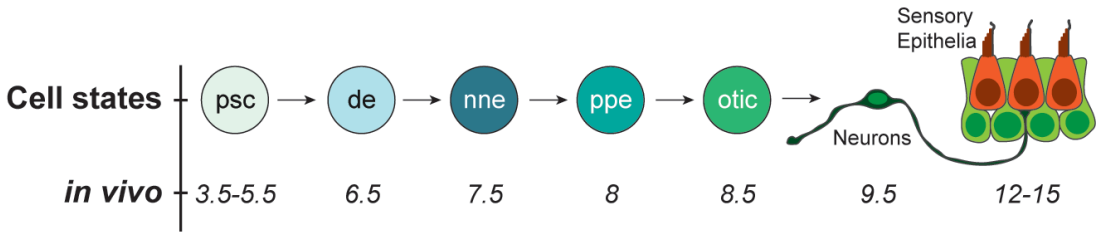

Figure 1: Cell state transitions during development of inner ear sensory cells.

The schematic shows a simplified model of the temporal progression of inner ear development in vivo. Beginning with a pluripotent state (psc), there is sequential acquisition of a definitive ectoderm (de), nonneural ectoderm (nne), preplacodal ectoderm (ppe), and otic prosensory progenitor cell (otic) state during inner ear development. Otic prosensory progenitors give rise to inner ear sensory neurons (i.e. spiral ganglion and vestibular ganglion neurons) and sensory epithelia containing hair cells (red) and supporting cells (green). The approximate timing of each fate transition is provided in mouse embryonic days.

I will critically analyze how closely stem cell researchers have characterized each step of the normal developmental process *in vitro*. Most of the stem cell research on the inner ear to date has been carried out using mouse PS cells. For this reason, my focus will be on literature deriving inner ear cells from mouse PS cells; however, I will also discuss work using human PS cells and adult stem cells (e.g. mesenchymal stem cells) when appropriate. Importantly, special emphasize will be given to the key morphological, biochemical, and physiological characteristics needed to identify inner ear cells derived *in vitro*.

Pluripotent stem cells

There are two types of PS cells: ES cells and iPS cells. ES cells are derived from inner cell mass cells in the blastocyst stage embryo (approximately embryonic (E) 3.5 in mice). In contrast, iPS cells are fully differentiated cells that have been reprogrammed to an embryonic stem cell-like state (Takahashi and Yamanaka, 2006; Yu et al., 2007). The methods for reprogramming are rapidly evolving, but typically involve the overexpression or modulation via small molecules of one or more transcription factors important for maintenance of pluripotency (Carey et al., 2011; Hou et al., 2013; Yamanaka, 2009; 2012). In general, ES and iPS cells can be considered equivalent in developmental potential, although subtle differences at the genetic and epigenetic level have been uncovered (Chin et al., 2010; Gore et al., 2011; Guenther et al., 2010; Hanna et al., 2010; Newman and Cooper, 2010). Moreover, culture conditions and laboratory specific practices may contribute to these apparent differences (Koehler et al., 2011; Newman and Cooper, 2010).

In recent years our understanding of pluripotency has advanced greatly. Critical to our ability to properly derive inner ear cells, or any other specific cell types, is an appreciation of the two distinct states of pluripotency, the "naïve" and "primed" states, which underlie the maintenance and initial differentiation of PS cells, respectively (Nichols and Smith, 2009; Ying et al., 2008). The naïve—also known as the ground—state of pluripotency refers to ES cells of the inner cell mass, which are in a stable state of pluripotency and express the marker genes *Nanog, Sox2, Oct4, Klf4* and *Rex1* (for additional markers refer to Young, 2011). Primed pluripotency is ascribed to cells in the epiblast (approximately E5.5 in mice) that are poised for differentiation down either of the ectoderm, mesoderm or endoderm lineages. These epiblast stem cells retain the capacity to self-renew and differentiate into cells from all three germ layers, but are more readily differentiated by signaling cues than naïve PS cells. This is achieved by epigenetic regulation of key developmental gene loci, which are maintained in a transcriptionally competent, but inactive state by both active and repressive histone marks, a configuration designated as a "bivalent domain" (Azuara et al., 2006; Bernstein et al., 2006). The epigenetic silencing ensures rapid transactivation of the genes in response to extracellular differentiation signals.

We now know that the manner in which stem cells are maintained in culture can influence the state of pluripotency. Undefined or fetal bovine serum-based methods of culturing mouse PS cells can lead to spontaneous differentiation, thus these conditions are more permissive of a primed pluripotent state (Ying et al., 2008). However, this spontaneous differentiation can be overcome by culturing

mouse PS cells in defined medium containing Leukemia inhibitory factor (LIF) and small molecule inhibitors of the mitotic activating protein kinase (MAPK) and Gsk3β (Wray et al., 2011; Ying et al., 2008). These conditions have been shown to force mouse PS cells into a naïve state of pluripotency. Removal from these conditions can rapidly initiate differentiation. In regards to differentiation studies, the purity (i.e. proportion of naïve vs. primed cells) of the cell population and its relative pluripotent state can affect the temporal progression of *in vitro* development. The mammalian embryo develops along a tightly regulated temporal schedule, with average gestational periods of 18 days and 9 months in mice and humans, respectively. During development, signaling and morphogenetic events occur in stereotyped anatomical locations and time points. For researchers to have any success in directing the differentiation of PS cells *in vitro* it is critical to know from which embryonic time point they are starting. Interestingly, human PS cells are thought to represent a primed state of pluripotency (Hanna et al., 2010). As a consequence, human PS cells share a similar gene expression and signal cue response profile with mouse epiblast-like cells. This gap in developmental timing is important for understanding the differences between how mouse and human PS cells differentiate *in vitro*.

The definitive ectoderm

The inner ear arises from the ectoderm germ layer. As such, following a primed pluripotent state, embryonic stem cells transition into a transient state known as the definitive ectoderm (approximately E6 in mice). In mice, the definitive ectoderm is not clearly defined due to its brief occurrence during development and,

thus has only been investigated directly in lower vertebrates (Hemmati-Brivanlou and Melton, 1997; Wilson and Hemmati-Brivanlou, 1995). The definitive ectoderm is a bipotent precursor of the neural and nonneural ectoderm. Collectively, these tissues give rise to the epidermis and the central and peripheral nervous systems (CNS and PNS). It is particularly challenging to define definitive ectoderm cells in an *in vitro* setting due to the lack of specific marker genes or proteins; however, definitive ectoderm cells can be defined by how they respond to signaling cues (Harvey et al., 2010). Seminal embryonic explant studies have revealed that undefined ectodermal tissue will differentiate into neural ectoderm in the absence of signaling factors (i.e. in a serum-free medium with minimal growth factors). This is known as the default model of neural ectoderm development (De Robertis and Kuroda, 2004; Stern, 2005; Ying et al., 2003). Later work in *Xenopus* showed that ectodermal explants cultured *ex vivo* in the presence of bone morphogenetic protein-4 (BMP4) differentiate into nonneural ectoderm, whereas control explants differentiated into neural ectoderm tissue (Wilson and Hemmati-Brivanlou, 1995; Wilson et al., 1997). Interestingly, PS cells treated with BMP4 will preferentially differentiate into mesodermal derivatives (Bernardo et al., 2011). From these studies and what we know about pluripotent states, we can define definitive ectoderm cells as cells that arise following a primed or epiblast-like state, but have not yet committed to a neural fate. Furthermore, in respond to BMP signaling definitive ectoderm cells transition to a nonneural fate instead of a mesodermal fate. Such cells have been described in ES cell cultures previously (Harvey et al., 2010). Harvey et al. observed a transient cell type in their mouse ES cell culture that

responded to BMP4 treatment by differentiating into nonneural ectoderm cells (Harvey et al., 2010).

The definitive ectoderm is likely under-characterized in stem cell cultures because neural ectoderm and various neuronal subtypes can be generated with relative ease. Neural cells develop efficiently in serum-free conditions, or using BMP inhibitors (e.g. Noggin, Dorsomorphin and LDN-193189). More generally, inhibition of transforming growth factor beta (TGFβ) signaling can promote ectodermal induction, likely by suppressing a primed pluripotent and mesodermal state, both of which all require TFGβ activity (Chambers et al., 2009). Notably, TGFβ inhibition (i.e. using small molecules such as selective inhibitor of smad3 [SIS3]) has been previously used to enhance production of inner ear cells from mouse ES cells by inhibiting the aberrant production of mesoderm and endoderm cells (Oshima et al., 2010).

The nonneural ectoderm

The nonneural ectoderm (also known as the surface ectoderm) is the next critical precursor during inner ear development (approximately E6.5 in mice). The nonneural ectoderm is the precursor to both the epidermis and preplacodal ectoderm; the latter of which gives rise to all cranial placodes including the otic (inner ear) placode. Our current understanding of nonneural ectoderm induction was primarily obtained from the *Xenopus* and zebrafish model systems. The consensus model stipulates that at the end of gastrulation, a gradient of BMP molecules patterns the ectodermal layer with high lateral concentrations and low medial concentrations of BMP molecules demarcating regions of nonneural and

neural ectoderm, respectively (Barth et al., 1999; Kishimoto et al., 1997; Neave et al., 1997; Reversade and De Robertis, 2005; Wilson et al., 1997). This gradient coincides with the upregulation of several nonneural associated markers, including *Dlx3, Dlx5, Gata2, Gata3* and *AP2.* As mentioned previously, high BMP activity steers definitive ectodermal cells towards a nonneural fate. Moreover, BMP antagonists secreted from cells at the midline of the embryo reinforce a lack of BMP signaling in cells destined to become neural ectoderm.

Consistent with its role during development, nonneural induction by BMP signaling has been recreated in mouse and human PS cell cultures for the production of epidermal cells such as keratinocytes (Coraux et al., 2003; Green et al., 2003; Itoh et al., 2011; Metallo et al., 2008). A similar approach has been taken to generate lens tissue from human PS cells (Leung et al., 2013; Yang et al., 2010). Despite these studies, researchers targeting the induction of inner ear cells from PS cells have largely failed to recognize the nonneural ectoderm as an essential precursor. Of note, Oshima and colleagues (2010) used medium containing fetal bovine serum to produce otic progenitor cells. Although not acknowledged by the authors, fetal bovine serum is known to contain BMP proteins, which likely contributed to nonneural induction in their cultures.

The preplacodal region

As mentioned above, the preplacodal ectoderm is derived from the nonneural ectoderm, which contains precursor cells that will ultimately give rise to the otic placode and then the inner ear. The preplacodal ectoderm develops in a U-shaped region of head ectoderm at the border of nonneural and neural ectoderm.

This region is often referred to as the preplacodal region (PPR) and gives rise to six cranial placodes: the adenohypophyseal (anterior pituitary gland), olfactory (olfactory sensory epithelium), lens, trigeminal (cranial nerve V), otic (inner ear/cranial nerve VIII) and epibranchial (cranial nerves VII, IX and X) placodes. Here I will focus on the induction of the PPR and subsequent otic placode induction, but for the interested reader there are several excellent reviews on development of the other cranial placodes from PPR (Grocott et al., 2012; Patthey and Gunhaga, 2011; Schlosser, 2006). An overview of the signaling mechanisms leading to preplacode induction and the various genetic/protein markers that can be used to characterize this process is shown in Figure 2.

The PPR is signified by expression of *Six1, Six4, Eya1* and *Eya2* in addition to nonneural markers such as *Dlx3, Dlx5, Gata2, Gata3* and *AP2*. Until recently, the underlying mechanisms leading to induction of the PPR were unclear. Several elegant zebrafish and chicken studies have now demonstrated that the BMP activity needed for nonneural induction must be subsequently attenuated for the PPR to develop properly (Ahrens and Schlosser, 2005; Brugmann et al., 2004; Glavic et al., 2004; Kwon et al., 2010; Litsiou et al., 2005). Furthermore, others have shown that fibroblast growth factor (FGF) signaling and inhibition of Wnt signaling are critical for PPR induction (Kwon et al., 2010; Litsiou et al., 2005; Patthey et al., 2009). From these studies it was clear that BMP and Wnt inhibition concomitant with activation of FGF signaling were critical for preplacode induction, however, the question of whether the entire preplacode is exclusively derived from the nonneural ectoderm was not resolved until more recently. In 2012, Pieper and colleagues used tissue

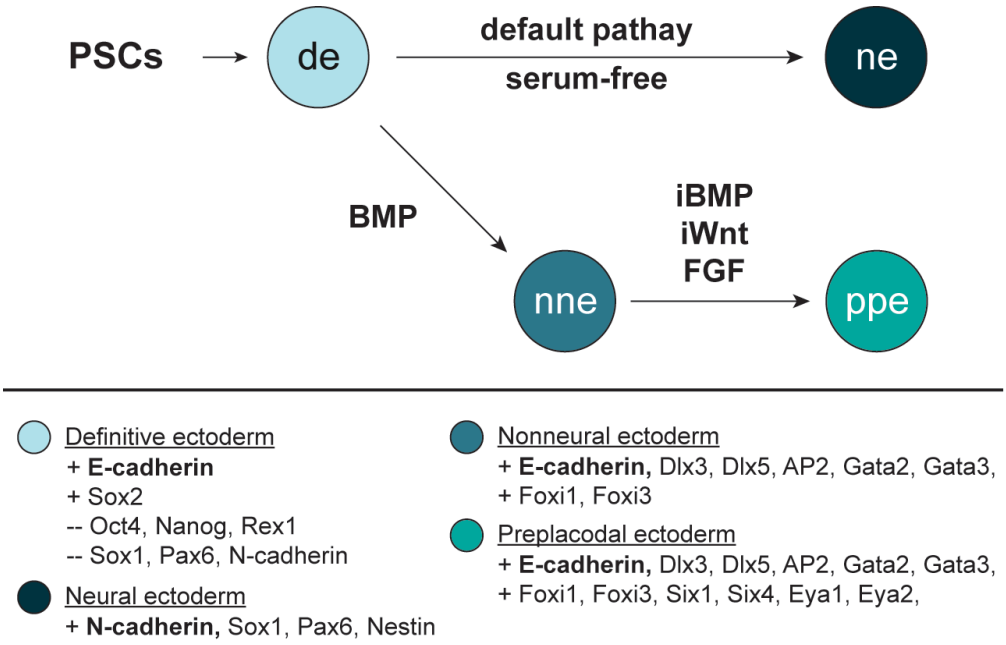

Figure 2: Schematic overview of the key signaling mechanisms underlying nonneural and preplacodal ectoderm induction.

Note that the "i" indicates signaling mechanisms that are inhibited. The lower panel lists makers that can be used to identify each tissue type. E- and N-cadherin are bolded to emphasize the importance of using these markers to distinguish nonneural and neural cell types.

grafting in the *Xenopus* model to reveal that the two neural plate border tissues, the PPR and the neural crest, are derived from the nonneural and neural ectoderm, respectively (Pieper et al., 2012). It should be noted, however, that a conflicting report seems to suggest that elevated FGF signaling can induce neural crest tissue from nonneural cells (Yardley and García-Castro, 2012). Despite the discrepancy surrounding the origin of neural crest tissue, there is a consensus that the preplacodal ectoderm is a nonneural ectoderm derivative. Moreover, PPR acquisition appears to be critical before cells can proceed towards an otic placode cell fate. Notably, Martin and Groves demonstrated that FGF2 treatment can induce otic cells in chicken preplacodal explants (Martin and Groves, 2006). By contrast, FGF2 treatment could not induce otic markers in more naïve surface ectoderm explants. Moreover, non-preplacodal ectoderm tissues could be converted into a preplacodal tissue upon grafting into the PPR and, once converted, this tissue became responsive to FGF2 treatment and gave rise to otic placode cells.

These basic developmental studies are critical to recreating inner ear development with PS cells because we must know precisely what intermediate cell types to expect in order to validate proper development *in vitro*. In other words, to prove that inner ear cells have been derived from stem cells, researchers will need to provide evidence that the cells have passed through a preplacodal intermediate. Towards this end, Oshima and colleagues recently used TGFβ and Wnt inhibitors to steer a heterogeneous cell population towards a preplacodal fate and then an otic progenitor fate (Oshima et al., 2010). To show preplacodal induction, however, the group used non-quantitative PCR analysis of several marker genes (e.g. *Dlx5*, *Six1,*

Eya1). As the sole method of verification, non-quantitative PCR is difficult to interpret because the transcripts being amplified could originate in disparate cell types within the heterogeneous population. For this reason, although Oshima and colleagues were able to show an upregulation of several preplacodal markers following their treatment plan, a demonstration that these markers were co-expressed is what was truly necessary to prove that preplacodal cells developed. Therefore, immunohistochemical analysis or single cell PCR is needed to verify these results.

The otic-epibranchial placode domain and the otic placode

In mice, FGF signaling originating from the neighboring hindbrain and the underlying mesenchyme is essential for otic placode induction in the PPR. In particular, two FGF isoforms, FGF-3 and FGF-10, are responsible for the induction process. Otic placode formation appears to occur in two steps. Initially, a broad region of the posterior PPR is defined by the aforementioned FGF signaling. Both the otic placode and epibranchial placodes arise from this region; therefore, it is often referred to as the otic-epibranchial placodal domain (hereafter, OPED; (Ladher et al., 2010). The transcription factors *Pax2* and *Pax8* are initially expressed throughout the OPED, however, *Pax2* expression is restricted to the otic placode over time. The segregation of the otic placode has been linked to Wnt mediated transcriptional control in the developing otic placode (Freter et al., 2008; Ohyama et al., 2006). Thus, FGF and Wnt signaling are the primary inducers of otic tissue in the PPR (Figure 3a).

Signaling mechanisms governing otic vesicle formation

Shortly after the otic placode is specified and acquires a thickened morphology, the placode invaginates into the mesenchyme to form the otic pit. Over a period of 12-24 hours the otic pit epithelium pinches off from the surface ectoderm to form the otic vesicle (also known as the otocyst). The otic vesicle is then partitioned into dorsal and ventral regions by opposing gradients of Wnt and BMP ligands, and Sonic hedgehog signaling, respectively. The ventral region of the otic vesicle contains prosensory otic progenitors that give rise to the primary sensory cells of the inner ear: sensory neurons and hair cells. Thus, acquisition of a prosensory otic fate is critical to generating inner ear sensory cells from PS cells.

Choosing the proper markers to identify otic progenitor cells deserves careful consideration. Figure 3b provides an overview of how to characterize authentic otic differentiation from other tissue types that express otic associated markers. From embryonic studies, Pax2 and Pax8 have emerged as markers of genuine otic progenitors; yet these proteins are not unique to the inner ear during development. For instance, at E9.5 in mice, Pax2/8 expression observed in the optic stalk, mid-hindbrain, kidney (i.e. the nephros), and the otic vesicle. Thus, additional markers are necessary to positively identify otic progenitors derived *in vitro*. For instance, the differential expression of cadherins can be used to identify nonneural (including otic progenitor cells) versus neural tissue. E-cadherin expression is maintained in the transition from definitive ectoderm to nonneural ectoderm, whereas it is downregulated in neural ectoderm tissue. Therefore, stem cell researchers can utilize the differential expression of E-cadherin/N-cadherin to

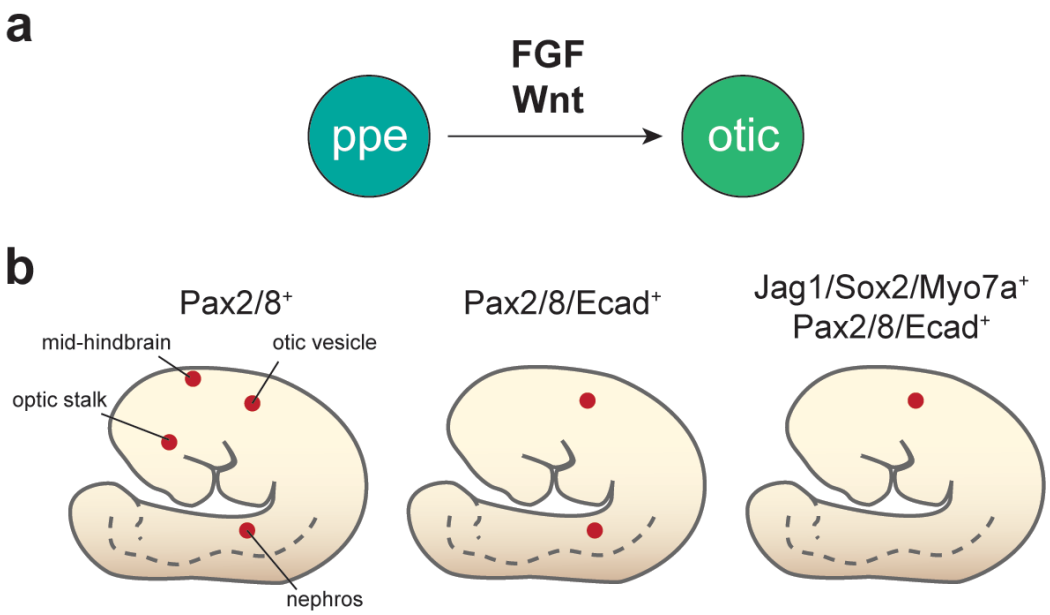

Figure 3: Mechanisms and markers indicative of otic induction.

a, FGF and Wnt activation are critical for conversion of preplacodal to otic progenitor cells. **b**, Several non-otic tissues express traditional otic markers. Researchers should be careful to rule out these tissues while characterizing *in vitro* otic development.

determine if their cultures are entering a nonneural or neural lineage. This distinction will preclude the mistaken identification of optic stalk or mid-hindbrain tissue for otic tissue, however, further characterization is needed to differentiate otic and kidney progenitors both of which express E-cadherin, Pax2 and Pax8. For this purpose other otic markers not seen in embryonic kidney, such as Dlx3 and Dlx5, can be employed. In addition, the Notch signaling associated protein Jagged1 and the transcription factor Sox2 are expressed throughout the otic placode and the nascent otic vesicle (Hartman et al., 2010; Neves et al., 2011; 2012; Oesterle et al., 2007). Both of these proteins are later restricted to the prosensory domain of the otic vesicle and sensory epithelium that produce hair cells and supporting cells. Moreover, the hair cell associated marker Myo7a is expressed at low levels in the otic vesicle, which appears to be a unique feature of inner ear development (Boëda et al., 2001; Sahly et al., 1997).

PATTERNING CELL FATE IN CULTURE

An important issue in stem cell biology is the format of the derivation culture. There are primarily three types of culture methods: (1) monolayer (i.e. two-dimensional; 2D) culture wherein the cells are attached to the bottom of a culture dish, (2) floating aggregate or embryoid body (i.e. three-dimensional; 3D) culture wherein cells remain floating in clumps, and (3) a combination of both 3D and 2D methods wherein the cells are cultured as aggregates for a period of time and then plated on a culture dish (Figure 4). Recent derivation studies in other fields have highlighted the relative merits of each approach. For instance, in monolayer culture,

Table 1: Previous attempts to derive inner ear sensory cells from pluripotent stem cells

Year	Group	Cell Type Used	Culture Method Used	Nonneural Cells	Preplacodal Cells	Otic Progenitor Cells	Cell Types Derived	Citation
2003	Heller	mESC	3D/2D, SFM[a], +EGF, +IGF1 +FGF2	N/A	N/A	Pax2+	Hair cell-like cells	Li et al., 2003
2010	Heller	mESC miPSC	3D/2D, SM[b], +IGF1, SIS3[c], Dkk1 +FGF2, Chick utricle cell co-culture	N/A	N/A	Pax2/Pax8/ Dlx5+ En1-	Hair cells-like cells	Oshima et al., 2010
2012	Rivolta	hESC	2D, SFM, +FGF3, FGF10	N/A	N/A	Pax8/Sox2+ Pax8/FoxG1+ Pax8/Nestin+	Hair cell-like and sensory neuron-like cells	Chen et al., 2012
2012	Yoshikawa	mESC	3D/2D, Stromal cell medium	N/A	N/A	N/A	Hair cell-like cells	Ouji et al., 2012

a, SFM, serum-free medium; *b*, SM, serum-containing medium; *c*, SIS3, selective inhibitor of smad3.

human PS cells can be rapidly and efficiently differentiated into neural and neural crest derivatives using small molecule inhibitor and recombinant protein treatments (Abranches et al., 2009; Chambers et al., 2009; 2012; Li and Ding, 2010). These studies suggest that the monolayer approach may yield a more homogenous population of a desired cell type. This is likely due to each cell receiving the same level of signaling inhibition or activation following a treatment. Conversely, cells aggregated in a 3D culture may receive varying levels of signaling modulation depending on their location within the aggregate and the diffusion properties of a particular molecule or protein (Kinney et al., 2011). Nonetheless, several 3D culture methods have been developed that lead to relatively efficient conversion of PS cells. Of particular note is the serum-free culture of embryoid body aggregates with quick aggregation (also known as SFEBq) method developed by Yoshiki Sasai and coworkers (Eiraku et al., 2008; Watanabe et al., 2005). In a series of elegant studies beginning in the mid-2000s, Sasai and colleagues demonstrated that this method can be used to generate a nearly 90% pure population of neural ectoderm cells, which can give rise to forebrain, midbrain and retinal tissue (Danjo et al., 2011; Eiraku et al., 2008; Ikeda et al., 2005; Muguruma et al., 2010; Sasai et al., 2012; Watanabe et al., 2005). A major advantage of SFEBq culture is that ectodermal tissues develop in the form of epithelia similar to their *in vivo* counterparts. Therefore, morphology can be used as a means of characterization in 3D culture—similar to the way structures can be identified in the embryo. Conversely, in 2D and 3D-2D cultures morphological properties are often lost because cells conform to the flat culture surface.

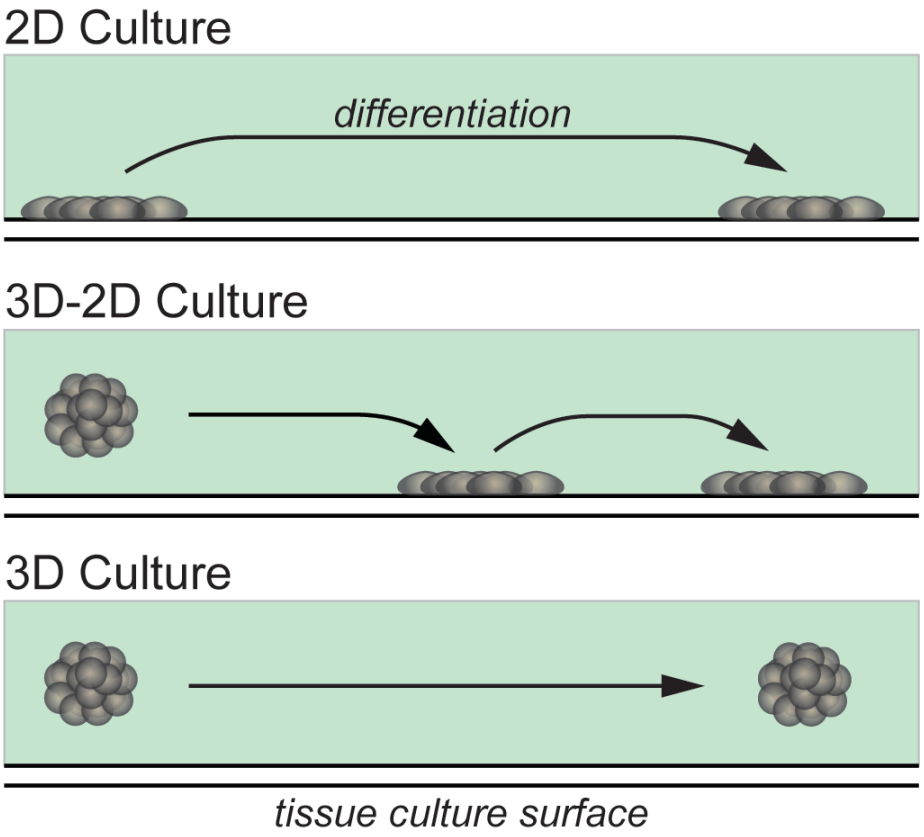

Figure 4: Differentiation culture formats

Illustrations of the 2D, 3D-2D and 3D culture formats.

To date, most inner ear derivation studies have adopted a 3D-2D approach. Table 1 summarizes the findings of recent attempts to derive inner ear sensory cells from PS cells. Li and colleagues were the first to provide evidence that inner ear hair cell-like progenitors could be derived *in vitro* using mouse embryonic stem cells (Li et al., 2003). A combined treatment of EGF, insulin-like growth factor 1 (IGF1) and, later, FGF2 were used in this study and subsequent studies using other stem cell types to promote development of inner ear cells (Chen et al., 2009; 2012; De Silva et al., 2006; Jeon et al., 2007; Li et al., 2003; Oshima et al., 2010; Qin et al., 2011). EGF-1 has been shown to have a role in preventing senescence and apoptosis in otic cells, while IGF1 has been found to be integral to proper otic neurogenesis (Aburto et al., 2012; Magarinos et al., 2010; White et al., 2012). Additionally, IGF1 has also been shown to be necessary for proper development of the anterior head region of the mouse embryo, but a more direct role in inner ear induction is less certain (Pera et al., 2001). As mentioned before, transient BMP signaling underlies the early inner ear induction process, so it is unclear how these mechanisms were recapitulated in this culture. Li and colleagues characterized putative otic progenitor cells by expression of Pax2 and Nestin, which are not exclusively expressed during inner ear development. Nonetheless, putative hair cells expressing Myo7a, Brn3c, and Atoh1 comprised ~5% of the culture after two weeks of differentiation. In apparent proof that these cells were of the inner ear lineage, the researchers demonstrated the *in vivo* survival of the otic progenitors and showed that they differentiated into hair cell like cells following injection into the avian inner ear. These results are compelling, however, a convincing reproduction of these results has not emerged

since publication in 2003. For instance, in a more recent study Chen et al. (2012), using human PS cells, were unable to produce hair cell-like cells using the EGF/IGF1/FGF2 method.

After testing the EGF/IGF1/FGF2 approach, Chen and coworkers developed a novel method for deriving otic progenitors, sensory neurons, and hair cell-like cells from human PS cells. For this approach, human PS cells were plated in a serum-free monolayer culture and treated with FGF-3 and FGF-10 for a period of 12 days. This method is intriguing because of its simplicity. Although, the use of FGF-3 and FGF-10 are developmentally accurate, the timing of treatment is much too early to have the same inductive affect seen on preplacodal cells *in vivo*. Thus, it is unclear how FGF-3 and FGF-10 function to generate otic progenitors in this culture. It is conceivable that endogenous BMP signaling mediates the spontaneous generation of nonneural cells. Nonetheless, strong evidence suggests that human PS cells, cultured under serum-free conditions, are biased toward neural development (Meyer et al., 2009; Pankratz et al., 2007; Zhang et al., 2001). Since most of these previous studies were performed using a 3D-2D method, it is possible that the exclusively monolayer format is more conducive to spontaneous nonneural differentiation (Chambers et al., 2009). Despite these mechanistic uncertainties, Chen et al. identified epithelial cells that expressed Pax2, Pax8, FoxG1, Sox2, Nestin and Six1 as evidence of their otic progenitor-like characteristics. They also found Myo7a/Brn3c^{+} cells in their cultures that appeared to have rudimentary apical protrusions with Espin-positive bundles—reminiscent of hair cell stereocilia. However, since the bundles do not have the same architecture as stereocilia on native hair cells further

characterization will be needed to determine the authenticity of these bundle-bearing cells.

Another recent study delineated a simple culture method that involves treating PS cells with stromal cell conditioned medium for a period of 14 days, which resulted in generating Myo7a/Brn3c^{+} hair cell-like cells (Ouji et al., 2012). Intriguingly, PS cells in this study first undergo neural ectoderm conversion before expressing hair cell-like marker proteins. It is difficult to determine whether these cells are truly inner ear hair cells or CNS cells that happen to share characteristics with hair cells. Notably, choroid plexus cells and retinal pigment epithelium cells, two neural ectoderm derivatives, are known to express Myo7a during development and may be mistaken for hair cells in a 2D culture (Boëda et al., 2001; Sahly et al., 1997). In addition to protein expression analysis, Ouji et al. attempted to show that these Myo7a/Brn3c^{+} cells have functional mechanosensitive channels by showing that they take up FM1-43 dye. FM1-43 dye becomes fluorescent upon entering cells through specific types of ion channels, including the mechanosensitive ion channels found in mature hair cells. If a putative hair cell does not become fluorescent when treated with FM1-43 dye, it likely does not contain functional mechanosensitive channels. Incidentally, choroid plexus epithelial cells are also known to take up FM1-43 dye (Meyers et al., 2003). Thus, the true identity of the cells derived by Ouji and colleagues remains equivocal without further examination. These results underscore the necessity to properly demonstrate the temporal progression of PS cells as they transition from one cell state to the next. Similarly, the cells in the Chen et al. study appear to transition through a neural ectoderm intermediate (Chen et al.,

2012). As we have discussed, neural ectodermal transition deviates from the established progression of inner ear development. It is conceivable that these results may reflect differences between the mouse and human inner ear developmental process and that of lower vertebrates such as the chicken and frog; however, early developmental events like the bifurcation of the ectoderm are likely conserved between species.

In 2010, Oshima and colleagues established a novel method for generating otic progenitors (Oshima et al., 2010). This method adopted the use of IGF1 from their previous method described in Li et al., but added several elements to more accurately model otic development. As I briefly mentioned before, their strategy was to induce cells from all lineages by treating cells with FBS and then selectively inhibiting mesoderm and endoderm cells using TGFβ and Wnt inhibitors. Although this approach led to a heterogeneous mixture of cells, the researchers were able to identify a small population (10-20%) of cells expressing a combination of marker proteins for otic progenitors, including Pax2, Pax8 and Dlx5. Moreover, the otic progenitors generated in this study did not express Engrailed-1, a protein expressed in Pax2/8^{+} cells of the developing hindbrain. This is a strong characterization, because Pax2/8 and Dlx5 only overlap in the developing inner ear, however the authors had difficulty quantifying the number of cells that were positive for all three markers (Oshima et al., 2010). This may be due to the fact that these proteins are expressed sequentially during inner ear development and do not overlap for an extended period in the embryo.

Oshima and coworkers used a 3D-to-2D format, making it easier to identify otic progenitor-like cells amongst a monolayer of cells (Oshima et al., 2010). Interestingly, when these cells were cultured for up to 20 days in a serum-free medium on a fibronectin substrate, the researchers observed the development of hair cell-like cells expressing GFP under control of the hair cell marker gene Atoh1. Atoh1-GFP^{+} cells also expressed Myo7a, but did not have stereocilia bundles seen in native hair cells. Remarkably, if the mixture of cells containing otic progenitor-like cells was plated on a layer of mitotically inactivated chicken utricle supporting cells (i.e. the cells that normally underlie and insulate hair cells in the sensory epithelium), more mature looking hair cell-like cells developed with stereocilia bundles (denoted by F-actin/Espin co-localization) and a kinocilium (denoted by acetylated-α-tubulin expression). Despite the fact that these cells represented less than one percent of the total cell population, the researchers were able to use the Atoh1-GFP reporter to identify cells for electrophysiological recordings. By deflecting the stereocilia bundles, they found that these hair cell-like cells were indeed mechanosensitive similar to native hair cells. These results marked the first demonstration that functional hair cells could be derived from PS cells *in vitro*. The findings also indicated that supporting cells might provide an important signaling cue missing in the monolayer culture system. Perhaps hair cells derived *in vitro* must be incorporated into an epithelium in a manner similar to native hair cells in order to develop properly. This would suggest that a 2D culture format might not be appropriate for proper hair cell differentiation. In support of this notion, recent studies on retinal derivation suggest that complex epithelia containing specialized

sensory cell types develop more authentically and reach later stages of maturity in a 3D culture environment (Eiraku et al., 2011; Gonzalez-Cordero et al., 2013; Nakano et al., 2012; Sasai et al., 2012).

Toward a framework for how to identify hair cell types in vitro

In the mammalian inner ear there are four distinct types of hair cells. Sensory epithelia in the vestibule contain type I and II hair cells, whereas the organ of Corti in the cochlea contains inner and outer hair cells. In the animal, hair cell types can be readily distinguished by gross anatomical characteristics; however, researchers deriving hair cells *in vitro* must rely primarily on genetic markers to distinguish one hair cell type from another. Figure 5 summarizes the defining characteristics of different hair cell types that can be used to identify hair cells *in vitro*.

Single cell electrophysiological recordings can be used not only to confirm acquisition of membrane properties comparable to those of native hair cells, but also to determine the hair cell phenotype. For example, stem cell-derived hair cells acquiring a vestibular phenotype should follow a stereotyped pattern of functional maturation characterized by the four distinct voltage-gated conductances: a delayed rectifier conductance (G_{DR}), a fast inward rectifier potassium conductance ($G_{K,L}$), a type-I-specific delayed rectifier potassium conductance (G_{K1}), and a tetrodotoxin-insensitive sodium conductance (G_{Na}), as well as the mechanotransducer conductance (Géléoc and Holt, 2003; Géléoc et al., 2004). The temporal order of conductance acquisition should be: G_{DR}, G_{K1}, G_{Na} and $G_{K,L}$ in cells destined for a type I vestibular phenotype. Moreover, G_{Na} expression in stem cell-derived hair cells may be of large enough to induce spiking patterns similar to that of immature cochlear

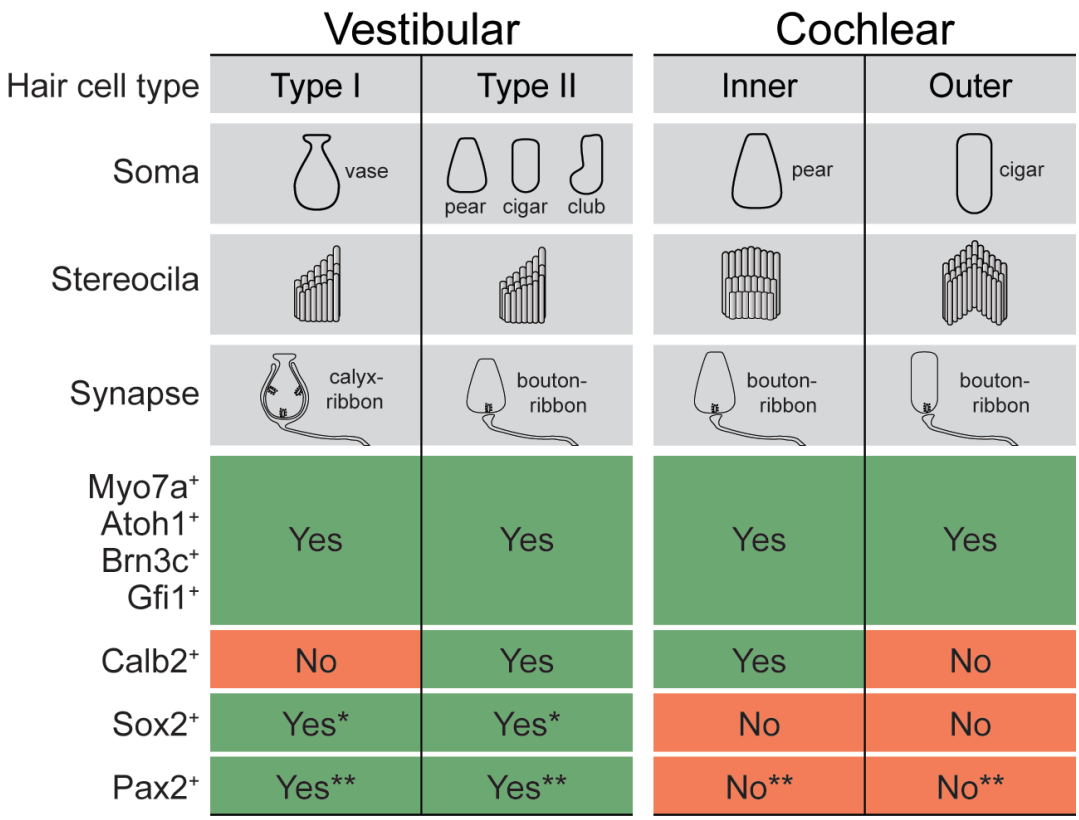

Figure 5: Defining different hair cell types by morphology and genetic markers.

Criteria for identifying certain types of hair cells derived *in vitro*. * Sox2 expression has been shown to persist in vestibular and not cochlear hair cells; however, whether Sox2 is localized to both or just one type of hair cell in the vestibule requires further investigation (see Oesterle et al., 2007). ** Pax2 restriction to vestibular hair cells has only been convincingly shown in chicken inner ears, so these results should be confirmed in the mouse system (see Warchol and Richardson, 2009).

inner hair cells (Kros et al., 1998; Marcotti, 2012). Additionally, voltage-gated calcium or ligand-gated (e.g. ATP or acetylcholine) conductance may be present in stem cell-derived hair cells (A J Hudspeth, 1988; Bao et al., 2003; Géléoc et al., 2004; Tritsch and Bergles, 2010; Tritsch et al., 2010). The ultimate validation of functional hair cells will rest on the presence of robust transduction currents upon mechanical stimulation of the stereocilia bundles (Gillespie and Müller, 2009; Oshima et al., 2010). The biophysical properties of mechanotransduction and adaptation may also help distinguish vestibular versus cochlear hair cells.

Inner ear neurogenesis

There are two general types of inner ear sensory neurons: the vestibular ganglion neurons (VGNs) and spiral ganglion neurons (SGNs). These glutamatergic bipolar neurons act as the primary relay between the vestibular organs or cochlea, and the CNS. Both neuronal types are derived from the same pool of otic progenitor cells, which delaminate from the otic vesicle at around E9.5 in mice. In recent years, mouse genetic studies have revealed much about how these two populations of neurons emerge from this progenitor pool and make stereotyped connections with hair cells (for an comprehensive review see (Appler and Goodrich, 2011). I will attempt to summarize this work and highlight key features of inner ear neurogenesis that can be used to generate inner ear neurons from PS cells. Importantly, degeneration or inflammation of the vestibular and spiral ganglia is associated with balance deficits and hearing loss, respectively. This has led many to postulate that transplantation of stem cell-derived inner ear neurons may be a

viable treatment option. The first step towards this goal, however, will be to successfully recapitulate inner ear neurogenesis *in vitro*.

The gene regulator networks governing delamination of neuroblasts from the otic vesicle and their specification into SGN and VGN neurons have been elucidated in recent years. Around E8.5, transient expression of *Ngn1* occurs in cells destined to become inner ear neurons within the prosensory domain of the otic vesicle epithelium. Ngn1 protein acts as a transcription factor promoting the expression of genes involved in inner ear neurogenesis, such as *NeuroD*, *GATA3*, *Islet1* and *Pou4f1* (Fritzsch, 2003; Fritzsch et al., 2010; Hanna et al., 2010; Ma et al., 2000; McCarroll et al., 2012; Raft et al., 2007). Shortly following the onset of Ngn1 expression, inner ear neuroblasts begin to delaminate into cochleovestibular ganglion (CVG) precursors (Fariñas et al., 2001; Yang et al., 2011). Within the otic vesicle epithelium, lateral inhibition via the Notch signaling pathway has been implicated in neuroblast delamination (Daudet et al., 2007). Additionally, IGF and Shh signaling appear to contribute to neuroblast proliferation and survival (Aburto et al., 2012; Bok et al., 2007).

The next step in otic neurogenesis is the division of the neuroblast pool into SGNs and VGNs. A recent study by Appler and coworkers elucidated the role of GATA3 in the SGN and VGN cell fate decision. In conditional *GATA3* knockout mice, neuroblasts delaminate from the otic vesicle; however, the SGN identity and neurite outgrowth was disrupted (Appler et al., 2013). They found that loss of *GATA3* decreased expression of the SGN associated gene *Mafb* and increased expression of the VGN associated genes *Onecut1* and *Pcdh19*. Thus, these results provide insight

into the cross-inhibitory mechanism that likely underlies the SGN and VGN fate decision.

Development of VGNs and SGNs is of course only one part of the puzzle; the guidance of axons from these cells to the appropriate locations is integral to proper inner ear development. While many factors likely play a role in the guidance of SGN the importance of hair cells may be overstated, as axons are capable of reaching the habenula perforate in *Atoh1* null mice which that lack hair cells (Fritzsch et al., 2005; Hu et al., 2004; Matsuoka et al., 2006; 2007; Okano et al., 2005; Sekiya et al., 2007). Earlier works suggested that two neurotrophins, BDNF and NT3, may be critical guidance cues for developing SGNs to innervate their target hair cells in the cochlea. BDNF is expressed in hair cells in the apical portion of the cochlea (starting at E12.5), followed by a gradual shift towards the basal region (Hegarty et al., 1997; Shepherd et al., 2005; Yang et al., 2011). In contrast, NT3 is expressed predominantly in hair cells in the basal and middle turns of the cochlea followed by expression proceeding apically. The strong and complementary expression patterns of these neurotrophins in hair cells at a developmental period when SGNs establish synaptic connections with hair cells led to the speculation that BDNF and NT3 may provide long-range guidance cues for SGN axons that express their cognate receptors trkB and trkC. However, subsequent studies have revealed that these neurotrophins function primarily as survival factors for SGNs (Ernfors et al., 1995; Silos-Santiago et al., 1997; Takahashi and Yamanaka, 2006; Yu et al., 2007). Recent studies, however, started to unravel true axon guidance cues for developing SGNs. Most notable of all are the axon repellant molecules Ephrin-A5 and EphA4. Ephrin-

A5 is expressed in outer hair cells, whilst EphA4 is expressed in type I SGNs. Defourny et al. (2013) elegantly demonstrated that EphA4-expressing type I SGNs are repelled by Ephrin-A5 in outer hair cells, therefore unable to enter the outer hair cell region, resulting in making synaptic connections solely with inner hair cells that do not express Ephrin-A5.

Derivation of inner ear sensory neurons from PS cells

To date, no group has successfully guided PS cells to a definitive SGN or VGN fate *in vitro*. Nevertheless, several attempts have been made toward this goal using guided differentiation as well as genetic engineering. For example, our group has shown that Shh activity promotes transdifferentiation of mesenchymal stem cells into *Gata3* positive glutamatergic neurons, whereas Wnt activity promotes transdifferentiation into *Tlx3* positive glutamatergic neurons (Kondo et al., 2005; 2011). Alternatively, overexpression of *Tlx3* in PS cells led to preferential differentiation of glutamatergic neurons (Kondo et al., 2008). However, the otic identity and functionality of these neurons needs further investigation. In another study, Reyes and colleagues found that forced expression of *Ngn1* in differentiating PS cells promoted development of otic-like neurons, but since *Ngn1* is essential for induction of many neuron types in the CNS and PNS, whether the derived neurons are authentic otic neurons is still unclear (Reyes et al., 2008; Young, 2011). More recently, Chen et al. provided evidence that human PS cell-derived otic-like progenitors could differentiate into functional otic-like neurons. These neurons were characterized as sensory neurons by the presence of Brn3a, Neurofilament

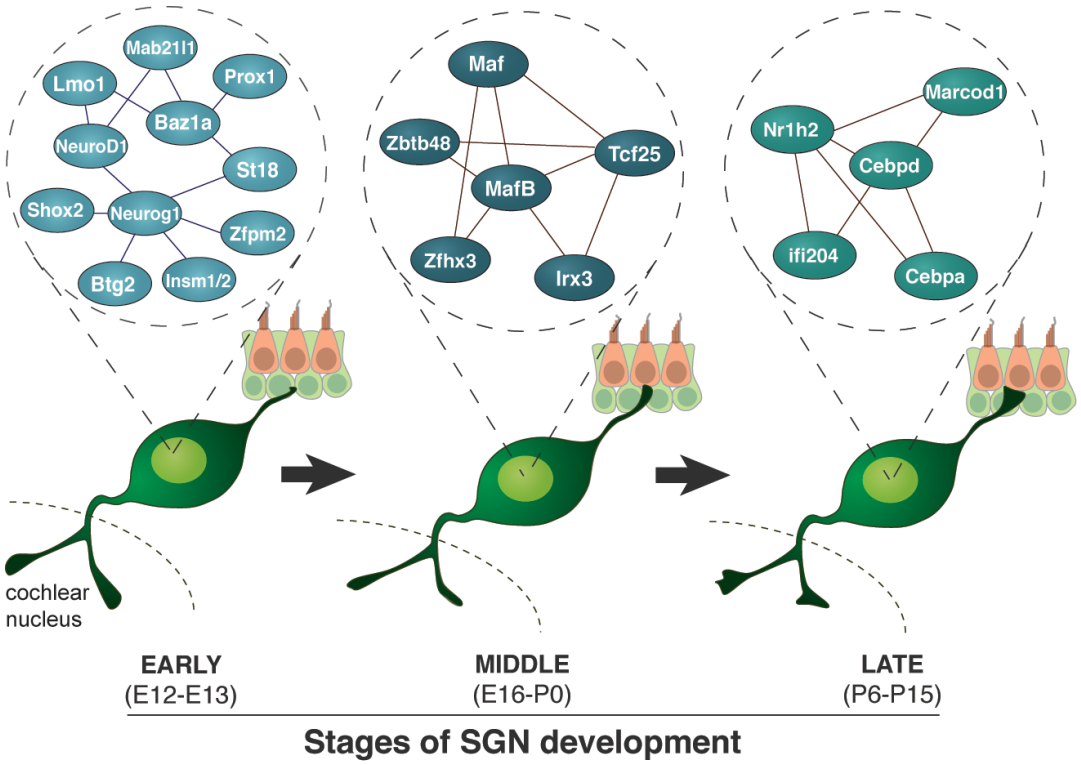

Figure 6: Gene expression profile of developing SGNs.

Each circle contains genes that were shown to be upregulated in SGNs compared to VGNs at each step of SGN development by Lu and colleagues (2011). This profile may be used to authenticate SGNs derived from PS cells.

(Nefl) and TuJ1, which defines a fairly broad subset of sensory neurons (Chen et al., 2012). Thus, more work is needed to fully recapitulate and characterize inner ear neurogenesis from PS cells.

A particularly difficult challenge confronting researchers trying to produce inner ear neurons from PS cells is identifying neurons produced *in vitro* as authentically otic. As it stands, SGNs and VGNs share many common traits with other sensory neurons. Therefore, as with the derivation of otic progenitors and hair cells, the derivation of authentic inner ear neurons will need to be carefully documented to show that each developmental step leading up to neurogenesis occurs. Beyond the neurogenic event, thorough gene and protein expression data will be critical to determining which neuronal subtypes are formed and what level of maturity they acquire. Recent work by Lu and colleagues has taken great strides toward outlining a gene expression profile of developing SGNs and VGNs (Appler and Goodrich, 2011; Lu et al., 2011). By meticulously microdissecting SGN and VGN tissues and performing microarrays at various stages of development, the researchers were able to obtain a temporal gene expression profile. This dataset is freely available and should provide a guide for stem cell researchers attempting to define inner ear neurons derived *in vitro*. Figure 6 highlights several genes revealed by Lu et al. to be specifically upregulated in SGNs.

PROSPECTS FOR CLINICAL TRANSLATION

Accumulating evidence has shown that PS cells can give rise *in vitro* to cells with phenotypic and functional properties comparable to native mechanosensitive

hair cells and, potentially, sensory neurons of the inner ear. Can these technical advances be translated and used to replace damaged sensory cells in the inner ear *in vivo*? The inaccessibility and delicacy of the inner ear structure present major challenges for clinical applications of cell-based therapy. The current consensus in the field is that replacing SGNs in the cochlea would be more feasible than replacing mechanosensitive hair cells (Brigande and Heller, 2009; Shi and Edge, 2013). Developing a method to deliver stem cell-derived hair cells to the organ of Corti and stimulate their integration into the epithelium is a significant challenge. In contrast, surgical approaches for delivering sensory neurons to the modiolus of cochlea have already been established.

Though the complete replacement of the cochlear implant may someday happen, currently the primary utility of stem cells appears to be their potential ability to modulate and improve the efficacy of cochlear implants by replacing lost SGNs. There are several reasons why this makes sense. The most obvious reason to combine the two modalities is that the inner ear is already accessed during a cochlear implantation surgery, and with some minor tweaking stem cell-derived cells could also be implanted with the hope of an added benefit to hearing following the procedure. Survival of SGNs and the efficacy of the growth of their axonal processes could be enhanced from electrical signals emitted from the electrodes of the implant, providing an additional benefit beyond that stem cells would otherwise have been capable of if implanted alone (Hegarty et al., 1997; Shepherd et al., 2005). Additionally, the outgrowth of axonal processes can be further enhanced by coating the array with neurotrophins to maximize its ability to attract the newly implanted

cells (Evans et al., 2009; Gonzalez-Cordero et al., 2013; Stern, 2005). While there are no current *in vivo* studies examining electrode arrays and the influence of stem cell engraftment and neuronal outgrowth, the development of cochlear implants for use in animal models will allow these theories to be tested and techniques further refined (Millard and Shepherd, 2007).

Stem cell transplantation in animal models of auditory neuropathy

Animals bearing selective loss of SGNs are desirable models to study the outcome of stem cell transplantation *in vivo*. Since mice are not an appropriate animal model for stem cell transplantation studies due to the small size of the inner ear, using genetically manipulated mice is not an option. Schmiedt and colleagues demonstrated that the Na,K-ATPase inhibitor Ouabain selectively damage SGNs while leaving hair cells intact in Mongolian gerbils (Lang et al., 2005; Schmiedt et al., 2002). This technique has been most widely used to create an animal model of auditory neuropathy for stem cell transplantation studies.

Seminal studies conducted in mid 2000s assessed whether undifferentiated or pre-differentiated PS cells could survive and engraft in cochlear tissues of host animals for an extended period of time (4-14 weeks). In most studies, gerbils, guinea pigs or rats were chosen as transplant recipient animals, whereas readily available mouse or human PS cells (embryonic stem cells, neural stem cells or mesenchymal stem cells) were used as donor cells (Hu et al., 2005; Regala et al., 2005; Sekiya et al., 2007). In these xenografting conditions, transplanted PS cells survived and gave rise to cells expressing neuronal proteins. Interestingly, a greater percentage of transplanted PS cells survived in the cochlea with selective loss of SGNs than the

untreated normal cochlea, suggesting that the damaged cochlea might provide a more permissive environment for donor PS cells (Matsuoka et al., 2007). The properties of the damage cochlear microenvironment that support better engraftment, however, are unclear at this time. Injections of PS cells directly into the modiolus of the spiral ligament appears to yield a significantly higher engraftment than injections into the scala tympani (Corrales et al., 2006; Matsuoka et al., 2006; 2007). In addition, *in vitro* neural induction of PS cells prior to transplantation promotes engraftment of donor cells in the host cochlea and suppress aberrant tumorigenesis that has been shown to be associated with ES cell transplantation (Chen et al., 2012; Corrales et al., 2006; Kondo et al., 2011). Some of these studies are largely descriptive without quantitative data or proper controls, however it is worth noting that generating animals with loss of SGNs and injecting stem cells into the tiny cochlear space in animals require extremely difficult multiple survival surgeries. These studies are very time-consuming and can be accomplished only by a very limited number of skilled ENT surgeons with knowledge on the anatomy of the animal inner ear.

Despite the daunting technical challenges, continued efforts to establish a means to replace lost or damaged SGNs with PS cells recently had some exciting developments. One of the most remarkable accomplishments in the advancement of surgical techniques enabled continued exposure of transplanted stem cells to biologically active molecules *in situ* in live animals (Kondo et al., 2011). In this study, gerbils with auditory neuropathy were transplanted with partially differentiated mesenchymal stem cells through modiolar injections. The animals were also

subcutaneously implanted with a mini-osmotic pump, which released neural induction medium followed by Wnt1 into the cochlea at a constant flow rate for 4 weeks. The extended supply of these factors in stem cell transplantation sites resulted in an increase in the number of engrafted cells due presumably to the effects of Wnt1 on cell survival. The study also revealed the remarkable ability of mesenchymal stem cells to migrate through the modiolus and reach the apical turn of the cochlea, where numerous donor cells were found in areas surrounding the spiral ganglion.

Another recent breakthrough in animal studies is the first demonstration of recovery in the auditory threshold after stem cell transplantation (Chen et al., 2012), in which Pax2/8-positive human ESC-derived cells were transplanted in the modiolus of ouabain-treated gerbils. Remarkably these transplanted ESC-derived otic progenitor-like cells, without any differentiation factors, appeared to migrate into the SG and gave rise to bipolar neurons extending their processes towards the organ of Corti. More strikingly, the thresholds of auditory brain stem responses (ABRs) in animals that received stem cell transplantation were approximately 20 dB lower than sham control animals at 6 weeks post-transplantation onward. Another important implication from the Chen et al. study was that authentic SGNs might not be necessary to recover function. Any excitatory glutamatergic neurons could be integrated into the auditory circuit if provided with the proper transplantation conditions. Interestingly, results from recent neural transplantation studies in the CNS seem to refute this notion (Kriks et al., 2011; Ma et al., 2012). Kirks and colleagues demonstrated that proper specification of dopaminergic neurons was

absolutely critical for the observed functional recovery in a mouse model of Parkinson's disease after transplantation into the striatum (Kriks et al., 2011). This work underscores the importance of authenticity in reconstituting a particular neuronal circuit. Whether the restored ABRs in the gerbils treated by Chen et al. actually signify restored audition in these animals will be an interesting question for future investigation. Moreover, it will be fascinating to see what bearing cellular identity might have on the outcome of cell therapy experiments in the inner ear.

In vitro disease models

In vitro disease modeling is another clinical application for stem cell-derived inner ear tissues. Stem cell-based disease models are a relatively new concept sparked by the development of iPS cell technology. It is now possible to derive iPS cells from patients with disorders or diseases with a genetic component. The patient-specific iPS cells can them be differentiated in vitro in to the tissue types most affected by the gene mutations. To date, iPS cell disease models have been established for a wide range of conditions including Alzheimer's disease, Parkinson's disease, Rett syndrome, schizophrenia, familial dysautonomia, microcephaly, and amyotrophic lateral sclerosis (ALS) to name a few (Brennand et al., 2011; Di Giorgio et al., 2008; Dimos et al., 2008; Dolmetsch and Geschwind, 2011; Kondo et al., 2013; Lancaster et al., 2013; Marchetto et al., 2010; Park et al., 2008; Sandoe and Eggan, 2013). One commonality between these models is a well-characterized differentiation method that produces a predictable number of specific type of cells or a population of cells with predictable heterogeneity (Han et al., 2011). For instance, ALS models have taken advantage of well-established methods

for deriving motor neurons (Dimos et al., 2008; Sandoe and Eggan, 2013). Another essential component of disease modeling studies is the use of clear endpoint analysis (i.e. neurite outgrowth, electrophysiological recordings, etc.). Disease modeling is not currently possible for genetic mutations impacting cranial placodes, including the inner ear, due to the lack of a well-characterized derivation method. The ideal method would reproducibly generate inner ear tissues that retain much of the structural and functional organization seen *in vivo*. Comparing morphology in animal models is a powerful means of determining the phenotypic consequences of gene mutations. For this reason, 3D culture systems that recapitulate the morphology of *in vivo* cell populations may be more appropriate for facilitating similar analysis *in vitro*. Interestingly, the 3D culture system for deriving cerebral tissue has recently been shown to be conducive to modeling human microcephaly (Lancaster et al., 2013). A similar model of inner ear development would facilitate investigation of genetic inner ear disorders.

RESEARCH SUMMARY/QUESTIONS

Before the clinical potential of stem cell research to alleviate inner ear dysfunction can be fully realized, we first need to establish a reproducible method to derive inner ear tissue *in vitro*. As I have discussed, efforts to derive inner ear tissues have been hampered by ill-defined culture systems that fail to faithfully recapitulate normal inner ear developmental mechanisms. During embryonic development, the inner ear arises from two progenitor cell types known as nonneural and preplacodal ectoderm cells. Surprisingly, previous studies aimed at deriving inner ear cells from PS cells have failed to emphasize the fact that the

derivation of nonneural and preplacodal cells is a critical first step towards deriving inner ear cells. To address this unmet need, I stringently defined a differentiation strategy to produce inner ear cells by carefully considering each transition in cellular identity; beginning with the nonneural and preplacodal identities. While the ultimate goal of this approach was to produce authentic SGNs, my methods turned out to be broadly applicable to the generation of other inner ear tissues such as mechanosensory hair cells and have the potential to generate other cranial placode derived tissues (e.g. trigeminal neurons, olfactory epithelium, lens, etc.). In the near-term this work will provide a reliable *in vitro* model of inner ear development for use in basic science or disease modeling studies. In the long-term, the culture system could be refined to produce highly pure populations of sensory cells for transplantation studies.

Based on key developmental mechanisms, I hypothesized that the temporally precise activation and/or antagonism of the BMP and FGF signaling pathways during *in vitro* differentiation of PS cells would lead to the generation of nonneural, preplacodal and inner ear cells. To test this hypothesis, I employed a combination of cell biology, molecular biology and electrophysiology methods to investigate the following specific questions:

1. Can precisely timed activation of BMP signaling induce nonneural cells in a three-dimensional mouse embryonic stem cell culture?

2. Can subsequent inhibition of BMP signaling and FGF signaling activation promote the induction of preplacode-like cells from nonneural cells?

3. If nonneural and preplacodal induction are accurately reproduced in three-dimensional culture, will inner ear tissues arise spontaneously via self-organization?

In the subsequent chapters of this dissertation I provide a detailed description of the methods (**Chapter 2**) used to address these questions as well as the results of these experiments (**Chapters 3, 4,** and **5**). Most of the results presented herein are modified from Koehler et al., Nature 2013 and a forthcoming manuscript in preparation for publication. Furthermore, I provide a general discussion (**Chapter 6**) to put the findings in perspective with regard to the current state of stem cell and inner ear research.

This introductory chapter was modified from a forthcoming book chapter in the 4th edition of Development of Auditory and Vestibular Systems published by Elsevier

Koehler KR, Malone A, Hashino E. Recapitulating inner ear development with pluripotent stem cells: biology and translation. Development of Auditory and Vestibular Systems 4 edition. Copyright Elseiver 2014.

CHAPTER 2: MATERIALS AND METHODS

ES cell culture

ES cells derived from blastocyst-stage embryos of R1 mice were maintained in feeder-free conditions using 2i-LIF medium as previously described (Hayashi et al., 2011; Ying et al., 2008). In brief, ES cells were maintained on gelatin and used for experimentation until passage 40. N2B27 Medium consisted of a 1:1 mixture of Advanced DMEM/F12 and Neurobasal medium (Invitrogen) supplemented with 1 mM GlutaMAX (Invitrogen) and 1 mM penicillin/streptomycin (STEMCELL Technologies). 2i-LIF medium was made by supplementing N2B27 medium with 1000 U ml^{-1} leukemia inhibitory factor (LIF; Millipore), 3 μM CHIR99021 (Stemgent) and 1 μM PD0325901 (Santa Cruz).

Days 0–3 of SFEBq differentiation were performed as described with major modifications (Eiraku et al., 2011). In brief, ES cells were dissociated with 0.25% trypsin-EDTA, re-suspended in differentiation medium and plated 100 ml per well (3,000 cells) on 96-well low-cell-adhesion U-bottom plates (Lipidure Coat, NOF). Differentiation medium was G-MEM supplemented with 1.5% knockout serum replacement (Invitrogen), 0.1 mM nonessential amino acids, 1 mM sodium pyruvate, 1 mM penicillin/streptomycin and 1 mM 2-mercaptoethanol. On day 1, half of the medium in each well was exchanged for fresh differentiation medium containing Matrigel (2% (v/v) final concentration). On day 3 of the protocol, BMP4 (10 ng ml^{-1}) and SB-431542 (1 μM) were added to each well at 5× concentration in 25 ml of fresh media. On days 4–5, FGF2 (25 ng ml^{-1}) and LDN-193189 (100 nM) were added to each well at 6× concentration in 25 ml of fresh media. The concentration of Matrigel

was maintained at 2% (v/v) throughout days 1–8. On day 8 of differentiation, cell aggregates were transferred to 24-well plates (Lipidure Coat, NOF; 4–8 aggregates per well) in N2 medium containing 1% (v/v) Matrigel. N2 medium contained Advanced DMEM/F12, 1× N2 Supplement, 1 mM penicillin/streptomycin or 50 mg ml^{-1} Normocin (Invivogen) and 1 mM GlutaMAX. For some experiments small molecules were added to N2 medium before plating the aggregates. Half of the medium was changed every day during long-term floating culture for up to 30 days.

Signaling molecules and recombinant proteins

The following small molecules and recombinant proteins were used: recombinant human BMP4 (10 ng ml^{-1}; Stemgent), human FGF2 (25 ng ml^{-1}; Peprotech), XAV939 (1 μM; Santa Cruz), SU5402 (10 μM; BioVision), SB-431542 (1 μM; Tocris Bioscience) and LDN-193189 (100 nM; Stemgent). Notably, we have obtained comparable results using concentrations of up to 1 μM LDN-193189.

Quantitative PCR

As described previously (Koehler et al., 2011), RNA was isolated using the RNeasy Minikit (Qiagen) and treated with TURBO DNase (Ambion). Single-stranded complementary DNA was synthesized using Omniscript reverse transcriptase (Qiagen) and Oligo-dT primers. All amplicons had standardized sizes of 100–110 base pairs. cDNA samples were amplified on an ABI PRISM 7900HT Sequence Detection System (Applied Biosystems) using the SYBR Green PCR Master Mix

(Applied Biosystems). For each PCR reaction, a mixture containing cDNA template (5 ng), Master Mix, and forward and reverse primers (400 nM each) was treated with uracil N-glycosylase at 50 °C for 2 min before undergoing the following program: 1 cycle, 95 °C, 10 min; 45 cycles, 95 °C, 15 s, 60 °C, 1 min; 1 cycle, 95 °C, 15 s, 60 °C, 15 s, 95 °C, 15 s; 72 °C, hold. Melting curve analysis was performed to confirm the authenticity of the PCR product. The mRNA level for each gene was calculated relative to L27 mRNA expression.

Primers used: *Dlx3* forward: CAGTACGGAGCGTACCGGGA, reverse: TGCCGTTCACCATGCGAACC; *Sox1* forward: AACCAGGATCGGGTCAAG, reverse: ATCTCCGAGTTGTGCATCTT; *brachyury* forward: CACACGGCTGTGAGAGGTACCC, reverse: TGTCCGCATAGGTTGGAGAGCTC; *Pax8*, forward: CGGCGATGCCTCACAACTCG, reverse: TGGGCCAAGTCCACAATGCG; *Pax2* forward: CCCGTTGTGACCGGTCGTGATAT, reverse: TGGGTTGCCTGAGAACTCGCTC.

Immunohistochemistry

Aggregates were fixed with 4% paraformaldehyde. The fixed specimens were cryoprotected with a graded treatment of 10, 20 and 30% sucrose and then embedded in tissue freezing medium. Frozen tissue blocks were sectioned into 10- or 12-mm cryosections. For immunostaining, a 3% goat or horse serum and 0.1% Triton X-100 solution was used for primary antibody incubation. An Alexa Fluor 488-conjugated anti-mouse IgG or anti-rat IgG and an Alexa Fluor 568-conjugated anti-rabbit IgG (Invitrogen) were used as secondary antibodies. A DAPI counterstain

was used to visualize cellular nuclei (Vector, VectaShield). For whole-mount staining, aggregates were placed directly into blocking solution with 1% Triton X-100 following fixation. For confocal imaging and three-dimensional reconstruction experiments, following secondary antibody incubation, aggregates were cleared using ScaleA2 solution for 1-2 days followed by ScaleB4 treatment for another 2 days as described previously (Hama et al., 2011). Microscopy was performed on a Nikon TE2000 Inverted Microscope or an Olympus FV1000-MPE Confocal/Multi-photon Microscope. Three-dimensional reconstruction was performed using Voxx (custom software developed by Indiana Center for Biological Microscopy).

The following antibodies were used: anti-E-cadherin (rabbit, Abcam; mouse, BD Biosciences); anti-N-cadherin (mouse, BD Bioscience); anti-Sox1 (rabbit, Cell Signaling Technologies); anti-Nanog (rabbit, Abcam); anti-brachyury (goat, Santa Cruz Biotechnology); anti-AP2a (mouse, DHSB); anti-Pax8 (rabbit, Abcam); anti-Pax2 (rabbit, Invitrogen; mouse, Abnova); anti-Sox2 (mouse, BD Biosciences); anti-Jag1 (rabbit, LSBio); anti-$p27^{kip1}$ (mouse, BD Biosciences); anti-myosinVIIa (rabbit, Proteus); anti-acetylated-a-tubulin (mouse, Abcam); anti-Tuj1 (mouse, Covance); anti-calretinin (Calb2; mouse, Millipore); anti-Caspr1 (mouse, NeuroMAB); anti-Caspr2 (mouse, NeuroMAB); anti-p63 (mouse, Santa Cruz Biotechnology); anti-cytokeratin5 (rabbit, Sigma); anti-neurofilament (rabbit, Millipore); anti-Brn3a (mouse, Millipore); anti-islet1 (mouse, DSHB); anti-synaptophysin (rabbit, Invitrogen); anti-Brn3c (mouse, Santa Cruz Biotechnology); anti-Ctbp1 and anti-Ctbp2 (mouse, BD Biosciences); anti-Rab3 (mouse, BD Biosciences); anti-Snap25 (mouse, BD Biosciences); anti-Pax6 (rabbit, Abcam); anti-Pax3 (mouse, DSHB); anti-

aPKC (rabbit, Santa Cruz Biotechnology); anti-laminin-B1 (rat, Abcam). For most antibodies, mouse embryonic tissue sections were used as positive controls. Mouse embryos were dissected from time pregnant ICR mice using a protocol approved by the Institutional Animal Care and Use Committee at Indiana University School of Medicine. The embryo fixation and processing procedure was identical to that used for cell aggregates.

The Alcian blue staining procedure was modified from a previously reported method (Jegalian and De Robertis, 1992). In brief, cyrosections were incubated in Alcian blue staining solution for 10 min and subsequently de-stained using 60% ethanol/40% acetic acid for 20 min. A final eosin stain was performed for 30 sec. For Oil Red O staining, cryosections were kept in 60% isopropanol for 2 min and then placed in freshly prepared Oil Red O stain for 5 min followed by a 30 sec hematoxyline stain.

Image analysis

The percentage of epithelial cells expressing Pax8 and Ecad was established by analysing serial sections of day 6 and day 8 aggregates. Data are representative of 6–8 aggregates from at least 3 separate experiments. For analysis of each aggregate, 5 cryosections were chosen at random positions along the *z*-axis of the aggregate. Using Nikon Elements or NIH ImageJ software, the Ecad$^+$ outer epithelium was outlined and cell counting of DAPI and Pax8$^+$ nuclei along the length of the epithelium established a percentage for each cryosection.

The apparent thickness of epithelia was determined by analysing cryosections stained with Ncad (control) or Ecad (all other conditions) on days 3–6. Data are representative of 6–8 aggregates from at least 3 separate experiments. For each aggregate, 3 serial sections were analysed. Five points along the epithelium were randomly chosen and the thickness was measured using Nikon Elements image analysis tools.

Similarly, the number of Myo7a$^+$ hair cells in each day 20 aggregate was determined by analysing 10 μm serial cryosections. Each biological sample represents the average number of hair cells counted in 4–6 cell aggregates and data are representative of the average from 3 separate experiments (15 aggregates total for each condition). Odd and even numbered cryosections were analysed separately and averaged to avoid double counting. The number of vesicles was quantified similarly, but every third section was analysed to avoid double counting and allow for analysis of 3 separate staining combinations. Vesicles with a long axis diameter larger than 30 mm were accounted for to avoid double counting.

Stereocilia heights were determined by measuring the apparent length of F-actin-labelled structures protruding from Myo7a$^+$ hair cells on day 20 and 24. Likewise, kinocilium heights were determined by measuring the apparent length of acetylated-α-tubulin-labelled protrusions from Myo7a$^+$ hair cells. Regions of interest were chosen randomly for analysis and >100 cells were analysed across 3–5 separate epithelia.

Synapses were quantified by analysing day 16, 20 and 24 aggregate sections stained for synaptophysin (Syp) and Ctbp2 using a previously described method (Coate et al., 2012). Regions of interest were chosen randomly for analysis and >100 cells were analysed across 4–5 separate epithelia from 3 separate experiments. Confocal *z*-stacks were taken of Ctbp2-stained hair cells. The maximum-intensity projections were used to count the number of $Ctbp2^{+}$ puncta surrounding each hair cell nuclei.

Statistical analysis

Statistical significance was determined using a Student's *t*-test for comparison of two groups or a one-way analysis of variance followed by Tukey's post-hoc test for multiple comparisons, unless stated otherwise. All data were analysed using Prism 6 or Microsoft Excel software.

FM1-43 labeling

The presence of functional mechanosensitive channels was confirmed using a FM1-43 dye uptake assay similar to previous studies (Gale et al., 2001; Hu and Corwin, 2007; Meyers et al., 2003). Large lumen aggregates (that is, >500-μm-long-axis diameter), identified by their translucency and spherical morphology relative to surrounding tissue, were used for these experiments. Aggregates were incubated in DMEM-F12 containing FM1-43FX (5 mM; Invitrogen) for 1 min and then washed 3× in fresh N2 Medium. A faint cellular outline caused by autofluorescence was used to

identify potential hair cells in the vesicle wall. In N2 Medium, a 0.25-mm tungsten needle was used to puncture each vesicle in an area away from the site of potential hair cells. The punctured vesicles were incubated in DMEM-F12 containing FM1-43FX (5 mM) for 1 min with gentle rocking and then washed 3× in fresh N2 medium. Vesicles were imaged to confirm dye uptake and immediately fixed with 4% paraformaldehyde. For some experiments, epithelia were fixed and incubated in PBS containing 1% Triton X-100 and phalloidin conjugated to Alexa Fluor 647 (Invitrogen) to confirm the identity of hair cells.

Electrophysiological recordings

On day 24 of differentiation, large lumen vesicles (>500-μm diameter) were dissected from cell aggregates following a 30-min incubation in DMEM/F12 containing dispase (STEMCELL Technologies). Epithelial regions containing hair cells were identified on the basis of a thickened morphology relative to the rest of the vesicle epithelium. Two incisions were made using tungsten needles on the opposite side of the vesicle in order to expose and flatten the hair-cell-containing epithelium. The flattened epithelium was mounted onto round glass coverslip and held in position by two wires glued to the coverslip using MDX4-4210 (Corning). The coverslip was then placed in a submersion-type slice chamber mounted on the stage of a Nikon E600FN Eclipse microscope. Electrophysiological recordings were performed under continuous perfusion of oxygenated artificial cerebrospinal fluid that contained the following (in mM): 130 NaCl, 3.5 KCl, 1.1 KH_2PO_4, 1.3 $MgCl_2$, 2.5 $CaCl_2$, 30 $NaHCO_3$, 10 glucose, pH 7.4 (320 mOsm kg^{-1}). Recording pipettes were

pulled from borosilicate capillary glass (WPI) with resistances ranging from 2 to 3 MΩ. Recording pipettes were filled with a potassium gluconate-based recording solution that contained the following (in mM): 130 K-gluconate, 3 KCl, 3 $MgCl_2$, 5 phosphocreatine, 2 K-ATP, 0.2 NaGTP, 10 HEPES, pH 7.3, 290 mOsm kg^{-1}. Whole-cell access resistances were monitored throughout each experiment and ranged from 5–20 MΩ; a change of 15% was deemed acceptable.

Hair cells were identified with a 40× water-immersion objective and differential interference contrast. Only cells with hair bundles on their apical surface were chosen for recording. Positive pressure was maintained as the recording pipette was lowered into the epithelium. When the recording pipette touched the membrane, positive pressure was released and tight seal was formed. Recordings were obtained at 30 °C using solution inline heater (Warner Instruments). The cells were held at −60 mV, and data were acquired using whole-cell technique in voltage-clamp mode using a Multiclamp 700B amplifier (Molecular Devices) coupled to a Digidata 1332A board (Molecular Devices). The data were analyzed using the pClamp 10.2 (Molecular Devices). All chemicals were purchased from Sigma-Aldrich. ***Electrophysiology was performed in collaboration with Andrei I. Molosh (experimental design, patch-clamp recordings, and data analysis) and Gerry S. Oxford (experimental design and data analysis)***

Transmission electron microscopy

Day 24 aggregates were fixed in 2% paraformaldehyde/2% glutaraldehyde in 0.1 M phosphate buffer. After fixation the specimens were rinsed with phosphate

buffered saline followed by post-fixation with 1% osmium tetroxide. Thereafter, the aggregates were dehydrated through a series of graded ethyl alcohols and embedded in Embed 812 (Electron Microscopy Sciences). Ultra-thin sections (70–80 nm) were cut, stained with uranyl acetate and viewed on a Tecnai BioTwin (FEI) transmission electron microscope at 80 kV. Digital images were taken with an Advanced Microscope Techniques couple-charged device camera. ***TEM was performed in collaboration with Caroline Miller at the IUSM Electron Microscopy Center***

Western blot analysis

Cell aggregates were lysed in radioimmunoprecipitation assay buffer supplemented with a protease inhibitor cocktail (Roche). Cell extracts were centrifuged at 13,000 r.p.m., 4 °C for 10 min to remove insoluble debris and chromosomal DNA. Proteins were separated by denaturing SDS–PAGE and transferred to PVDF membranes (Biorad). After blocking, membranes were incubated with a primary antibody overnight at 4 °C. An anti-b-actin (Sigma) antibody was used for confirmation of equal loading of the samples. Blots were detected with a horseradish peroxidase-conjugated goat anti–rabbit or rabbit anti-mouse antibody (Invitrogen) and visualized with the SuperSignal West Pico or -Femto chemiluminescent detection system (Pierce) and exposed to X-ray film. ***Western blot analysis was performed in collaboration with Dharmeshkumar Patel***

This chapter is modified from work previously published in Nature

Koehler, K. R., Mikosz, A. M., Molosh, A. I., Patel, D. & Hashino, E. Generation of inner ear sensory epithelia from pluripotent stem cells in 3D culture. *Nature* 500**,** 217–221 (2013).

CHAPTER 3: INDUCTION OF A NONNEURAL EPITHELIUM IN THREE-DIMENSIONAL CULTURE

INTRODUCTION

The inner ear contains specialized sensory epithelia that detect head movements, gravity and sound. It is currently unclear how to derive these sensory epithelia from pluripotent stem cells, a process which will be critical for modeling inner ear disorders *in vitro* or developing cell-based therapies for profound hearing loss and balance disorders (Bermingham-McDonogh and Reh, 2011; Brigande and Heller, 2009). To date, attempts to derive inner ear mechanosensitive hair cells and sensory neurons have relied on genetic manipulation or co-culture with embryonic inner ear tissues (Chen et al., 2012; Kondo et al., 2008; Oshima et al., 2010; Reyes et al., 2008). These efforts have resulted in inefficient and incomplete phenotypic conversion of stem cells into inner ear-like cells. A key insight lacking from these previous studies is the importance of the nonneural and preplacodal ectoderm, two critical precursors during inner ear development (Groves and Fekete, 2011; Lleras-Forero and Streit, 2012; Patthey and Gunhaga, 2011; Pieper et al., 2012; Schlosser, 2006). Moreover, the optimal format of culture (e.g. monolayer or floating culture) for inducing the inner ear-like cells is unknown.

Recent studies have demonstrated how organogenesis of complex neural ectoderm tissues such as the cerebral cortex and retina can be faithfully reconstituted *in vitro* using the SFEBq method (Eiraku et al., 2008; 2011; Nakano et al., 2012). Culturing aggregates in a serum-free medium containing knockout serum replacement promotes development of a neural epithelium via the default pathway

of neural ectodermal development. Modifying the signaling factors (e.g. Insulin, FGF2, Shh, RA, etc.) presented to the neural epithelium can induce specific regions of the forebrain, midbrain and hindbrain. Until recently, developing neuroepithelia within these cultures took the form of dispersed epithelial vesicles embedding in unorganized tissue. In a critical evolution of the method, Eiraku and colleagues demonstrated that extracellular matrix proteins (e.g. a laminin/entactin complex or Matrigel) could be added to the culture medium to promote the development of a basement membrane on the surface of the aggregate. With structural support, the entire surface layer of cells self-organizes into a neural epithelium after 5 days in culture. These aggregates spontaneously developed optic cups, which matured into complete neural retinas in about 18-20 days. This work provided proof-of-principle for guiding the organogenesis of complex sensory organs *in vitro*.

The aforementioned studies were successful at deriving mature neural ectoderm tissues; however, the cranial placodes and the inner ear are derived from the nonneural ectoderm. Suga and coworkers recently demonstrated that by increasing the size of the aggregate, a nonneural ectoderm layer spontaneously arises on the surface of the cell aggregates leaving a neural layer underneath. Their data suggest that an endogenous source of BMP signaling is likely mediating nonneural induction in 3D culture; however, the precise signaling mechanisms are unclear. Using a sonic hedgehog agonist they induced the development of adenohypophyseal placodes, vesicles, and functional anterior pituitary tissue from the induced nonneural epithelium. These results showed that cranial placode morphogenesis could be recapitulated in 3D culture. Specifically, placodal

invagination and vesicle formation, two critical morphological steps in both anterior pituitary and inner ear development, were well preserved in this culture system. Here we report the step-wise differentiation of a nonneural epithelia from mouse embryonic stem (ES) cells in three-dimensional culture (Eiraku et al., 2011; Suga et al., 2011). During neurulation *in vivo*, the definitive ectoderm is subdivided into the neural ectoderm and nonneural ectoderm, the latter of which gives rise to the inner ear (Figure 7). Since the inner ear shares a common precursor with the neural tissues derived in previous studies, the definitive ectoderm, we proposed that SFEBq culture could be redirected to generate inner ear epithelia using carefully timed morphogenetic cues (Figure 8). Drawing on previous 3D culture studies, we attempted to garner more control over the nonneural induction process by treating smaller, Matrigel-conditioned, aggregates with BMP4.

RESULTS

We identified a definitive ectoderm-like epithelium on day 3 of SFEBq culture, prior to expression of neuroectoderm-associated proteins on day 5 (Figure 9 and 10). During early embryogenesis, activation of bone morphogenetic protein (BMP) signaling is critical for induction of the nonneural ectoderm from the definitive ectoderm epithelium (Grocott et al., 2012; Wilson and Hemmati-Brivanlou, 1995). Consistent with this role, in aggregates treated with BMP4 (hereafter, BMP), the nonneural ectoderm marker *Dlx3* was upregulated, while the neuroectoderm marker *Sox1* was downregulated (Figure 11).

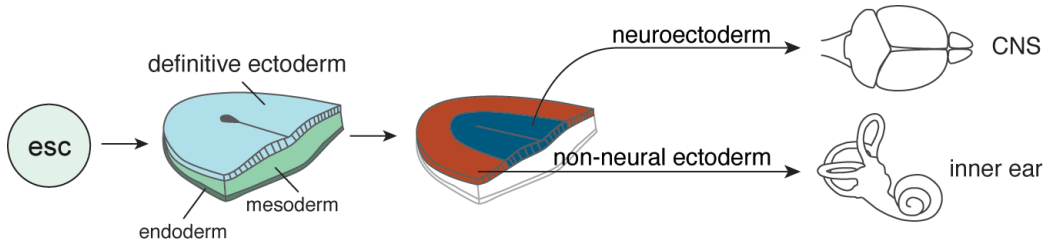

Figure 7: Bifurcation of the ectodermal germ layer

The cell fate decision between nonneural ectoderm and neuroectoderm is the critical point of departure between central nervous system and inner ear development.

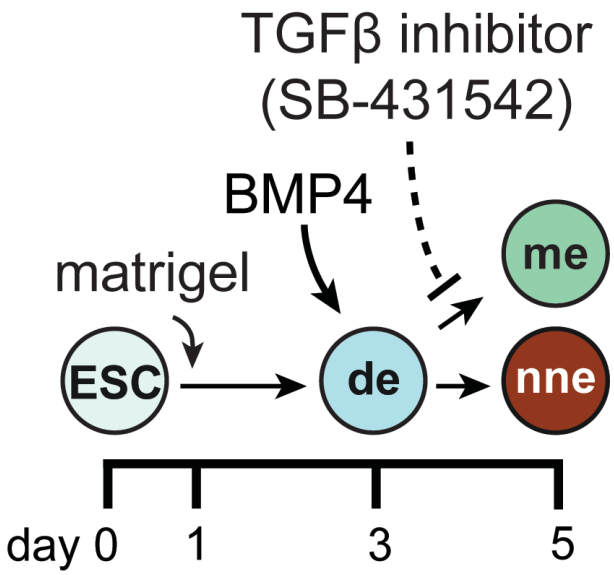

Figure 8: Nonneural ectoderm induction strategy.

ESC, embryonic stem cells; de, definitive ectoderm; me, mesendoderm; nne, nonneural ectoderm.

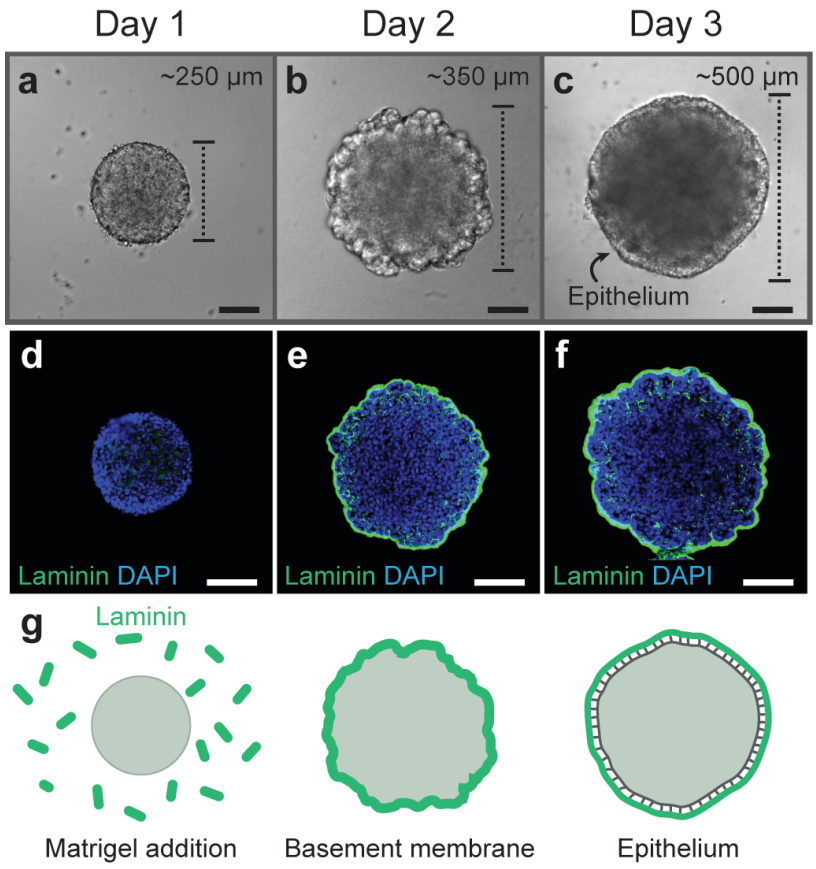

Figure 9: Development of an epithelium on ES cell aggregates.

a-c, DIC images of representative aggregates on days 1, 2, and 3 of 3D culture. **d-g**, Following Matrigel addition on day 1, Laminin is incorporated into a basement membrane on the surface of the aggregate. An epithelium develops on the aggregate surface by day 3. Scale bars, 100 µm.

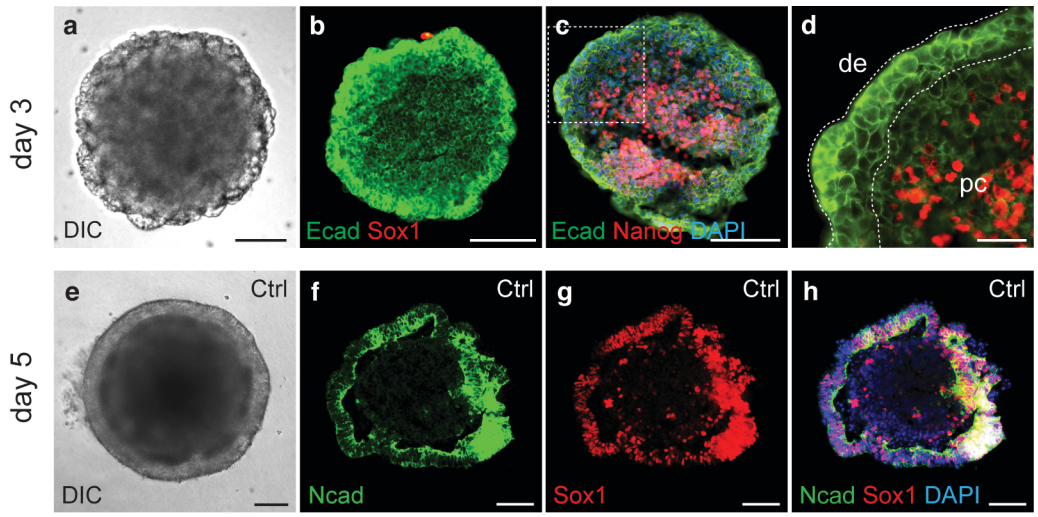

Figure 10: Definitive ectoderm and neural ectoderm in 3D culture.

a-d, On day 3 of SFEBq differentiation, a Nanog$^-$ Sox1$^-$ and Ecad$^+$ epithelium forms on the outer surface of each aggregate. SFEBq has been shown to generate a nearly pure population of neuroectodermal cells (see Eiraku et al. 2008, 2011 and Kamiya et al. 2011); therefore, this epithelium may be roughly equivalent to embryonic definitive ectoderm because it is in-between a state of pluripotency (Nanog$^+$) and neuroectoderm (Sox1$^+$ Ncad$^+$; (Eiraku et al., 2008; 2011; Kamiya et al., 2011). No *unique* markers of the definitive ectoderm are known. esc, embryonic stem cells; me, mesendoderm; de, definitive ectoderm; nne, nonneural ectoderm; ne, neuroectoderm; ppe, preplacodal ectoderm; epi, epidermis; otic, otic placode; pc, pluripotent cell. **e-h**, By day 5 of differentiation, vehicle control (Ctrl) aggregates develop a Ncad$^+$ Sox1$^+$ epithelium similar to the neuroectoderm *in vivo* and previous reports using SFEBq culture (see Eiraku et al. 2008, 2011 and Kamiya et al. 2011). Scale bars, 100 μm (**a-c, e-h**), 25 μm (**d**).

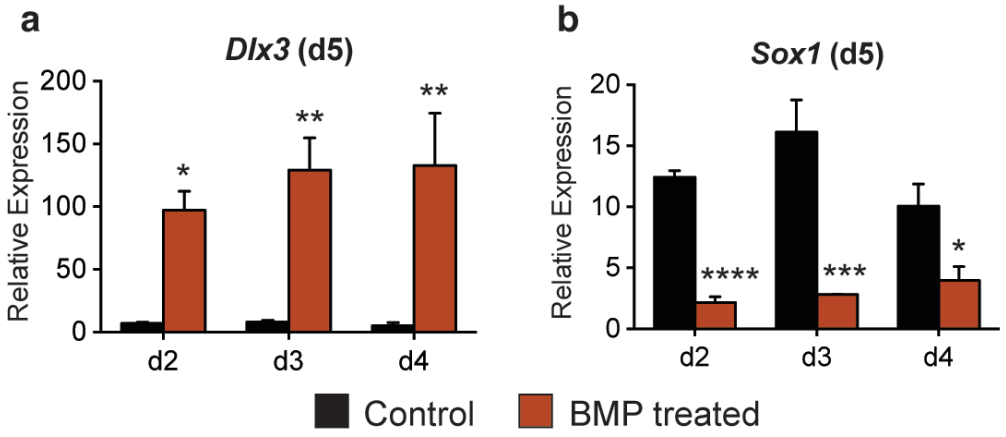

Figure 11: *Dlx3* and *Sox1* expression following BMP treatment.

a, **b**, qPCR analysis of day 5 samples after the addition of 10 ng ml^{-1} BMP or a vehicle control to the medium on day 2, 3 and 4. The nonneural ectoderm *Dlx3* (**a**) was upregulated in response to BMP4 treatment, whereas the neuroectodermal marker *Sox1* (**b**) was downregulated ($n = 3$; mean ± s.e.m.). A two-way ANOVA with Bonferroni's post hoc test for multiple comparisons was used to determine significance (*$P < 0.05$, **$P < 0.01$, ***$P < 0.001$, ****$P < 0.0001$). No significant differences were observed between control groups.

BMP-treated aggregates also expressed the mesendoderm marker *brachyury*, indicating the undesirable induction of mesoderm or endoderm cell types (Figure 12; Bernardo et al., 2011). By day 5, 60.8 ± 3.9% of cells in BMP-treated aggregates were brachyury$^+$ and the presumptive ectodermal layer on the surface of each aggregate had been disrupted, prohibiting further analysis (Figure 12). To suppress aberrant mesendoderm induction, we combined BMP treatment with the transforming growth factor β (TGFβ) inhibitor SB-431542 (hereafter, SB; Figure 8; Chambers et al., 2009). A combined treatment of SB and BMP (hereafter, BMP/SB) on day 3 completely abolished brachyury$^+$ cells in the outer-epithelium, while maintaining mesendoderm tissue in the inner layer of the aggregates (Figure 12; Bernardo et al., 2011; Chambers et al., 2009; Eiraku et al., 2011).

To test whether BMP/SB treatment indeed induced nonneural ectoderm, we assessed the cellular composition of BMP/SB-treated aggregates by immunofluorescence at differentiation day 5. Western blot analysis revealed that the nonneural ectoderm marker AP2 was only detectable in the BMP/SB-treated samples (Figure 13). Remarkably, AP2 expression was found predominantly in the Ecad$^+$ outer-epithelium, but was absent in other regions of treated aggregates (Figure 14). Moreover, we identified an intermediate layer of each aggregate with Sox1$^+$ and N-cadherin (Ncad)$^+$ cells, indicative of the formation of neuroectoderm (Figure 14). Importantly, Ncad was not observed in the AP2$^+$ outer-epithelium (Figure 14), demonstrating a complete transformation of the outer-epithelium into nonneural ectoderm (compare with control day 5 sample in Figure 10).

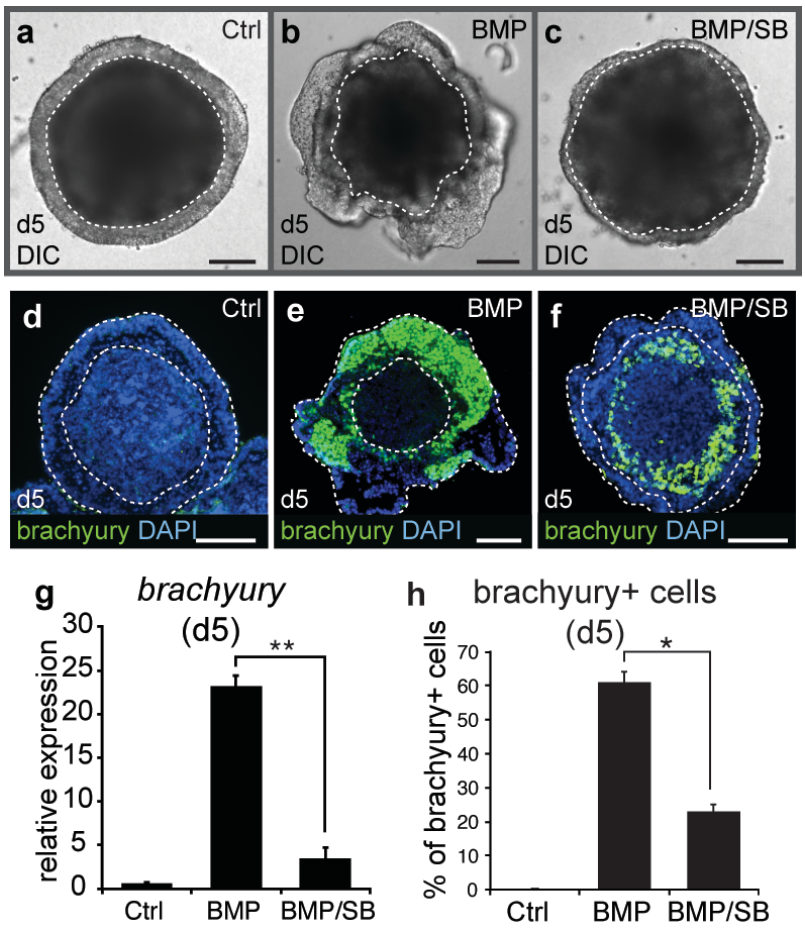

Figure 12: Control of BMP induced mesendoderm by TGFβ inhibition.

a–c, Morphology of control (Ctrl), BMP and BMP/SB aggregates. DIC, differential interference contrast. **d–f**, Brachyury⁺ cells are less prevalent in BMP/SB aggregates. DAPI, 4′,6-diamidino-2-phenylindole. **g**, SB decreases the level of brachyury expression induced by BMP ($n = 3$; $^{**}P < 0.01$; mean ± s.e.m.). **h**, Quantification of brachyury+ cells on day 5 ($n = 3$; $^{*}P < 0.05$; mean ± s.e.m.). Scale bars, 100 μm.

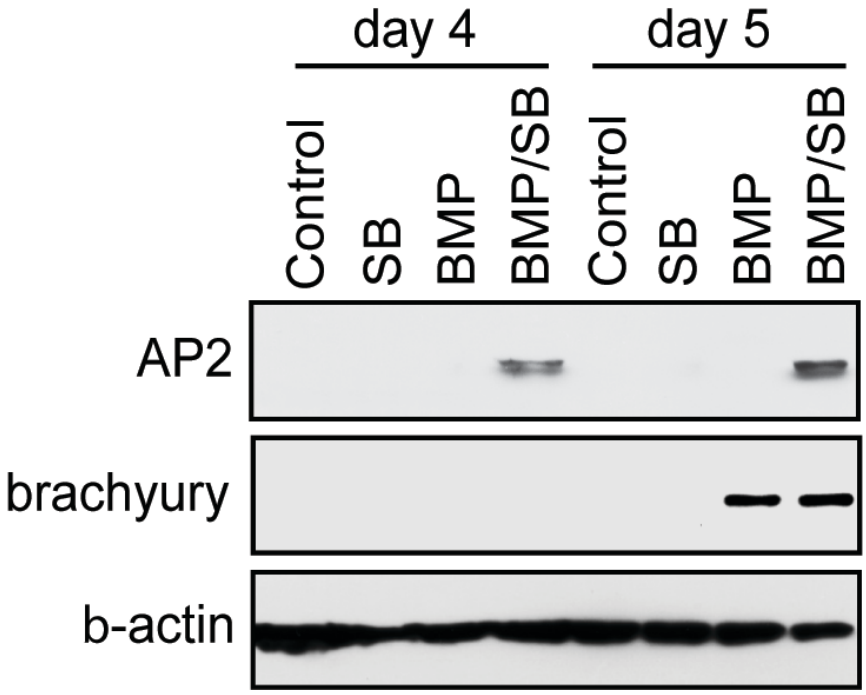

Figure 13: AP2 is only upregulated in BMP/SB treated aggregates.

Western blot analysis reveals that AP2 protein is only detectable in BMP/SB treated aggregates beginning on day 4 (i.e. 24 hours after treatment). Consistent with qPCR and immunostaining, brachyury is detectable on day 5 in both BMP and BMP/SB treated aggregates. ***Western blot data produced by Dharmeshkumar Patel***

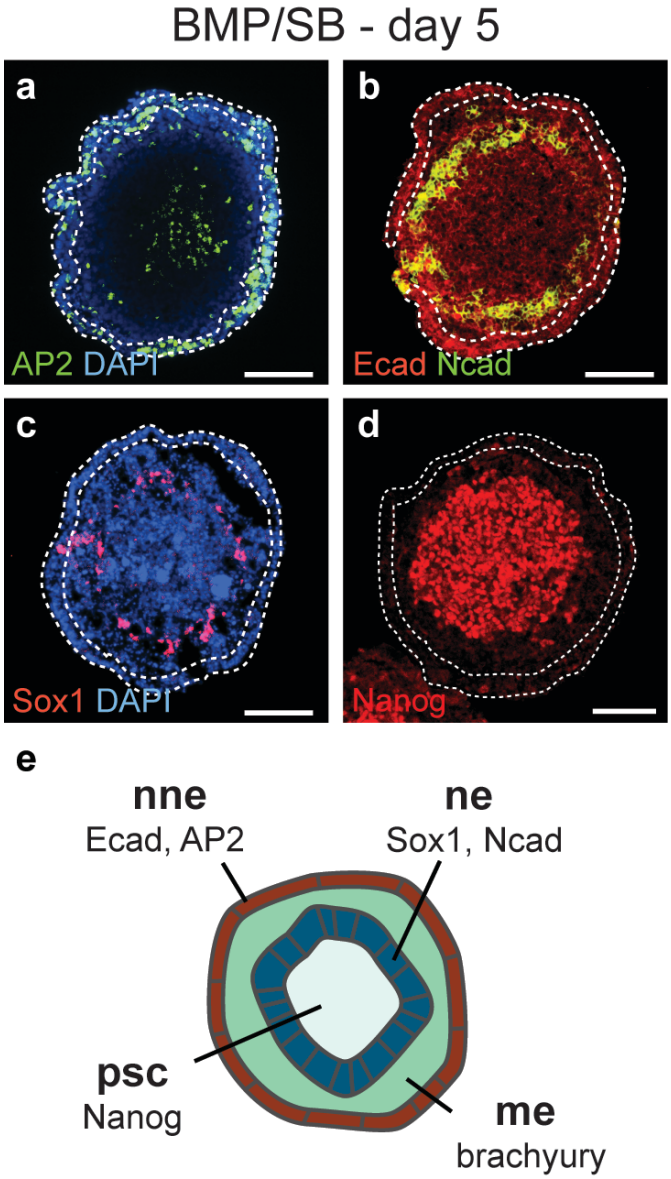

Figure 14: Lineage composition of BMP/SB treated aggreagates.

a-d, BMP/SB aggregates contain an outer AP2^{+} Ecad^{+} epithelium, an interior Sox1^{+} Ncad^{+} cell layer, and a core of Nanog^{+} cells. **e**, BMP/SB aggregate composition on day 5. ne, neuroectoderm. Scale bars, 100 μm.

In addition, the pluripotency marker Nanog was restricted to cells at the core of each aggregate (Figure 14). Altogether, these data strongly suggest that the outer-epithelium of day 5 BMP/SB-treated aggregates represents nonneural ectoderm, which surrounds an interior layer containing a mixture of mesendodermal and neuroectodermal tissues and a central core of uncommitted pluripotent cells (see Figure 14e for an illustration of BMP/SB aggregates). In support of this conclusion, the outer-epithelium of BMP/SB samples grown for 20 days without additional treatments developed into a Krt5/p63^{+} epithelium, mimicking the normal embryonic development of the epidermis from the nonneural ectoderm (Figure 15). Altogether, these results show that BMP/SB treatment is important for *in vitro* nonneural induction in floating stem cell aggregates. The later development of epidermal tissue denotes that stem cell-derived nonneural tissue has the same potential as *in vivo* potential. **Chapter 4** of this dissertation describes our investigation into whether epidermal induction can be suppressed in favor or a preplacodal fate to ultimately produce inner ear tissue.

This chapter is a modified version of work previously published in Nature and a manuscript in revision

Koehler, K. R., Mikosz, A. M., Molosh, A. I., Patel, D. & Hashino, E. Generation of inner ear sensory epithelia from pluripotent stem cells in 3D culture. *Nature* **500,** 217–221 (2013).

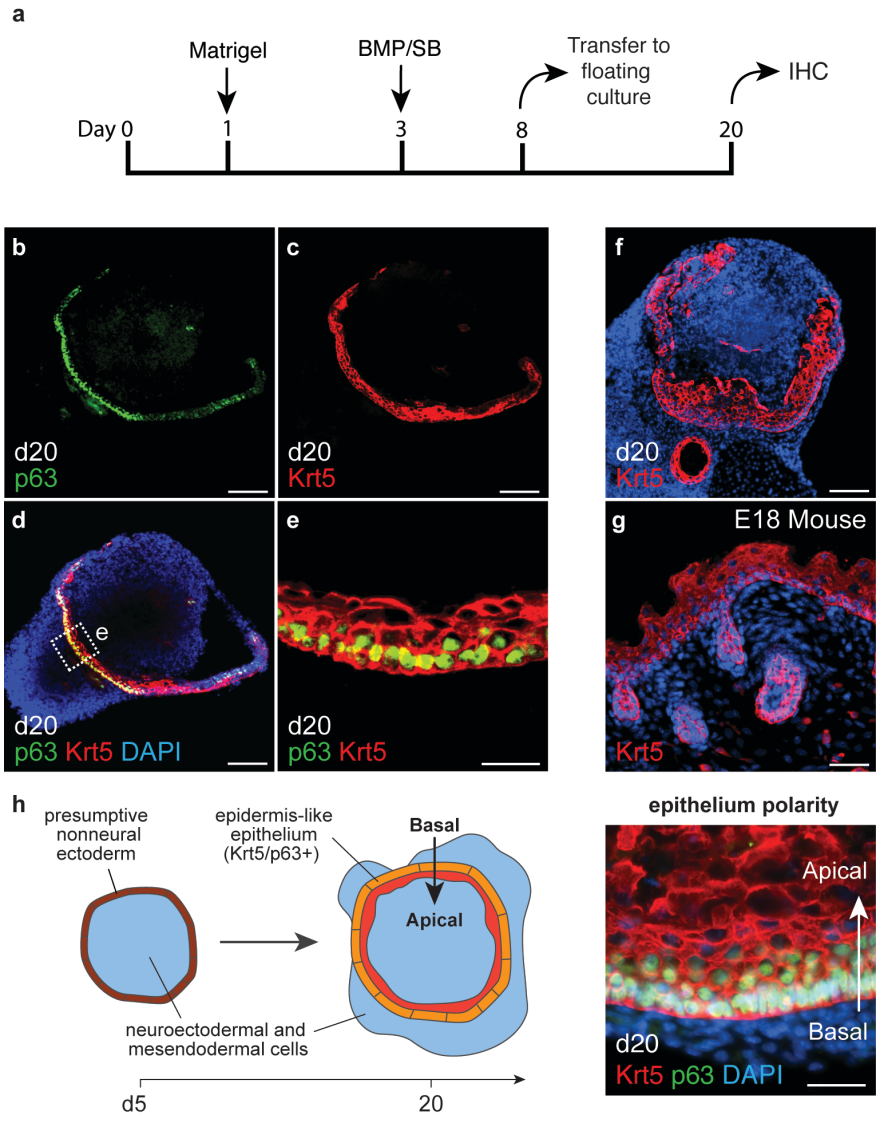

Figure 15: Epidermis-like epithelium in BMP/SB treated aggregates after 20 days in culture.

a, Following 8 days of differentiation in 96-well plates, BMP/SB aggregates were washed with N2 Medium and transferred to floating culture for self-guided development. **b-e**, A Krt5$^+$ p63$^+$ epithelium develops in BMP/SB aggregates cultured for 20 days. These results were confirmed in 3 separate experiments. **f, g**, The staining pattern and morphology of the Krt5$^+$ epithelium is consistent with epidermis on the surface of E18 mouse embryos. **h**, The basal to apical polarity of the epidermis is oriented toward the interior of the aggregate. These results are consistent with *in vivo* induction of epidermis from the nonneural ectoderm. Interestingly, BMP/SB treatment on day 3 appears to be necessary and sufficient to initiate self-organized induction of epidermis. No Krt5$^+$ p63$^+$ epithelium was observed in vehicle treated aggregates (data not shown). Scale bars, 100 μm (**b-c, f, g**), 25 μm (**e, h**).

CHAPTER 4: INDUCTION OF PREPLACODAL AND OTIC PLACODE EPITHELIUM FROM THE NONNEURAL EPITHELIUM

INTRODUCTION

Having established a nonneural induction culture system (see **Chapter 3**), we next investigated whether the nonneural epithelia could be steered toward a preplacodal fate. As previously mentioned, Suga et al. (2011) proved that adenohypophyseal placodes could be generated in 3D culture; however, the underlying mechanisms remained elusive. Specifically, it was unclear from their study, whether BMP inhibition was necessary for induction of a preplacodal epithelium prior to adenohypophyseal placode induction, which would be consistent with *in vivo* findings. Recall from **Chapter 1** that the preplacodal epithelium is a contiguous band of head ectoderm that arises from the nonneural ectoderm at the neural tube border and is the precursor to all of the cranial placodes (Figure 16; Grocott et al., 2012; Lleras-Forero and Streit, 2012). While BMP signaling is required for induction of nonneural ectoderm, recent studies suggest that subsequent BMP inhibition along with active fibroblast growth factor (FGF) signaling is necessary for nonneural cells to select a preplacodal over an epidermal fate (Kwon and Riley, 2009; Kwon et al., 2010; Pieper et al., 2012). Thus, we hypothesized that a properly timed treatment with a BMP inhibitor and/or FGF2 could promote the development of a preplacodal epithelium at the expense of epidermis in BMP/SB treated aggregates (Figure 17). In mice, the preplacode arises approximately 24-48 hours following nonneural specification; therefore, we speculated that BMP inhibition and/or FGF2 treatment 24-48 hours

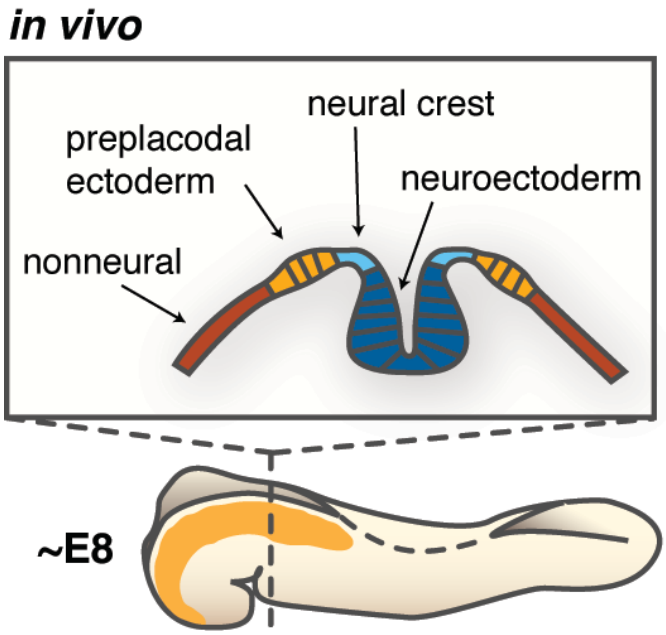

Figure 16: The location and timing of preplacodal induction *in vivo.*

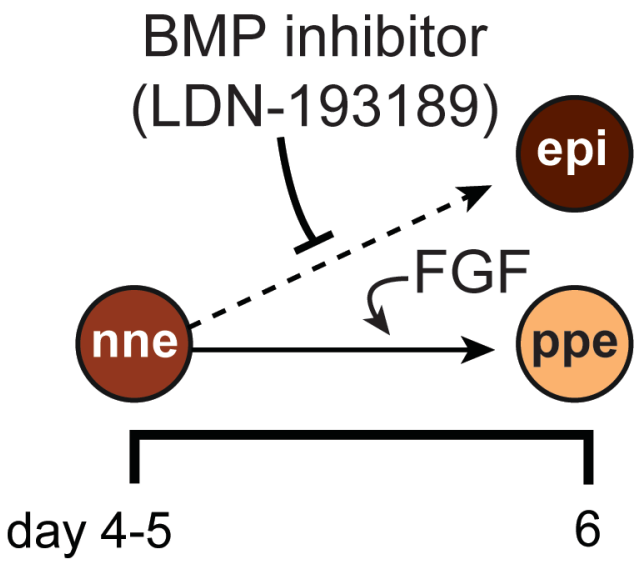

Figure 17: *In vitro* preplacodal induction strategy.

Once a nonneural fate is acquired a combination of BMP inhibition and FGF activation should steer a cell toward a preplacodal ectoderm fate. In our culture model nonneural identity is signified by AP2 expression on day 4; thus, BMP inhibition and FGF activation should take place at some point between days 4 and 5. Based on the normal timing of development, beyond day 5 (i.e. >48 hours after nonneural induction) an epidermal cell fate may be fixed and recalcitrant to reassignment. epi, epidermis; ppe, preplacodal ectoderm.

after BMP/SB treatment would be a suitable starting point for experimentation (Figure 17).

RESULTS

We began treating BMP/SB aggregates with various combinations of the specific BMP inhibitor, LDN-193189 (hereafter, LDN) and FGF2 (Figure 17). We found that BMP/SB aggregates treated with LDN on day 4.5 maintained expression of *Dlx3*, which indicated that BMP inhibition after nonneural ectoderm induction does not reverse nonneural fate specification (Figure 18). In the embryo, the epithelium of the preplacodal ectoderm is characterized by a thickened morphology relative to the surrounding surface ectoderm (Grocott et al., 2012; Lleras-Forero and Streit, 2012; Schlosser, 2006). Thus, we examined the thickness of epithelia in BMP/SB-LDN samples and found thickened epithelial patches that were not present in BMP/SB epithelia (Figure 19). As observed *in vivo*, this morphological change appeared to be dependent on endogenous FGFs, as inhibition of FGF signaling by the small molecule SU5402 abolished epithelial thickening (Figure 20). Similarly, a combined treatment of recombinant FGF2 and LDN (hereafter, BMP/SB-FGF/LDN) caused significant thickening of the $AP2^{+}$ epithelium relative to epithelia in BMP/SB treated aggregates (Figure 21 and 22). The outer-epithelium of BMP/SB-FGF/LDN aggregates co-expressed $Gata3^{+}$ $Six1^{+}$ $AP2^{+}$, mimicking the embryonic preplacodal epithelium (Figure 23). These and the following data strongly suggest that the outer-epithelium of BMP/SB-FGF/LDN-treated aggregates is representative of preplacodal ectoderm.

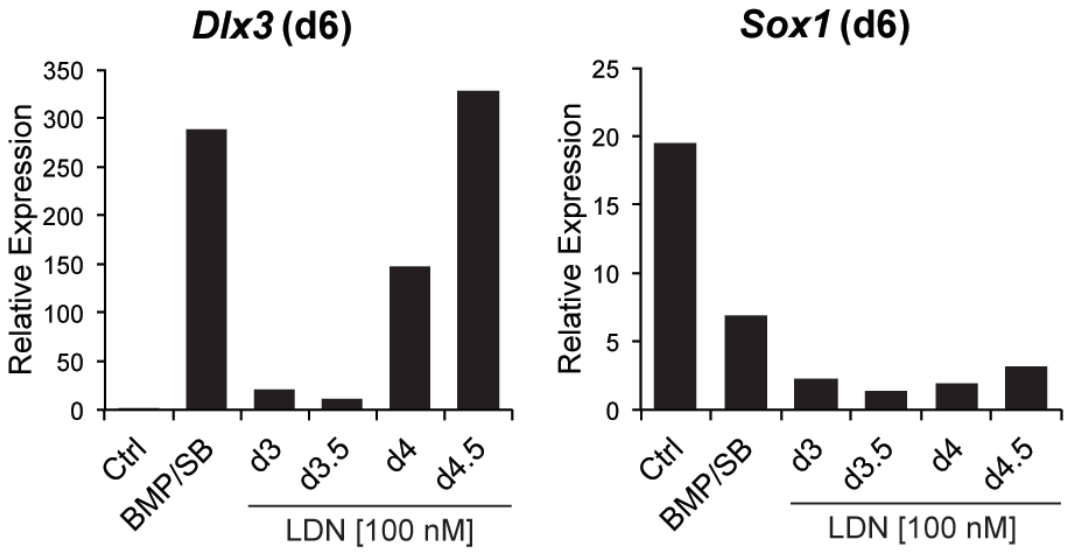

Figure 18: *Dlx3* and *Sox1* gene expression following LDN treatment on various days.

LDN treatment does not appear to induce *Sox1* expression, but suppresses *Dlx3* expression if treatment occurs on or before day 4 (data are representative of 2 separate experiments).

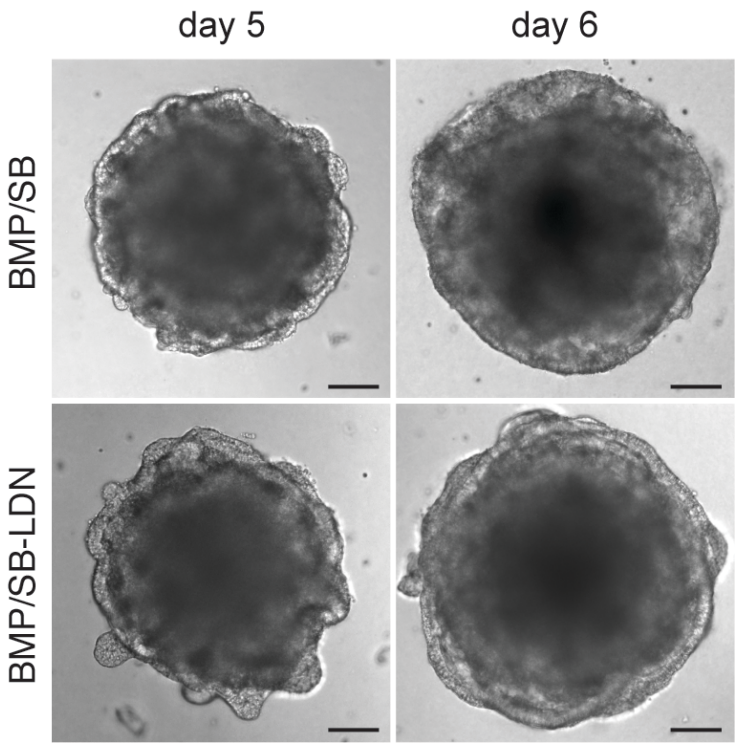

Figure 19: Morphological changes occur following BMP/SB-LDN treatment on days 5 and 6.

Note that the apparent thickness of the outer-epithelium of BMP/SB-LDN aggregates is greater than BMP/SB treated aggregates. Scale bars, 100 μm.

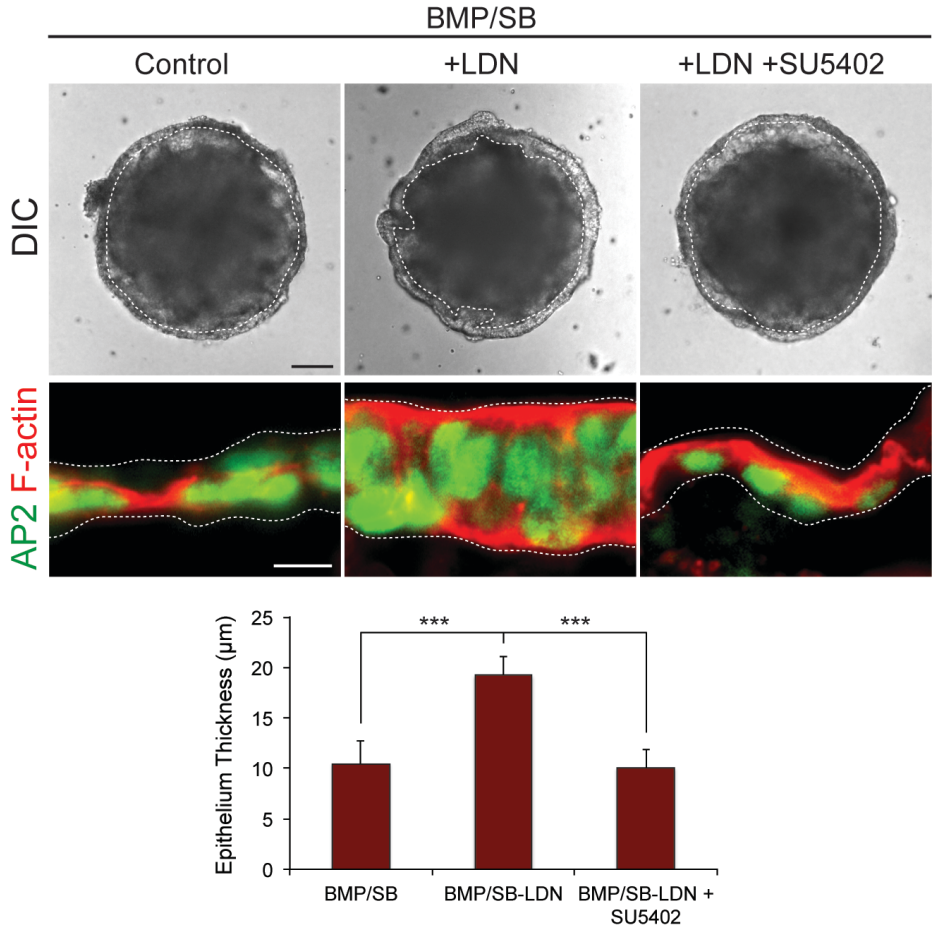

Figure 20: Outer epithelial thickening following LDN treatment is FGF-dependent.

Inhibition of FGF using SU5402, abolishes epithelial thickening following BMP/SB-LDN treatment (n = 9 aggregates, 3 separate experiments, ***P < 0.001). AP2 expression, however, is still found in the outer epithelium following SU5402 treatment. Scale bars, 100 µm (top panels) and 10 µm (middle panels).

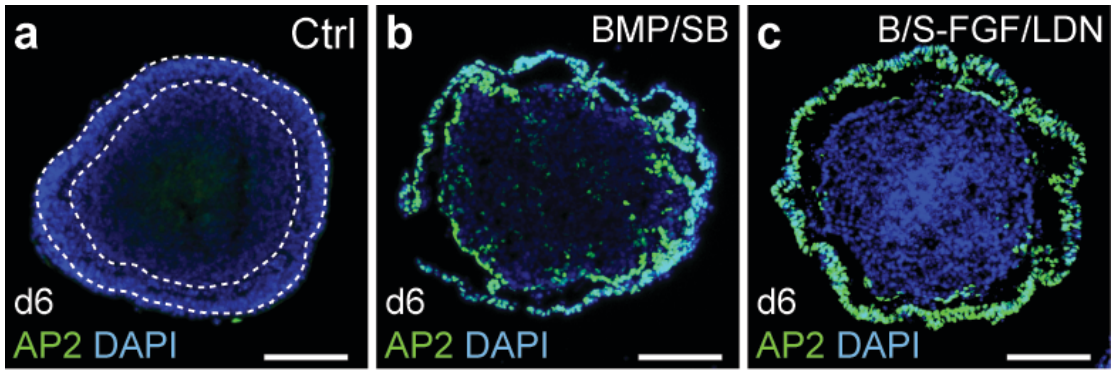

Figure 21: AP2 expression in the outer-epithelium of BMP/SB and BMP/SB-FGF/LDN treated aggregates.

a-c, On day 6, AP2 is expressed in both BMP/SB and BMP/SB-FGF/LDN samples. BMP/SB-FGF/LDN aggregates are distinguished by a thickened epithelium relative to BMP/SB aggregates. Scale bars, 100 μm.

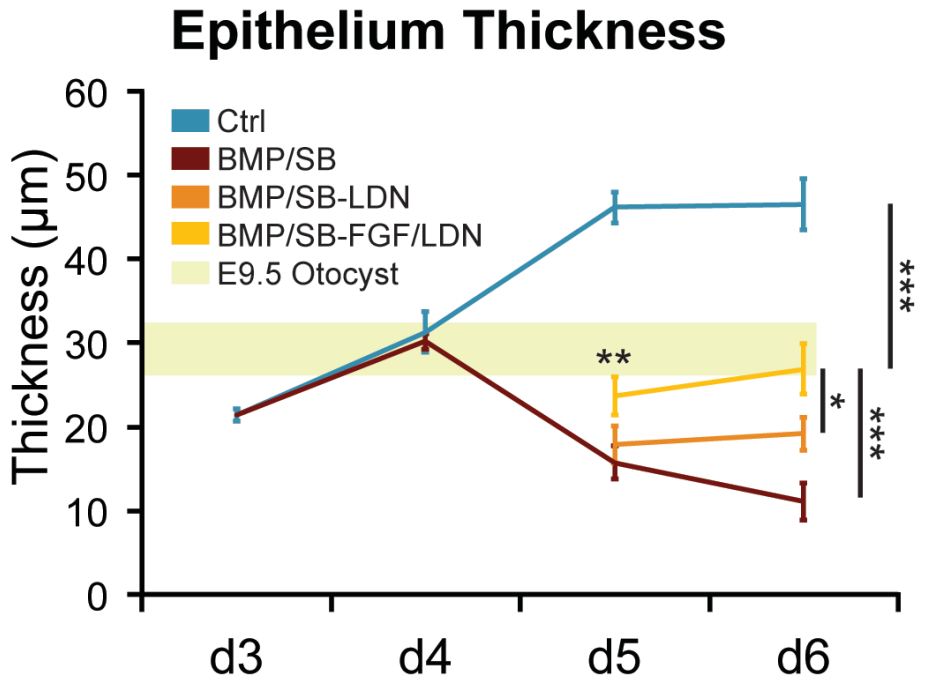

Figure 22: Outer-epithelial thickness over time in culture.

The apparent thicknesses of Control, BMP/SB, BMP/SB-LDN and BMP/SB-FGF/LDN epithelia on days 3-6. For comparison, the apparent thickness of the E9.5 otic vesicle is superimposed. Data represent 15-20 aggregates from 3-4 separate experiments and 6 otocysts from 3 embryos (mean ± s.e.m.). A one-way ANOVA was used to determine significant differences between groups (*$P < 0.05$, **$P < 0.01$, ***$P < 0.001$). On day 5, BMP/SB-FGF/LDN was significantly different from all other groups.

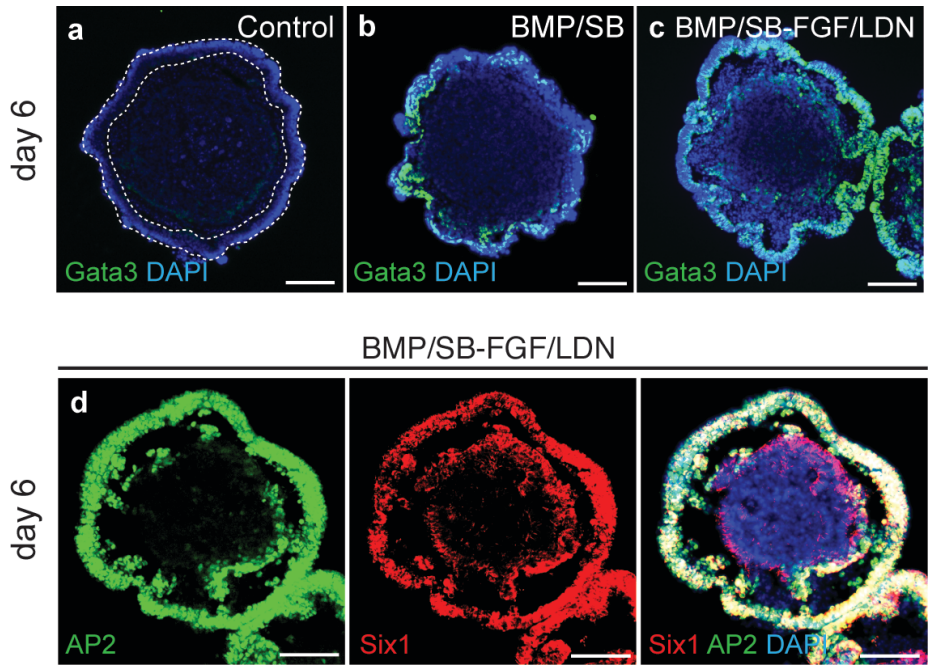

Figure 23: Gata3 and Six1 expression in the outer-epithelium of BMP/SB-FGF/LDN treated aggregates.

a-c, Gata3 was detected in the outer epithelium of BMP/SB and BMP/SB-FGF/LDN treated aggregates. **d**, The outer-epithelium of BMP/SB-FGF/LDN aggregates co-expressed AP2 and Six1. Scale bars, 100 μm.

In vertebrates, the otic placode is derived from a posterior preplacodal region known as the otic-epibranchial placode domain (OEPD; Figure 24). The otic placode is demarcated from other developing placodes by expression of the transcription factors Pax8 (Figure 24 and 25; Ladher et al., 2010). We next examined whether the thickened preplacode-like epithelium observed following BMP/SB-FGF/LDN treatment expressed OEPD associated markers. Our qPCR analysis revealed that *Pax8* and the otic-specific marker *Pax2* were significantly upregulated in BMP/SB-FGF/LDN samples compared to other conditions (Figure 26). *Pax8* expression appeared to be dependent on the concentration of FGF2 in the medium (Figure 27). By day 6, we observed $Pax8^+$ cells distributed in placode-like patches throughout the outer $AP2^+$ $Ecad^+$ epithelium of BMP/SB-FGF/LDN aggregates (Figure 28). Notably, we also observed a population of $Pax8^+$ $TuJ1^+$ $Ncad^+$ $Ecad^-$ cells in the interior of each aggregate, suggesting formation of mid-hindbrain in this region (Figure 29). The percentage of $Pax8^+$ $Ecad^+$ epithelium markedly increased between days 6 and 8 (Figure 30) and the $Pax8^+$ $Ecad^+$ epithelium bore a striking morphological resemblance to the developing otic placode (Figure 25). Pax8 expression was only observed in BMP/SB-FGF/LDN treated aggregates that received FGF/LDN treatment between days 4 and 5 (Figure 30). Of note, we did not observe expression of Pax3 or Pax6 in the outer epithelium, ruling out the development of other cranial placodes (Figure 31). Moreover, the population of $Nanog^+$ pluripotent cells appeared to diminish over time in culture (Figure 32).

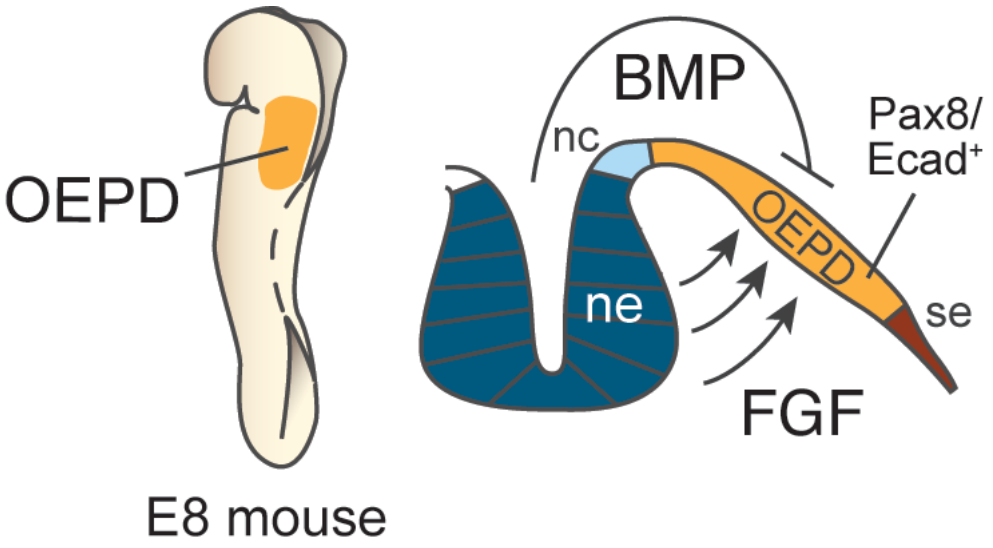

Figure 24: Mechanism and location of OEPD induction in vivo.

The otic-epibranchial placode domain (OEPD) is approximately located in the yellow shaded region on an E8 mouse embryo. The OEPD expresses Pax8 and E-cadherin. FGF signaling from the underlying mesenchyme and neural tube are thought to work synergistically with BMP antagonists to induce the preplacodal ectoderm and the OEPD. ne, neural ectoderm; nc, neural crest; se, surface ectoderm.

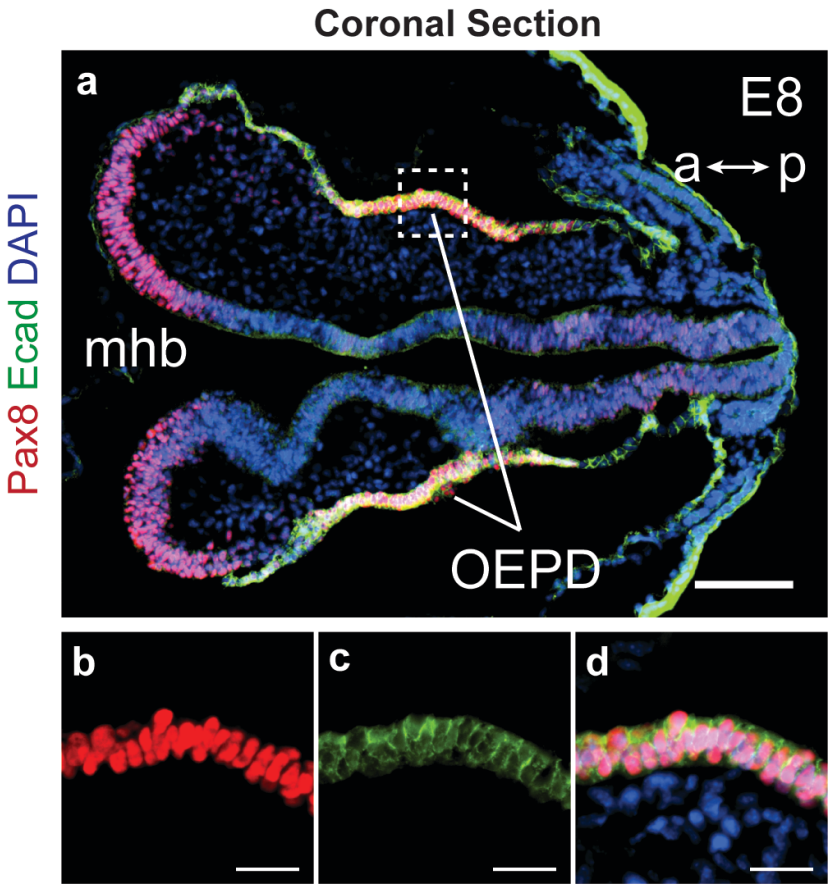

Figure 25: OEPD in an E8 embryo.

a-d, At E8, Pax8 and Ecad expression in the surface ectoderm marks the otic-epibranchial placode domain (OEPD). Pax8 expression is also detected in the mid-hindbrain region of the neuroepithelium (mhb). a, anterior; p, posterior. Scale bars, 100 (**a**), 25 (**b-d**) μm.

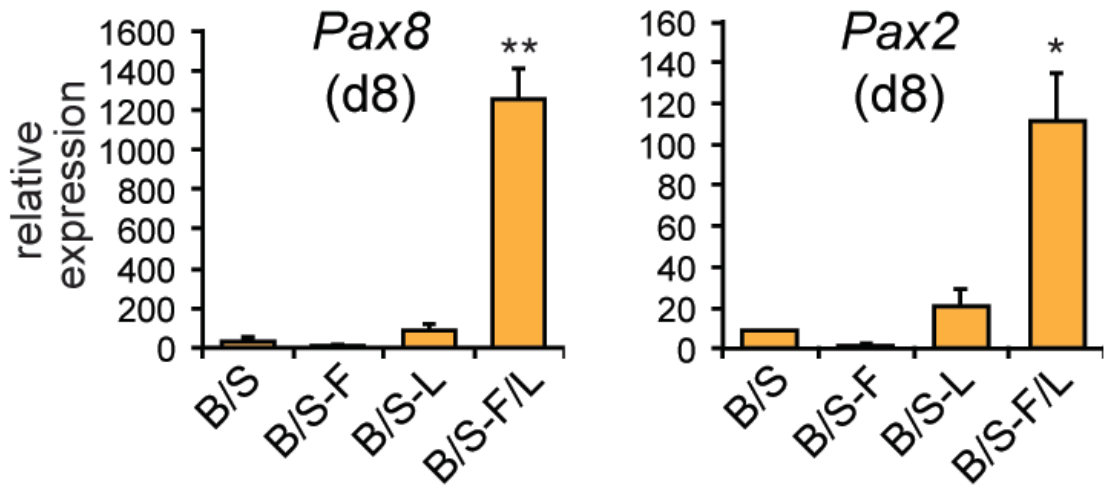

Figure 26: *Pax8* and *Pax2* gene expression on day 8 of differentiation.

Relative *Pax8* and *Pax2* mRNA expression on day 8 of differentiation (n = 3–4; *P < 0.05, **P < 0.01; mean ± s.e.m.). B, BMP4; S, SB413542; F, FGF2; L, LDN193189.

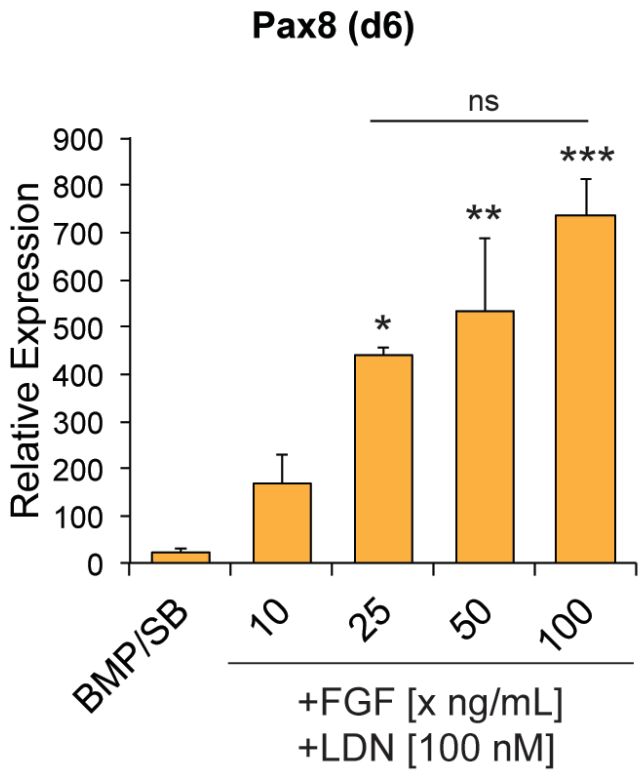

Figure 27: FGF2 induces *Pax8* gene expression in a dose-dependent manner.

qPCR analysis shows that relative *Pax8* expression is dependent on FGF dosage. FGF dosages >25 ng ml^{-1} showed an upward trend in *Pax8* expression, however, differences between 25, 50 and 100 ng ml^{-1} were not significant using a one-way ANOVA with Tukey's post hoc test for multiple comparisons. 25 ng ml^{-1} was chosen as the appropriate dosage for all subsequent experimentation (n = 4, *P < 0.05, **P < 0.01, ***P < 0.001; mean ± s.e.m.).

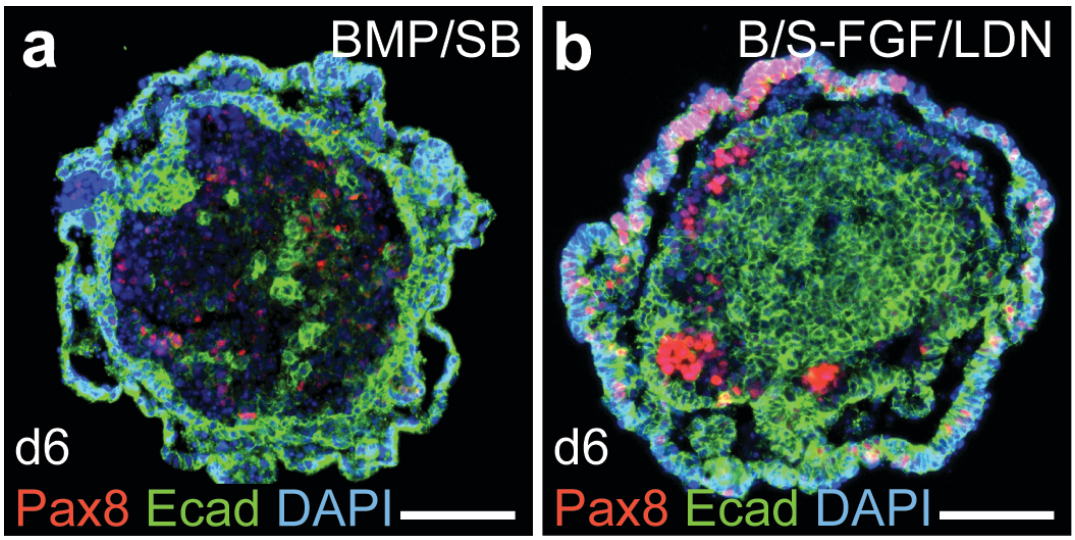

Figure 28: Pax8 and Ecad expression in the outer epithelium.

a, **b**, Representative images of Pax8 and E-cadherin (Ecad) expression in (**a**) BMP/SB aggregates and (**b**) BMP/SB-FGF/LDN aggregates on days 6. Scale bars, 100 μm.

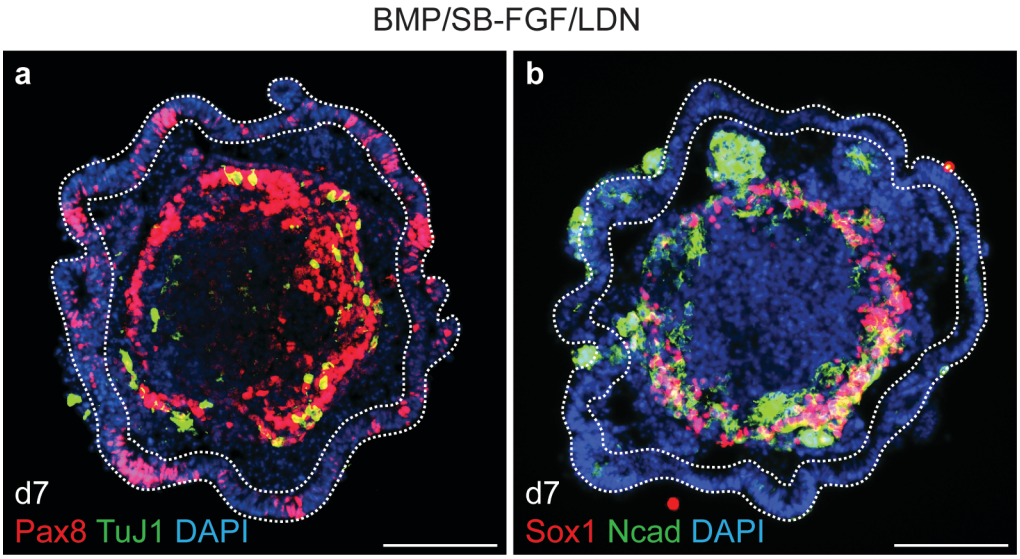

Figure 29: Hindbrain-like neural induction in BMP/SB-FGF/LDN treated aggregates.

a, b, An interior layer of Pax8 and Sox1^{+} Ncad^{+} cells develops in BMP/SB-FGF/LDN aggregates. This expression pattern is consistent with developing mid-hindbrain tissue. βIII-tubulin (Tuj1; shown)$^{+}$ neurons developed within this region, confirming a neural identity. Scale bars, 100 μm.

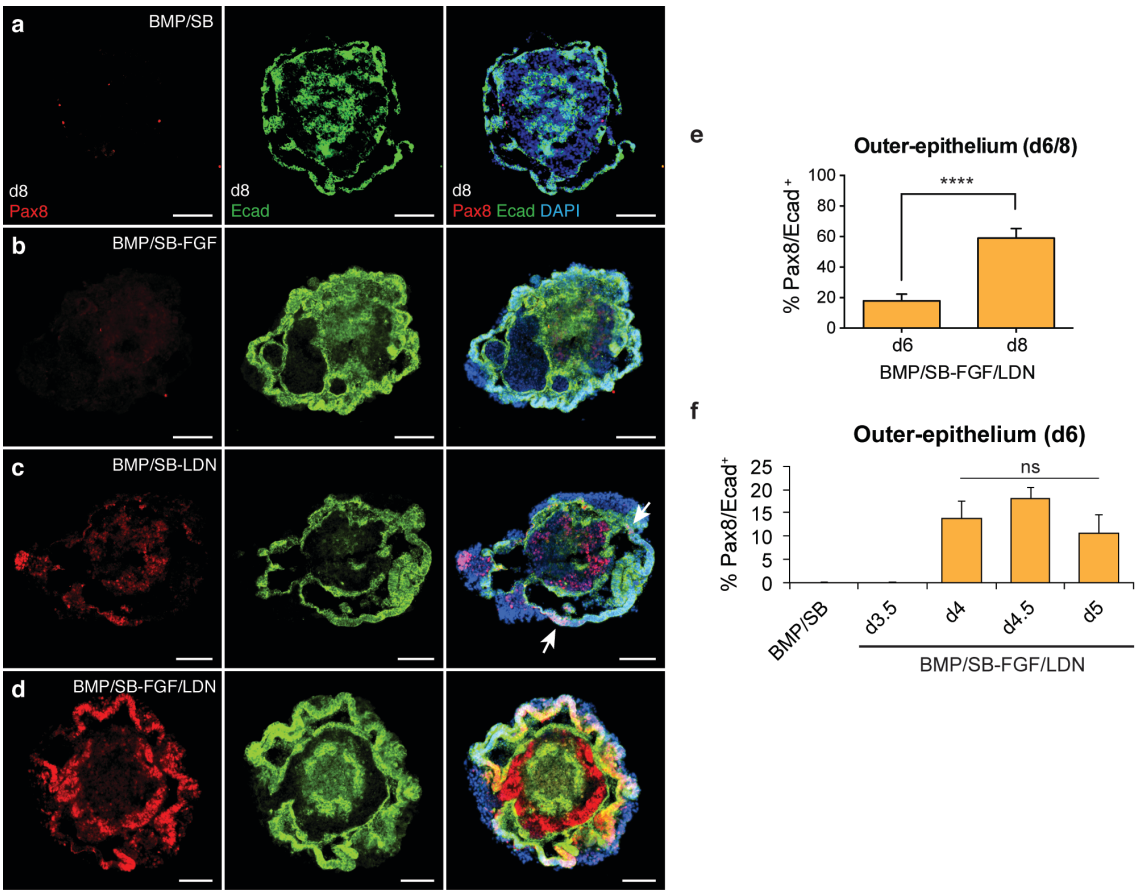

Figure 30: Sufficiency and proper timing of FGF/LDN treatment for Pax8 induction.

a-d, Representative immunostaining for Pax8 and Ecad on day 8 of differentiation. For BMP/SB-LDN treated aggregates arrows identify the patches of Pax8$^+$ Ecad$^+$ cells. We conclude from these results that the combined treatment of FGF/LDN or, potentially, LDN combined with endogenous FGFs is sufficient to induce Pax8$^+$ Ecad$^+$ epithelium. **e**, Percentage of Ecad$^+$ epithelium expressing Pax8 on day 6 and 8 (n = 9 aggregates, 3 separate experiments, ****P < 0.0001, mean ± s.e.m.). For these experiments FGF/LDN treatment was performed on day 4.5. ns, not significant. Scale bars, 100 μm.

f, FGF/LDN treatment only generated Pax8$^+$ Ecad$^+$ epithelium following treatment on days 4-5. FGF/LDN treatment after d5 did not result in epithelial thickening (data not shown). The graph shows quantification of the average percentage of Pax8$^+$ Ecad$^+$ epithelium on day 6 (n = 12 aggregates, 4 separate experiments; mean ± s.d.).

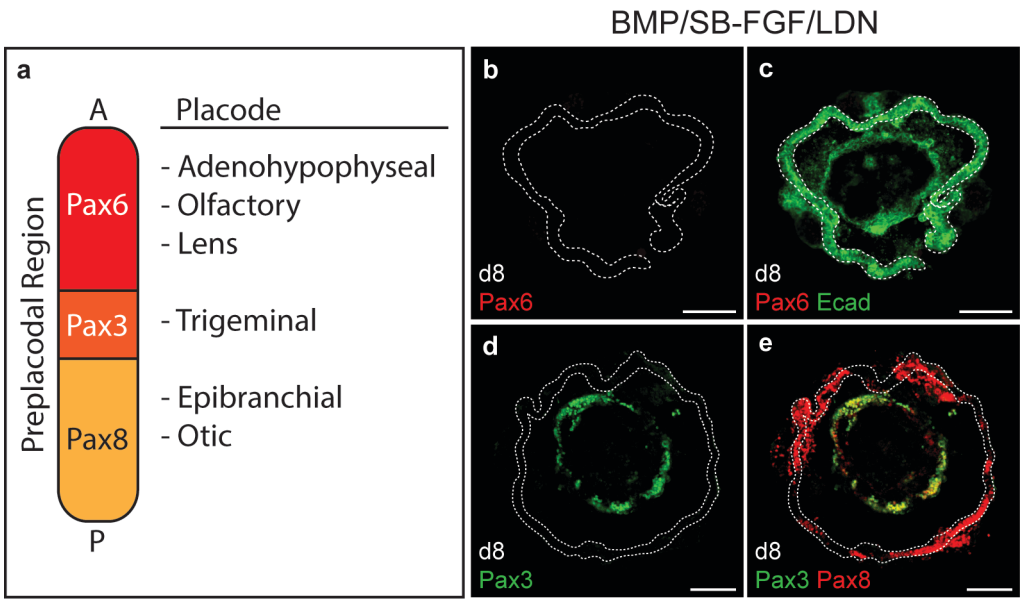

Figure 31: Absence of other cranial placode markers.

a, In the preplacodal region of the embryo, Pax6 expression delineates the anterior placodes (i.e. the adenohypophyseal, olfactory and lens placodes), whereas Pax3 is expressed in the trigeminal placode. **b**, **c**, Pax6 is not expressed in day 8 BMP/SB-FGF/LDN treated aggregates. **d**, **e**, Pax3 is expressed in $Pax8^{+}$ cells located in the interior layer, however, no Pax3 expression was observed in the outer-epithelium. Scale bars, 100 μm.

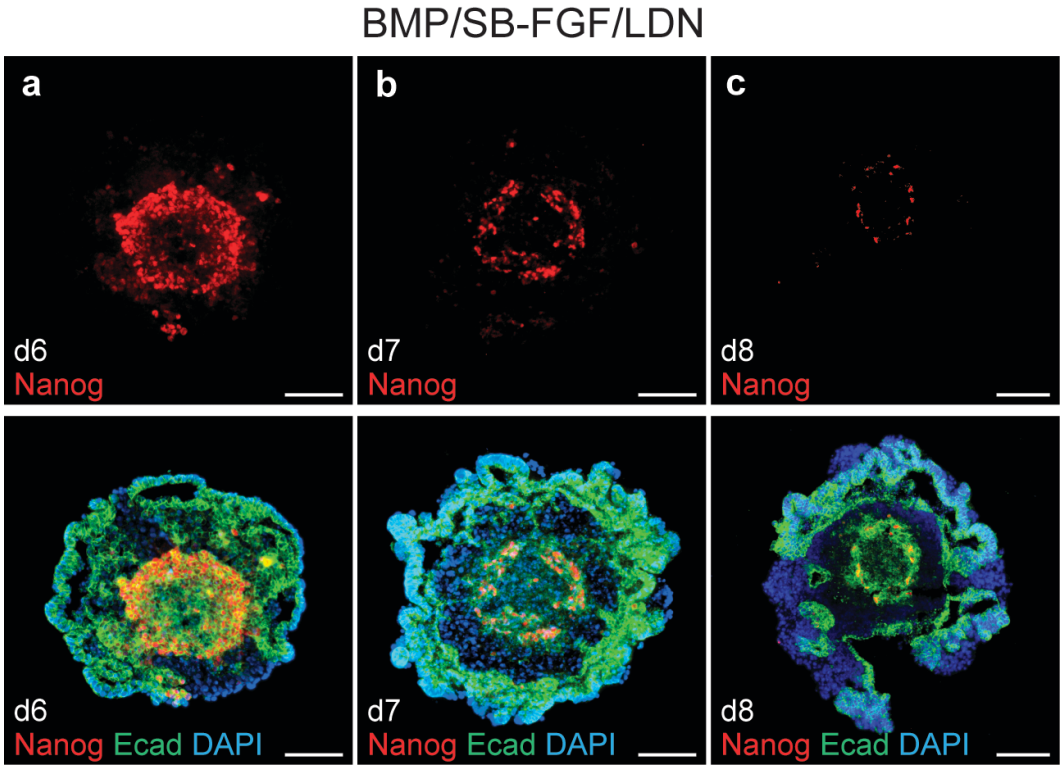

Figure 32: Loss of pluripotent cells over time in BMP/SB-FGF/LDN treated aggregates.

a-c, Representative images showing that the population of Nanog$^+$ (i.e. presumptive pluripotent cells) diminishes over time in culture—days 6, 7, and 8. Scale bars, 100 μm.

Taken together, these findings show that FGF/LDN treatment is critically important for OEPD induction and that treatment is most effective when performed between days 4 and 5 in our model system. The increased relative expression of *Pax2* also suggests that otic placode development may take place following BMP/SB-FGF/LDN treatment. **Chapter 5** of this dissertation describes our investigation into whether an otic placode-like epithelium can be generated from the putative OPED epithelium.

This chapter was modified from work previously published in Nature and a manuscript in revision

Koehler, K. R., Mikosz, A. M., Molosh, A. I., Patel, D. & Hashino, E. Generation of inner ear sensory epithelia from pluripotent stem cells in 3D culture. *Nature* **500,** 217–221 (2013).

CHAPTER 5: SELF-ORGANIZED FORMATION OF INNER EAR TISSUE: SENSORY NEURONS AND HAIR CELLS

INTRODUCTION

The proper development of organs requires the synchronized organization and coordinated differentiation of large cell populations. To date, a full appreciation of the chemical and mechanical signaling methods that govern cellular behaviors and cell fate decisions remains elusive. Nonetheless, culturing ES cells as a floating cell aggregate in 3D culture has emerged as an effective method to generate complex organs *in vitro*; thus, a complete knowledge of the underlying mechanisms is not necessary to recreate organogenesis *in vitro* (Sasai, 2013a; Sasai et al., 2012). Presently, mouse and human cortical tissue, neural retina, intestinal epithelia, liver buds, spermatozoa, and anterior pituitary gland tissue have been generated in 3D culture from PS cells (Eiraku and Sasai, 2012; Eiraku et al., 2008; 2011; Gonzalez-Cordero et al., 2013; Koehler et al., 2013; McCracken et al., 2011; Nakano et al., 2012; Nasu et al., 2012; Spence et al., 2010; Suga et al., 2011). Moreover, in a 3D culture variant using tissue specific stem cells, the villi of the small intestine and liver tissue can be reconstituted from a single cell (Huch et al., 2013; Sato et al., 2009). A common theme that unifies all of these approaches is that the differentiating cells are granted the freedom to self-organize into epithelia. The epithelia typically assemble into larger structures that are nearly identical in organization to the functional units of *in vivo* organs; therefore, the stem cell-derived structures are often denoted as 'organoids.' In a 2D culture, by contrast, the cells adhere to a culture plate; thus, they are restricted to conform to a flat shape. In

essence, the 3D environment allows cells to develop more naturally, as they would in the embryo.

In **Chapters 3 and 4** we showed that by faithfully recapitulating *in vivo* development with precise temporal control of BMP, TGFβ and FGF signaling, ES cell aggregates transform sequentially into nonneural, preplacodal and OEPD-like epithelia. During embryonic inner ear development, an otic placode arises and invaginates from within the OEPD to form the otic vesicle. We hypothesized that the OEPD-like epithelium in BMP/SB-FGF/LDN aggregates would produce otic placodes and vesicles if we provided the proper culture environment. Drawing on previous 3D culture studies, we hypothesized that placing the OEPD-induced aggregates in a minimal medium for an extended amount of time (e.g. 5-10 days) would initiate self-organized development of otic tissue. Remarkably, vesicles containing prosensory cells emerge from the presumptive OPED epithelium and give rise to hair cells bearing stereocilia bundles and a kinocilium following 14-20 days of culture. Moreover, we demonstrate how these vesicles are structurally and biochemically comparable to developing vestibular end organs (i.e. the utricle and saccule). Our data thus establish a novel 'inner ear organoid' culture that can be used to gain deeper insight into inner ear development and disorder.

RESULTS

The prosensory domain of the otic placode (otic vesicle at later stages) gives rise to the vestibular/cochlear sensory epithelia and inner ear sensory neurons. To initially assess whether otic induction occurred in our cultures we looked for a

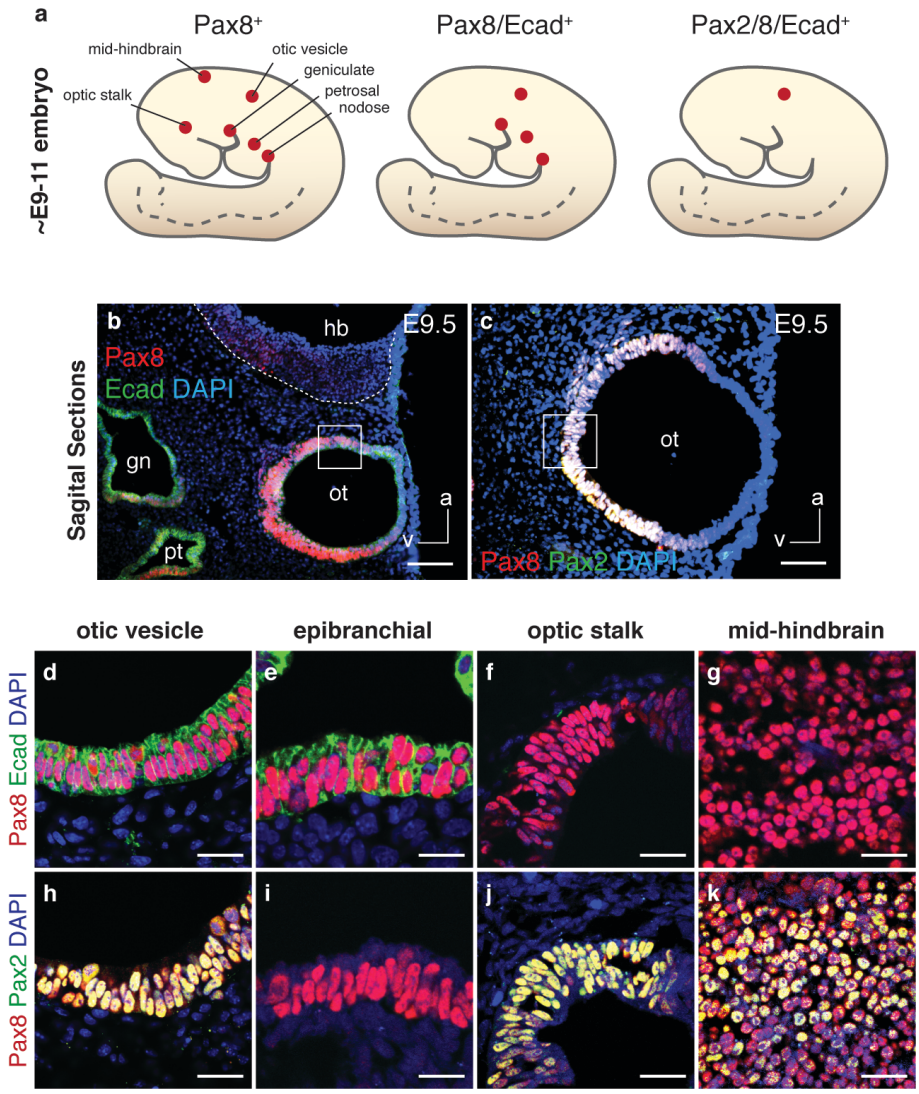

Figure 33: Markers that identify otic vesicle in the embryo.

a-k, The well-established otic markers Pax2 and Pax8 are not unique to the inner ear during development. On E9.5 Pax2 and Pax8 expression co-localizes in the optic stalk, mid-hindbrain and kidney as well as the otic vesicle. We found that the combination of Pax2, Pax8 and Ecad provides a unique signature of otic placode or vesicle fate. At ~E9-11, Pax8 is expressed in the otic vesicle, epibranchial placodes (i.e. geniculate, petrosal and nodose), optic stalk, and mid-hindbrain. Pax8 and Ecad expression is restricted to the otic vesicle and epibranchial placodes. Pax2, Pax8 and Ecad expression is restricted to the otic vesicle (**d, h**). a, anterior; v, ventral. Scale bars, 100 μm (**b, c**), 25 μm (**d-k**).

combination of otic prosensory markers, Pax2, Pax8, Ecad, and Sox2, seen during normal development (Figure 33). On day 8 of differentiation, BMP/SB-FGF/LDN aggregates were transferred to a serum-free floating culture to allow self-guided differentiation. Approximately 24 hours after transfer, the interior cell mass of each aggregate breached the outer-epithelium and formed a heterogeneous cell layer on the exterior of the aggregate (253 aggregates analyzed, 4 separate experiments; Figure 34). This indicates that the outer-epithelium transitions to an inner-epithelium lining the core of each aggregate. During days 9-12 we observed the continuous invagination of vesicles containing Pax2/Ecad, Pax2/8, and Sox2/Pax8^{+} cells from the presumptive OEPD epithelium into the exterior cell layer (Figure 35 and 36), which resulted in ~20-28 Pax2/8/Sox2^{+} vesicles per aggregate (Figure 37). We hypothesized that endogenous Wnt signaling may underlie induction of vesicles bearing otic prosensory markers in our culture because Wnt signaling is necessary for otic placode formation *in vivo*. Confirming this hypothesis, treatment of aggregates with the Wnt inhibitor XAV939 from day 8-10 significantly decreased the number of prosensory vesicles and, specifically, reduced the prevalence of Pax2^{+} vesicles (n=4; Figure 37). These data indicate that endogenous Wnt signaling induces formation of otic vesicles from the presumptive otic placode using similar mechanisms as observed *in vivo*. Interestingly, the remaining inner-epithelium developed into Keratin 5 (Krt5)$^{+}$ p63^{+} epidermis (Figure 38). The basal (p63^{+}) layer of the inner-epithelium was oriented so that the apical surface of the epithelium was facing the interior of the aggregate; thus, the process of vesicle

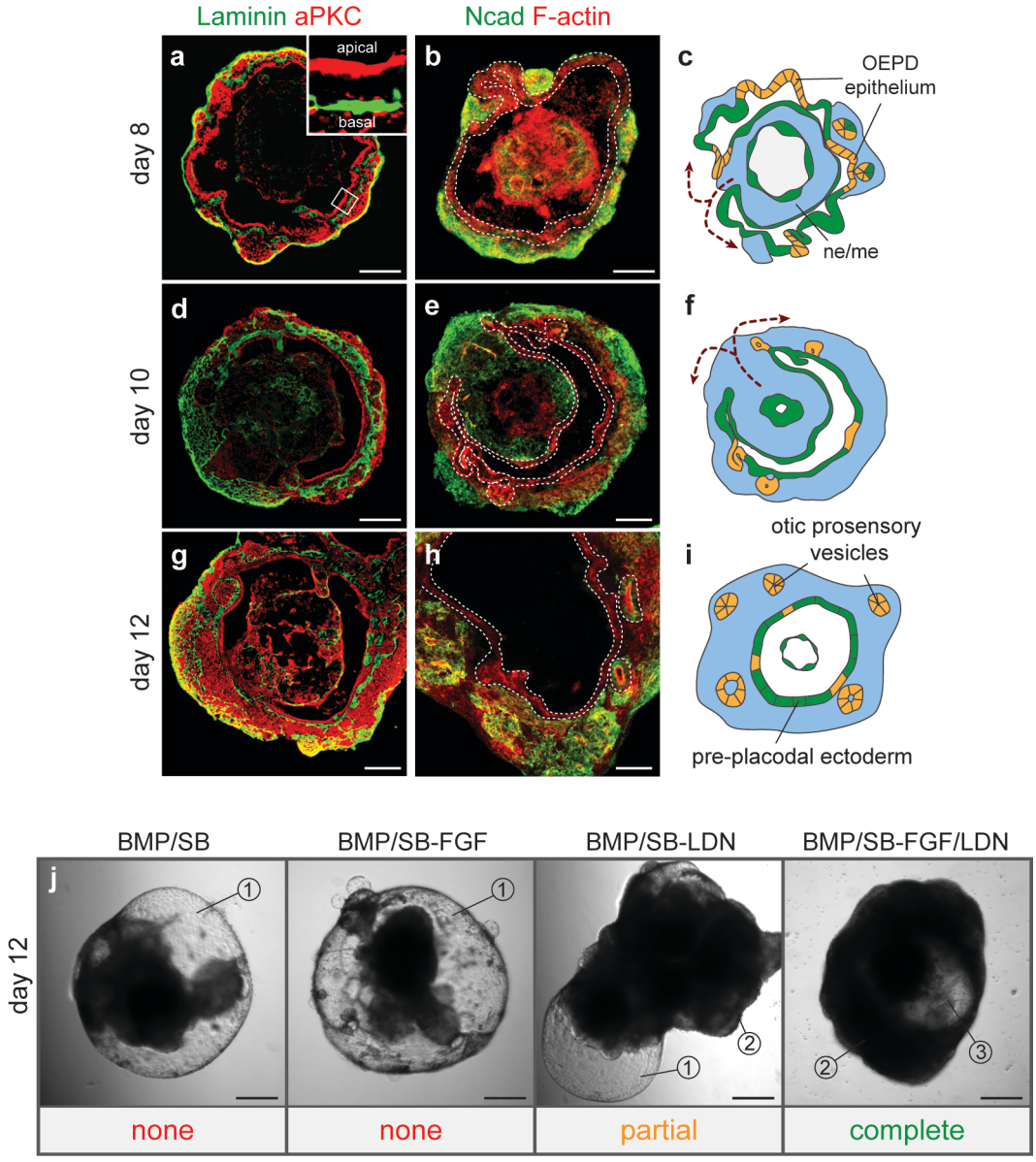

Figure 34: Cellular re-organization in BMP/SB-FGF/LDN treated aggregates.

a-i, To elucidate the process of cellular re-organization during days 8-12, aggregates were stained for basal (laminin) and apical (atypical protein kinase C; aPKC) polarity markers (**a, d, g**). Note that the basal surface of the epithelium remains oriented toward the outside of the aggregate as the inner cell mass relocates to the out surface of the aggregate. Ncad (a marker for both neuroectoderm, mesoderm and the otic vesicle *in vivo*) labeled most cells in the inner cell mass and helps visualize the topographical change (**b, e, h**) depicted in **c**, **f** and **l**. F-actin staining was used to identify the epithelium. Presumptive otic vesicles (dotted outline in **h**) express Ncad. **j**, Representative DIC images of aggregates on day 12 could be

assessed for cellular re-organization based on morphology. Note the translucent epithelium found in all conditions except BMP/SB-FGF/LDN treated samples. (1) This translucent epithelium is indicative of incomplete or partial re-organization. (2) An opaque outer cell mass was indicative of partial or complete re-organization. (3) Fully re-organized aggregates display a hallow core that is clearly visible through the aggregate surface (images are representative of ~90-95% of aggregates for each condition; 4 experiments). Scale bars, 250 μm (**j**), 100 μm (**a-i**).

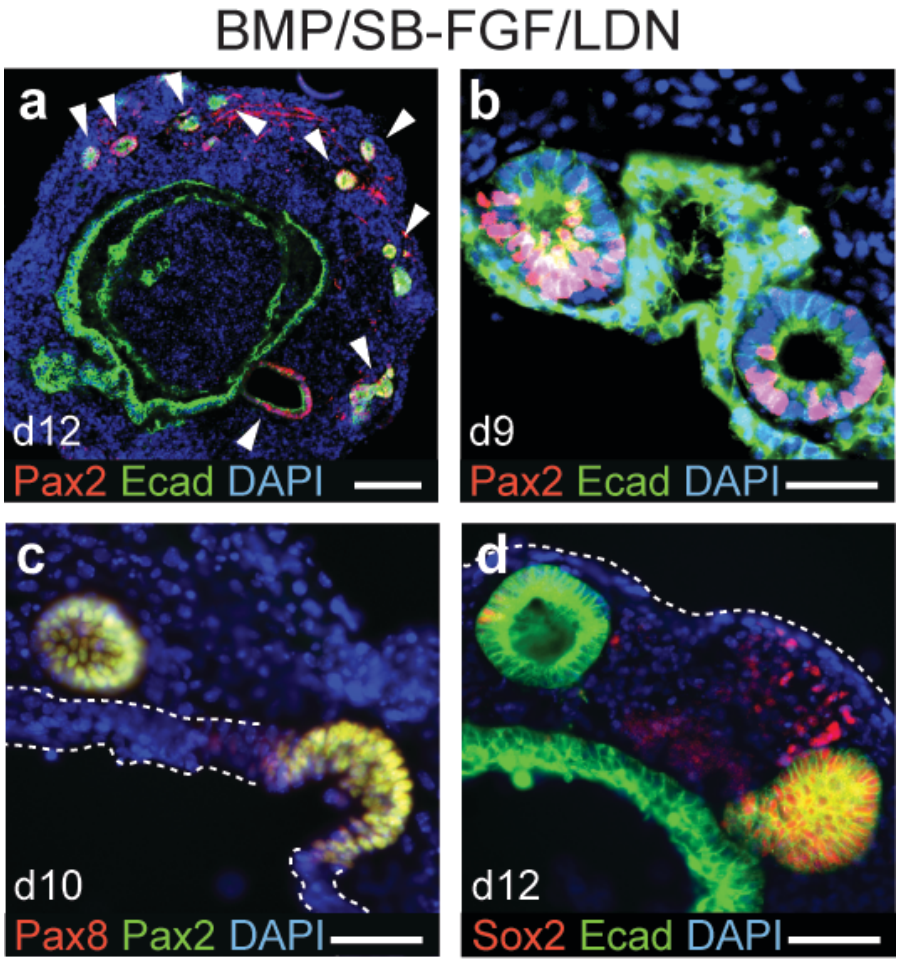

Figure 35: Otic vesicle formation in BMP/SB-FGF/LDN treated aggregates.

a, Day 12 BMP/SB-FGF/LDN aggregate with Pax2⁺ Ecad⁺ vesicles (arrowheads). **b–d**, Pax2⁺ Ecad⁺ (**b**), Pax2⁺ Pax8⁺ (**c**) and Ecad⁺ Sox2⁺ (**d**) vesicles invaginate from the inner epithelium from days 9–12. Scale bars, 100 μm (**a**), 50 μm (**b–d**).

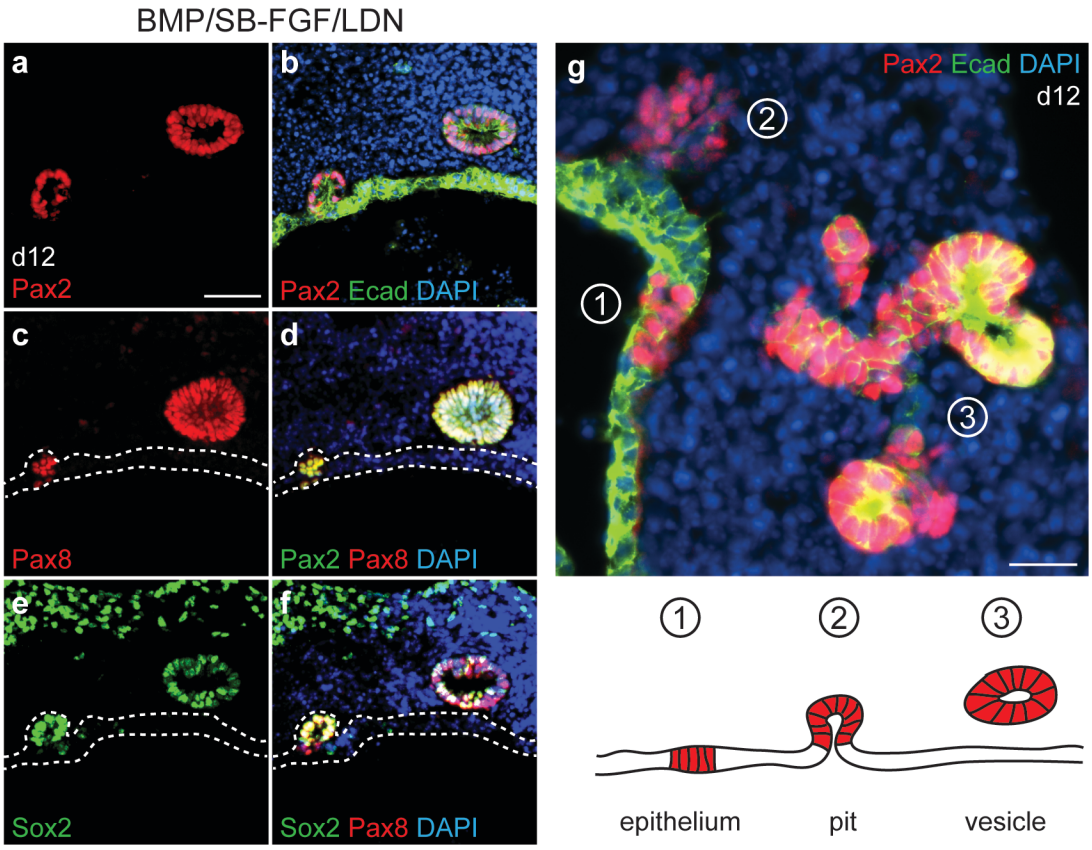

Figure 36: Prosensory otic vesicles emerge from the epithelium.

a-f, Serial sections show co-expression of Pax2, Pax8, Ecad, and Sox2 in vesicles, indicating an inner ear prosensory fate. **g**, A fortuitous section of a day 12 aggregate illustrates the 3 steps of vesicle formation. The separation of the vesicles labeled 3 was confirmed by analyzing cyrosections above and below the section shown. Scale bars, 50 μm (**a-g**).

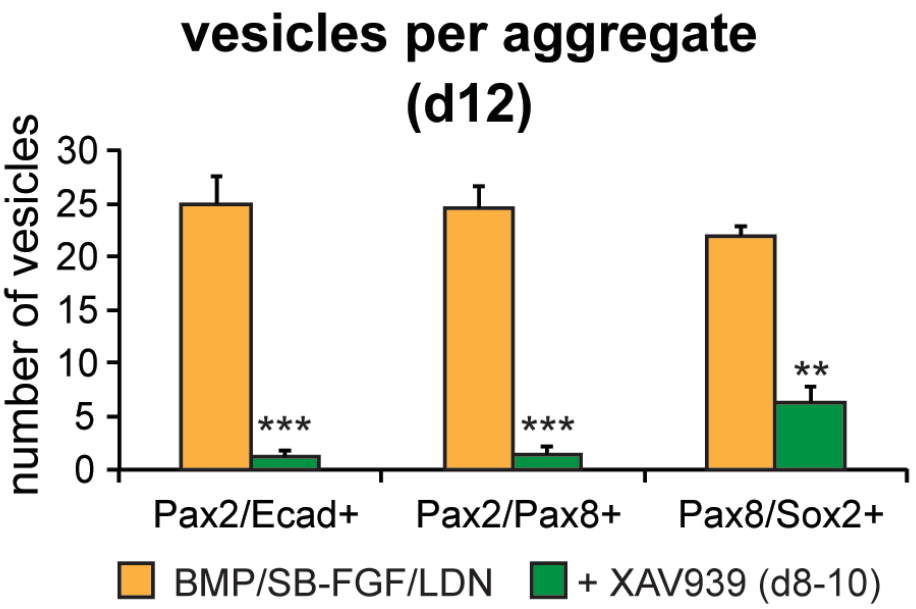

Figure 37: Otic vesicle formation is dependent on endogenous Wnt signaling.

A pulse treatment with a selective Wnt inhibitor, XAV939, between days 8-10 decreases the number of vesicles expressing Pax2 and Ecad, Pax2 and Pax8, and Pax8 and Sox2 on day 12. (n = 9 aggregates; $^{**}P < 0.01$, $^{***}P < 0.001$; mean ± s.e.m.).

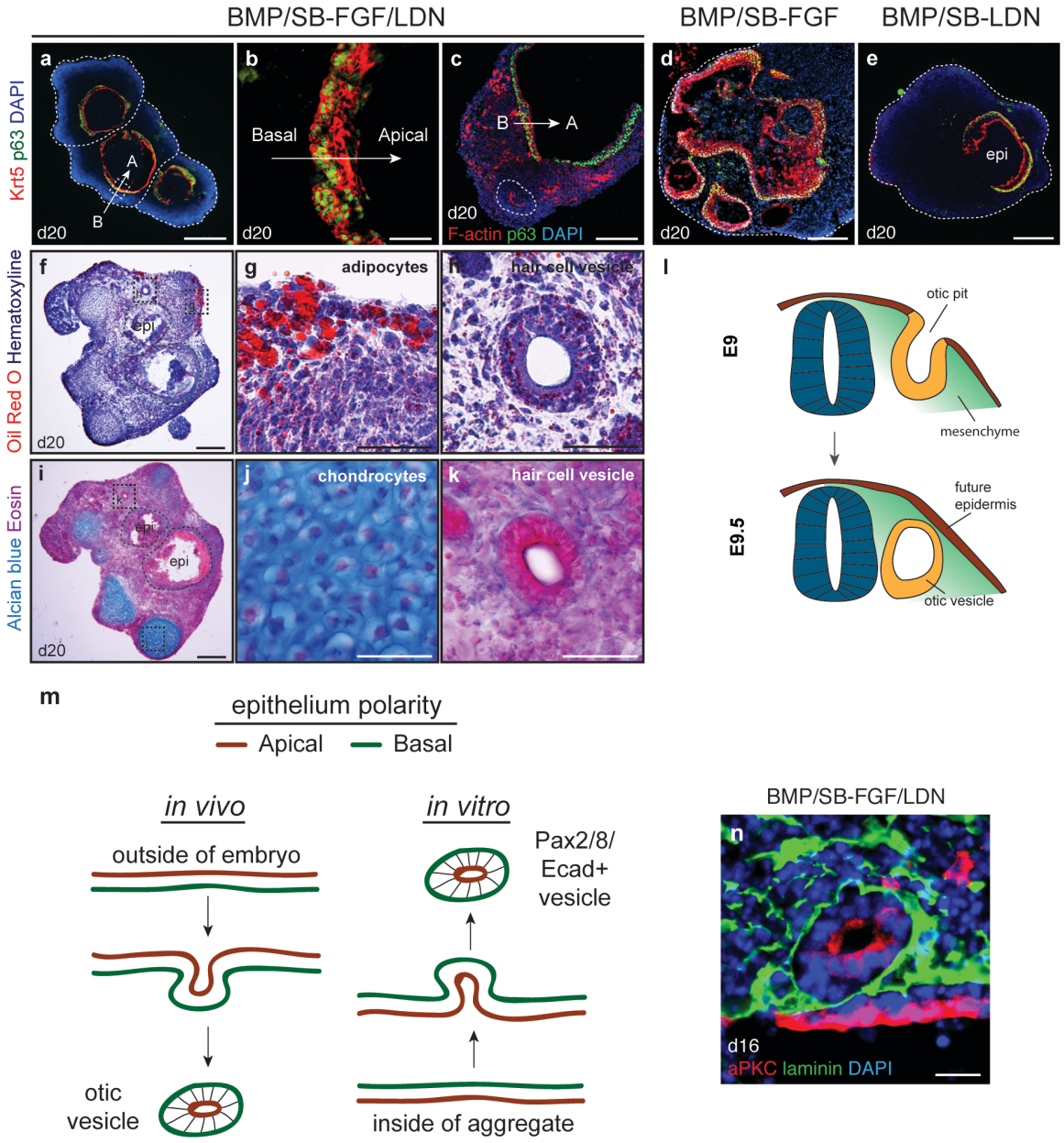

Figure 38: Epidermis arises under all BMP/SB treated conditions and vesicles evaginate into mesenchyme-like tissue.

a-e, Krt5⁺ p63⁺ epidermis-like epithelium forms in BMP/SB-FGF, -LDN and -FGF/LDN aggregates. In BMP/SB-LDN and BMP/SB-FGF/LDN aggregates the Krt5⁺ p63⁺ epithelium lines the central cavity of the aggregate with the apical surface oriented toward the interior of the aggregate (**b**). F-actin staining with phalloidin reveals that vesicles (outlined) are located basal to the p63⁺ epithelium (**c**). **f-l**, Oil Red O and Alcian Blue staining shows that adipocytes and chondrocytes develop adjacent to hair cell-containing vesicles in the outer cell mass. This confirms that presence of mesenchymal development in this region of the aggregates. The development of hair cell vesicles surrounded by mesodermal tissue in BMP/SB-

FGF/LDN aggregates mimics the development of the inner ear in the head mesenchyme (**l**).

m, One apparent discrepancy between *in vitro* and *in vivo* otic vesicle formation is that the otic placode *invaginates* into the body to form the otic vesicle (**l**, ~E9-9.5) and, conversely, *in vitro* vesicles *evaginate* out into the medium or exterior cell layer. From the Krt5 and p63 staining results, we can see that the basal-to-apical polarity of the inner epithelium is oriented outside-to-inside relative to the surface of BMP/SB-FGF/LDN aggregates (note that a similar orientation was observed in BMP/SB aggregates; see Figure 15). The schematic illustrates how vesicles that appear to *evaginate* toward the exterior of the aggregate *in vitro* are, in actuality, *invaginating* relative to the polarity of the epithelium. Staining for apical (aPKC) and basal (laminin) polarity markers (**n**) confirms this model. Scale bars, 250 μm (**a**), 100 μm (**c-f, i**), 50 μm (**g, h, j, k**) 25 μm (**b**,**n**)

invagination toward the outside of the aggregate is consistent with the orientation of embryonic otic vesicle invagination (Figure 38).

During development, the prosensory domain of the otic vesicle is destined to become sensory epithelia harboring Myo7a$^+$ sensory hair cells. Surprisingly, the epithelia of Sox2$^+$ Jag1$^+$ vesicles became Myo7a$^+$ by day 14, mimicking the diffuse Myo7a staining pattern in the E9.5 otic vesicle (Figures 39 and 40). CyclinD1 was also expressed throughout the vesicle epithelium, consistent with *in vivo* expression patterns (Figure 39). By day 16, we found that each aggregate contained 15.4 ± 4.8 (n = 12 aggregates) vesicles lined with Myo7a$^+$ Sox2$^+$ cells bearing the stereotyped morphology of sensory hair cells with a large nuclei (~8-μm diameter) positioned basal to an elongated apical end (Figures 40 and 41). The Myo7a$^+$ Sox2$^+$ cells were organized in a radial pattern with the apical end abutting a lumen of varying sizes (~5–1,100-μm-long-axis diameter; Figure 40). Basal to each layer of Myo7a$^+$ Sox2$^+$ cells was a tightly arranged layer of Sox2$^+$ cells reminiscent of supporting cells (Figure 40). Mimicking the *in vivo* sensory epithelia, hair cells and supporting cells could be further distinguished by expression of Brn3c (also known as Pou4f3) and cyclin D1, respectively (Figure 41 and 42; Laine et al., 2010). Due to their strong resemblance to inner ear sensory epithelia and compartmentalization into discrete vesicles we designated these structures inner ear organoids. Using wholemount staining and 3D reconstruction, we were able to gain an appreciation of the structural organization of inner ear organoids (Figure 43). F-actin staining revealed tight cell–cell junctions along the luminal surface as well as F-actin$^+$ Espin$^+$ stereocilia bundles (Figure 44). Every Myo7a$^+$ cell analyzed also had an acetylated-

α-tubulin$^+$ kinocilium protruding from the apical end into the lumen (Figure 44). Stereocilia and kinocilium were not visible at day 16, but the average height increased from day 20 to day 24 and fell within the range of heights recorded from an adult mouse utricle (Figure 44j; Li et al., 2008). The hair cells also appeared to be functional on the basis of rapid uptake of FM1-43 dye and the diversity of voltage-dependent currents (Figure 45 and 46; Géléoc et al., 2004; Meyers et al., 2003). In all cells included in this study we observed outwardly rectifying potassium currents with voltage-dependent activation kinetics to amplitudes ranging from 194 pA to 3,612 pA with a mean of 1,003 ± 527 pA (*n* = 6; Figure 46). In addition, some cells were distinguished by the presence of a transient inward current, probably reflecting calcium channel activity (Figure 46). By day 20 each BMP/SB-FGF/LDN aggregate contained 1,552.3 ± 83.1 Myo7a$^+$ cells with typical hair cell morphology, in marked contrast to other conditions that yielded no Myo7a$^+$ cells (~1–2% of all cells in the aggregate; *n* = 12–16 aggregates per condition; Figure 47). We conclude from these data that the cytoarchitecture, cellular morphology and functional characteristics observed in inner ear organoids are similar to sensory epithelia in the inner ear.

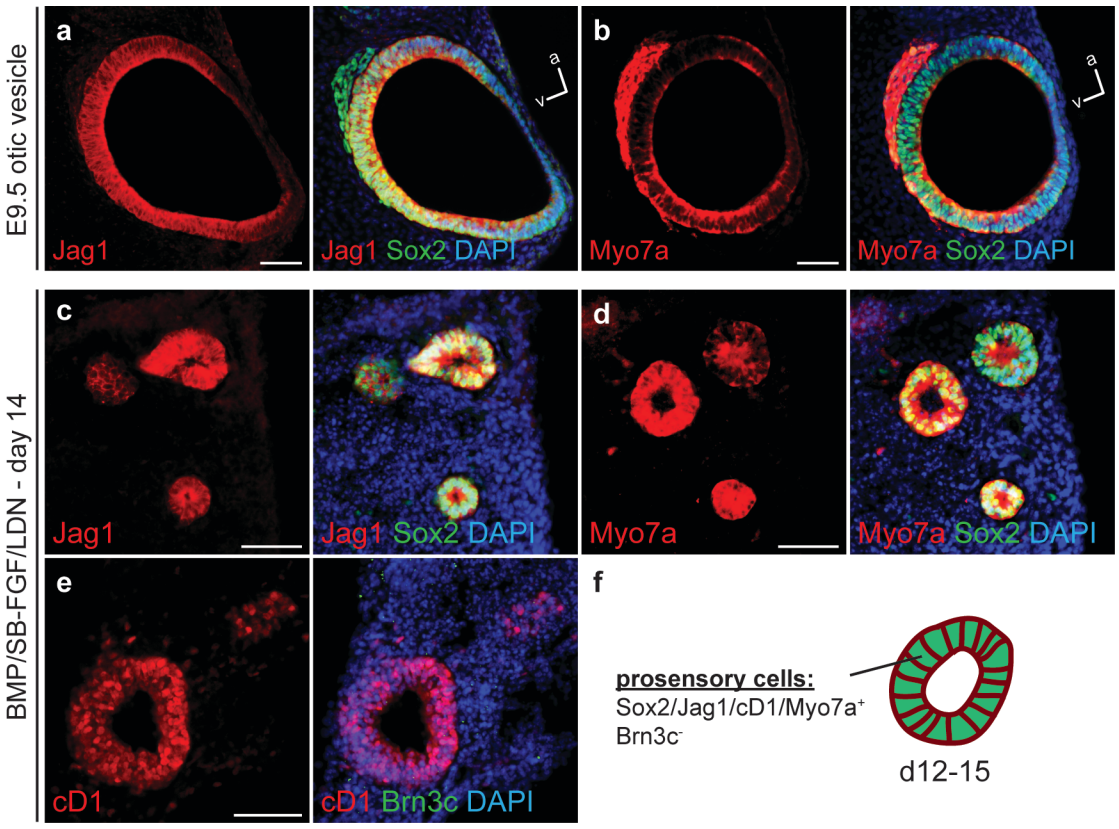

Figure 39: Jagged1, Myo7a and cyclinD1 expression mimics in vivo expression.

a-d, At day 14 of differentiation, prosensory vesicles express Sox2, Jag1 and Myo7a, mimicking the expression pattern of the E9.5 otic vesicle. **e**, Prosensory cells also expressed cyclinD1 (cD1), but did not express the hair cell marker Brn3c. Scale bars, 50 µm (**a-e**).

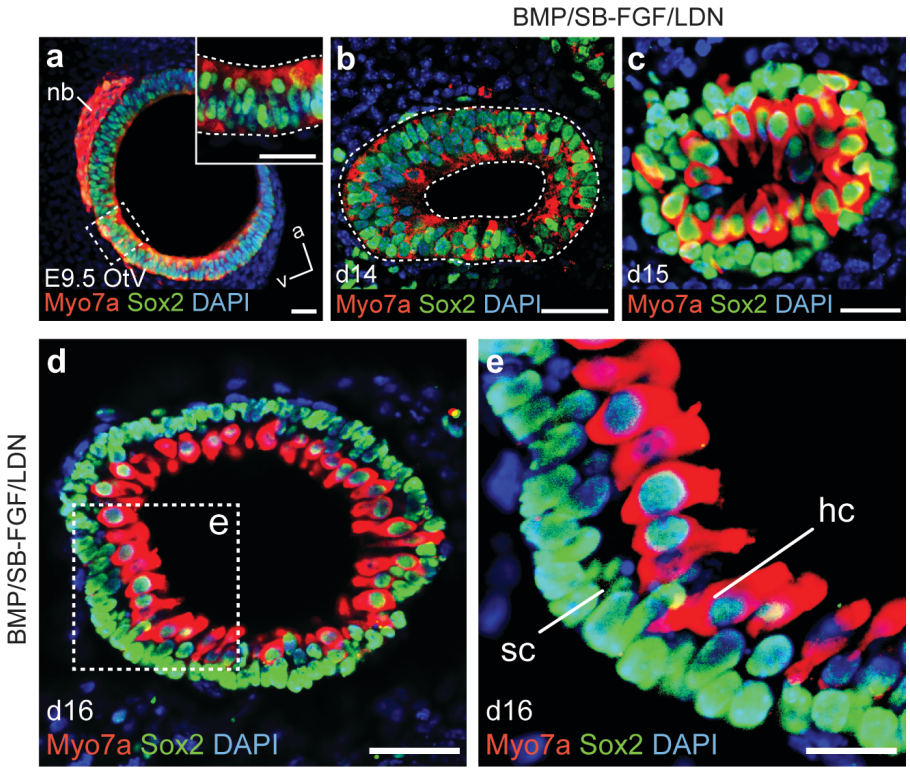

Figure 40: Emergence of hair cells in stem cell-derived otic vesicles.

a, **b**, Expression of Myo7a in the E9.5 otic vesicle (OtV) (**a**) and day 14 vesicles (**b**). nb, neuroblasts. **c**–**e**, Myo7a$^+$ Sox2$^+$ hair cells (hc) with underlying Sox2$^+$ supporting cells (sc) on days 15 (**c**) and 16 (**d**, **e**). Scale bars, 100 μm (**a**), 50 μm (**d**), 25 μm (**b, c, e**).

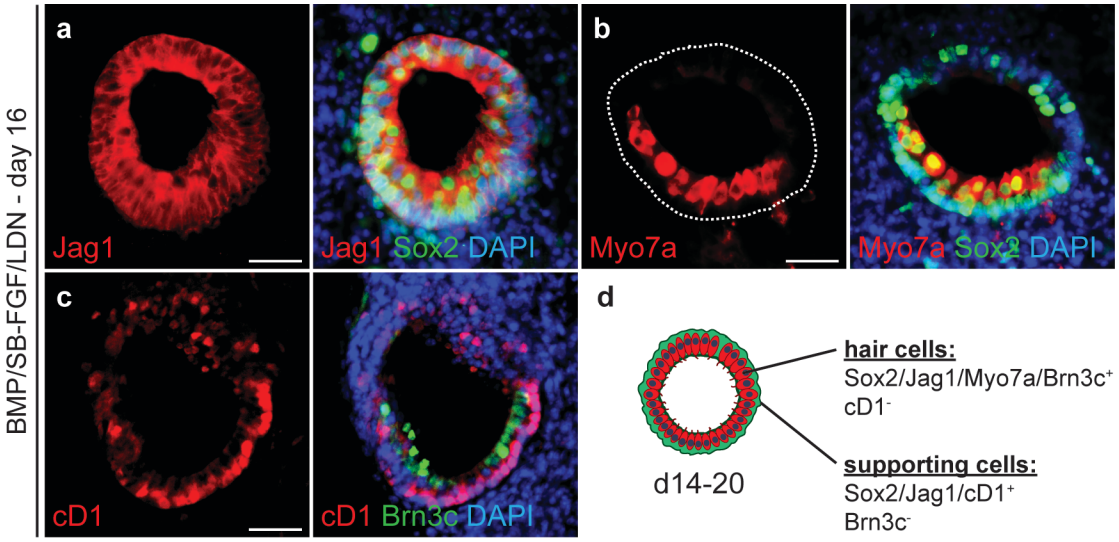

Figure 41: Distinct supporting cells and hair cells.

a-d, Maturing prosensory otic vesicles express Jag1 and Sox2 in both supporting cells and hair cells, while Myo7a and Brn3c, and cD1 expression in confined to hair cells and supporting cells, respectively. **d**, Schematic representing vesicles with sensory epithelia containing hair cells and supporting cells observed between days 14-20. Scale bars, 25 μm.

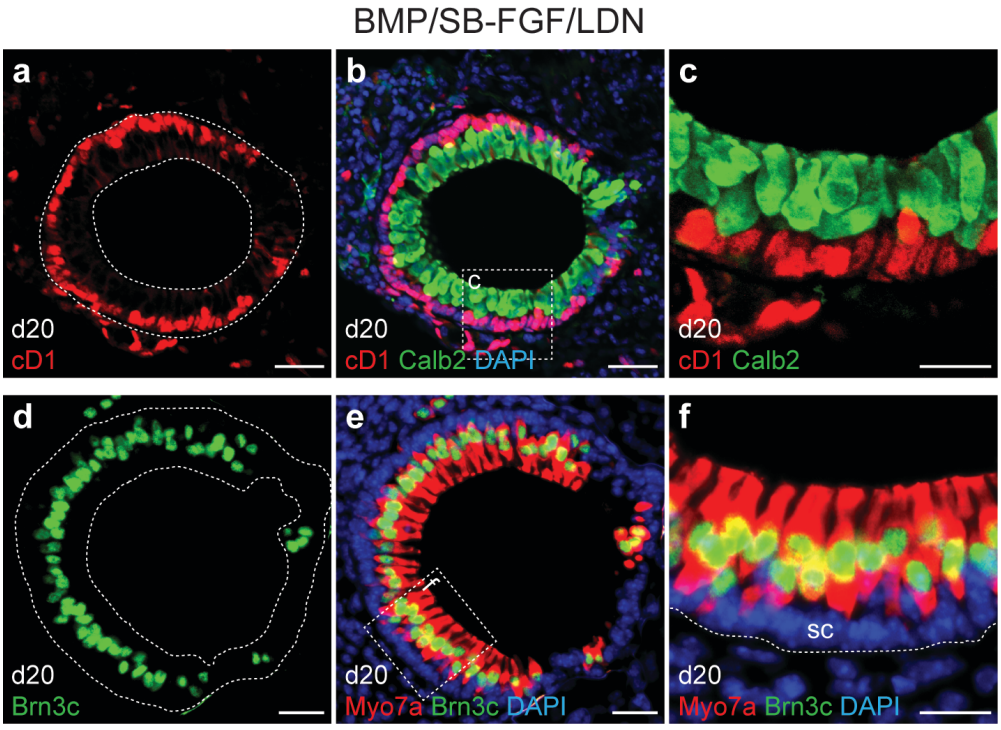

Figure 42: Brn3c and cylcinD1 expression in hair cells and supporting cells.

a-f, Brn3c and cyclinD1 (cD1) delineate hair cells from supporting cells in d20 epithelia. Calb2 is expressed in hair cells. Data represent two separate sections of a single vesicle. Scale bars, 25 μm.

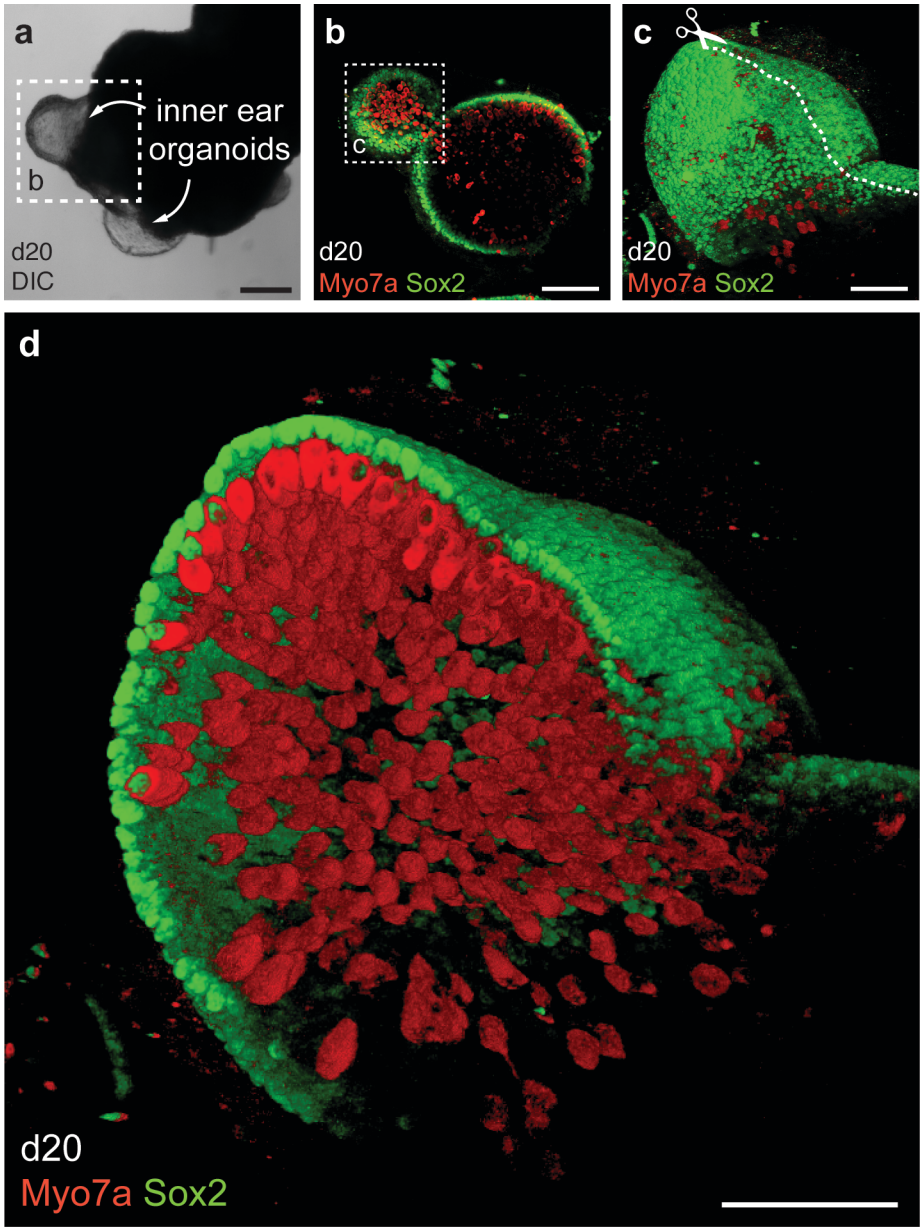

Figure 43: 3D reconstruction of inner ear organoids.

a, Representative DIC image of an aggregate with two protruding inner ear organoids. **b–d**, Whole-mount immunofluorescence for Myo7a and Sox2 (**b**) and three-dimensional reconstruction (**c, d**) of an organoid in a day 20 BMP/SB-FGF/LDN aggregate. Note that the same organoid is represented in **a-d**. Scale bars, 250 µm (**a, b**), 50 µm (**c, d**).

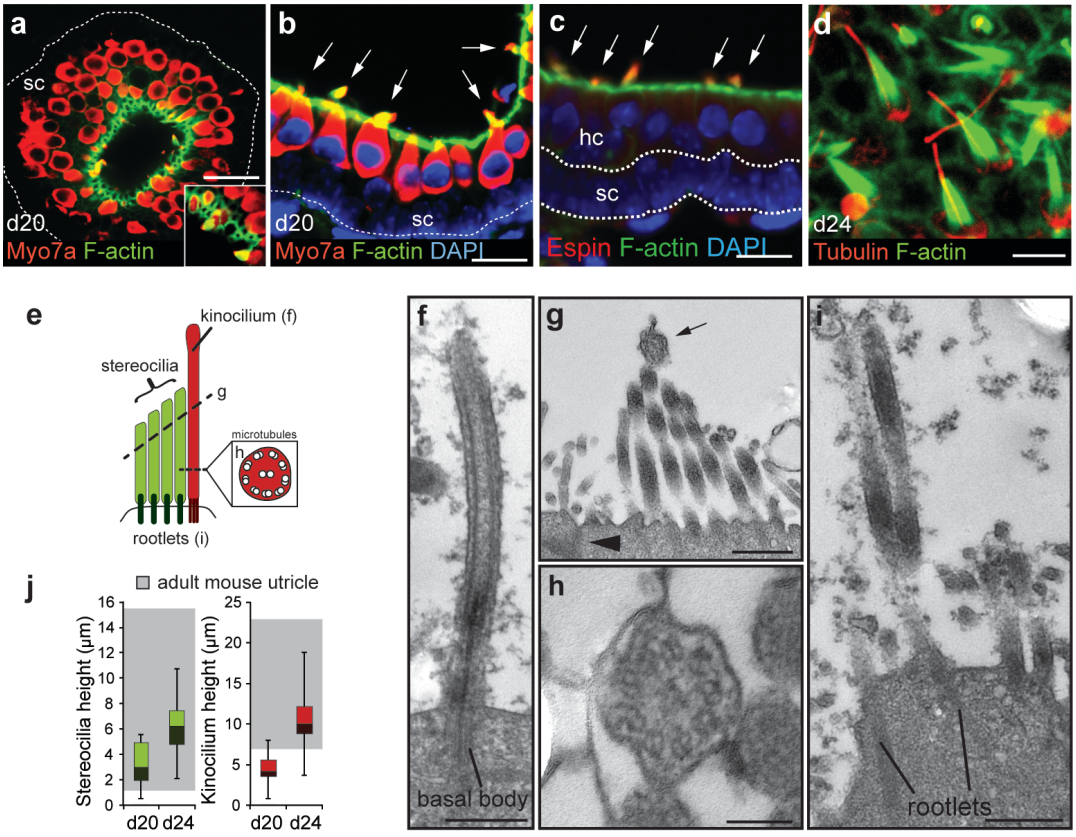

Figure 44: Stereocilia and cell-cell tight junctions on the apical surface of stem cell-derived sensory epithelia.

a, b, F-actin labels cell–cell junctions on the luminal surface and stereocilia bundles. **c**, Stereocilia bundles express Espin, characteristic of stereocilia on authentic inner ear hair cells. **d**, Acetylated-α-tubulin (tubulin) labels kinocilium and the cuticular plate. **e**, Transmission electron microscopy reveals several ultrastructural hallmarks found in stem cell-derived hair cells. Notably, a single kinocilium with basal body (**f**) was associated with each bundle of stereocilia. Cross-sections of kinocilia (**h**) displayed the characteristic configuration of 9 microtuble doublets surrounding 2 central microtubules. **g**, Stereocilia bundle, kinocilium (arrow) and tight junctions (arrowhead) were visible at the apical surface of hair cells. Also, stereocilia have rootlets (**i**) that extended into the cell body. **j**, Distribution of stereocilia and kinocilium heights on days 20 and 24 compared to adult mouse utricle, with range indicated by grey boxes (n > 100 cells; ± max/min). Scale bars, 25 µm (**a-c**), 5 µm (**d**) 500 nm (**f, g, i**), 100 nm (**h**).

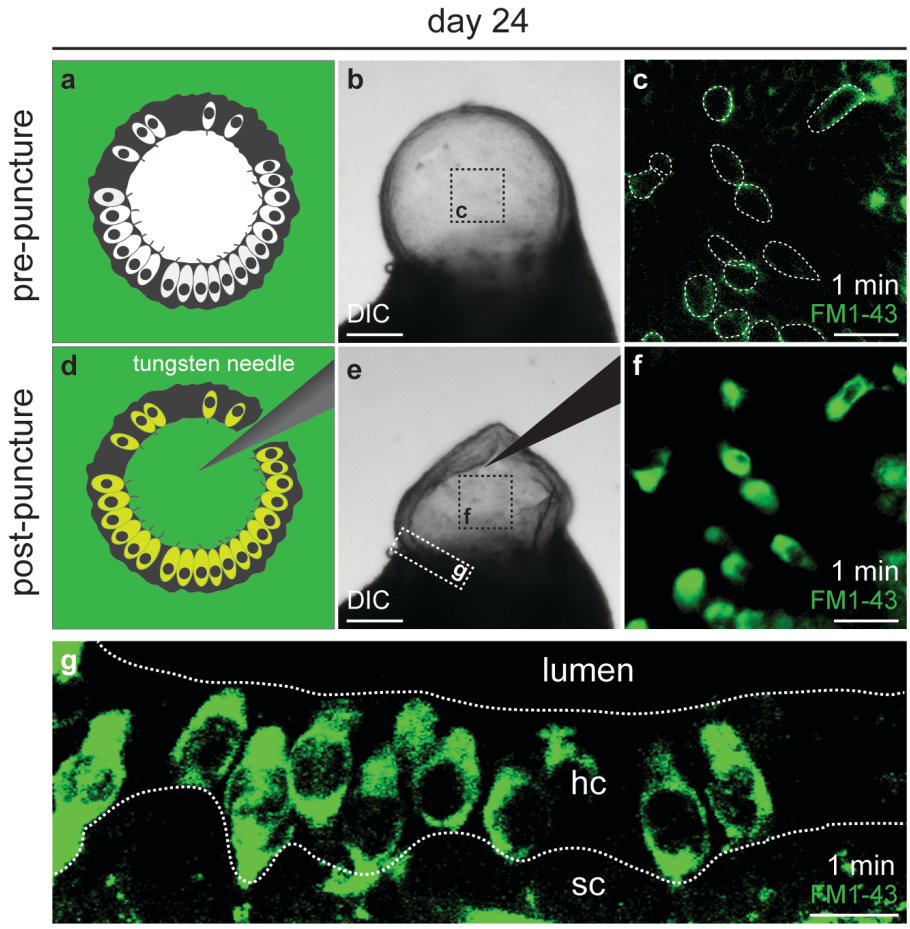

Figure 45: FM1-43 uptake by hair cells.

a-c, Inner ear organoids containing hair cells were identified by morphology as translucent cysts protruding from the side of cell aggregates. Hair cells in the epithelium could be identified through the organoid wall following treatment with FM1-43FX for 1 minute. **d-g**, After puncturing the organoid with a 0.25 µm tungsten needle and another 1 minute incubation, previously outlined hair cells became fluorescent (**f**). Confocal imaging of the epithelial sheet revealed FM1-43FX labeled cells with the same morphology as hair cells. The underlying supporting cells did not take up the dye (**g**; sc). These results are consistent with previous investigations (see Meyers et al., 2003) and were confirmed using 10 vesicles from 3 different experiments. Scale bars, 250 µm (**b, e**), 25 µm (**c, f, g**).

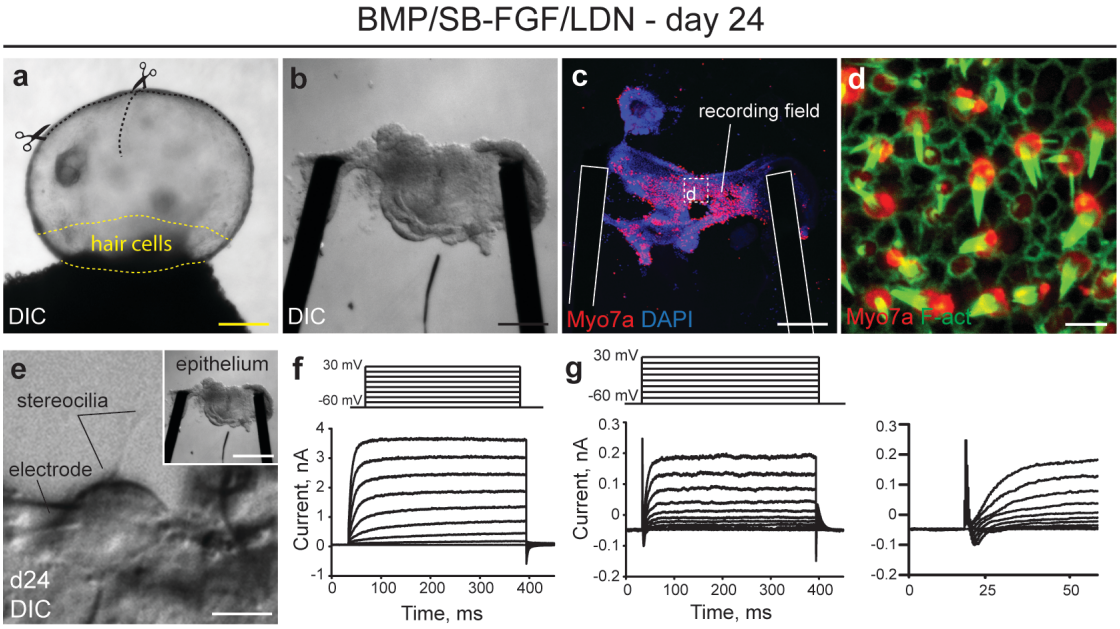

Figure 46: Functional analysis of stem cell-derived hair cells.

a, For electrophysiological recording, organoids were dissected to flatten the sensory epithelium (typically found in the portion of the organoid abutting the aggregate). **b**, The sensory epithelium was secured to a coverslip by two needles during recording. **c**, **d**, Post-recording, samples were fixed and stained for Myo7a and F-actin (phalloidin) to confirm the identity of hair cells. **e**, Representative epithelium preparation (inset) and hair cell during electrophysiological recordings. **f**, Representative voltage–current responses recorded from hair cells. The voltage protocol is shown at the top. **g**, Representative traces of complex current which include the inward and outward components. The voltage protocol is shown at the top. (**g**, **right panel**) Expanded view of transient inward current, which could be calcium or a transient voltage-gated sodium current observed in immature vestibular hair cells (see Bao et al., 2003 and Géléoc et al., 2004). Outward current was truncated for clarity. Scale bars, 250 µm (**a-c**), 10 µm (**e**), 5 µm (**d**).

There are four distinct populations of hair cells in the mammalian inner ear; type I and type II vestibular and inner and outer cochlear hair cells. We wished to reveal which type of hair cells populated the stem-cell-derived sensory epithelia in our culture. Previous studies have suggested that expression of Pax2 and Sox2 may distinguish vestibular from cochlear hair cells (Oesterle et al., 2007; Warchol and Richardson, 2009). In addition, expression of the calcium-binding protein Calbindin (Calb2; also known as Calretinin) and Sox2 uniquely label type II vestibular hair cells, whereas calyceal innervation from sensory neurons identifies type I vestibular hair cells (Figure 48; Desai et al., 2005; Lysakowski et al., 2011; Oesterle et al., 2007). On day 20, nearly all stem-cell-derived hair cells were $Sox2^+$ $Pax2^+$ ($n > 250$ hair cells; Figure 48). Moreover, every hair cell expressed Calb2, suggesting a uniform population of type II vestibular hair cells (Figure 48). From a structural standpoint, we noted the presence of larger lumen organoids (3.7 ± 0.3 per aggregate, defined as >50-μm-long-axis diameter, $n = 15$ aggregates) with regions of sensory (with hair cells) and non-sensory (without hair cells) epithelia identical in organization to a vestibular end organ (Figure 48 and 49). Intriguingly, we also observed discrete populations of $Calb2^+$ and $Brn3a^+$ Tuj1 (also known as $Tubb3)^+$ neurofilament $(Nefl)^+$ neurons extended processes towards the sensory epithelia (Figure 50 and 51). We were surprised to find that, by day 16, hair cells exhibited punctate expression of ribeye (revealed by anti-Ctpb2 staining) co-localized with the postsynaptic and neuronal markers Tuj1, Synaptophysin (Syp), Snap25 and Rab3, indicating the formation of ribbon synapses with adjacent neurons (Figure 50 and 51). Notably, the average number of $Ctbp2^+$ puncta

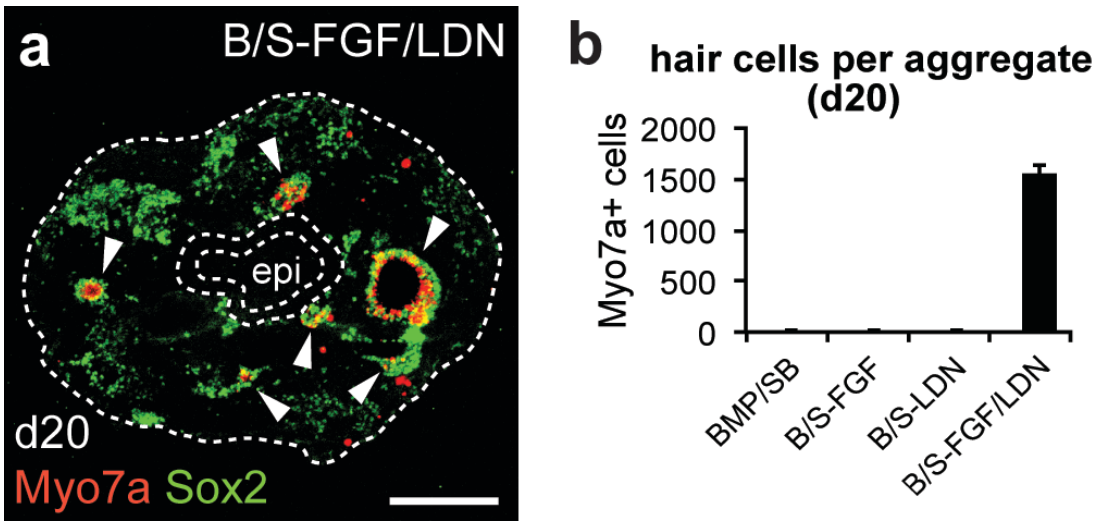

Figure 47: Hair cells per aggregate on day 20.

a, Day 20 aggregate with Myo7a$^+$ Sox2$^+$ vesicles. Epidermis is indicated by dashed outline. **b**, Number of hair cells on day 20 (*n* = 12–16; mean ± s.e.m.). Scale bars, 250 μm (**a**).

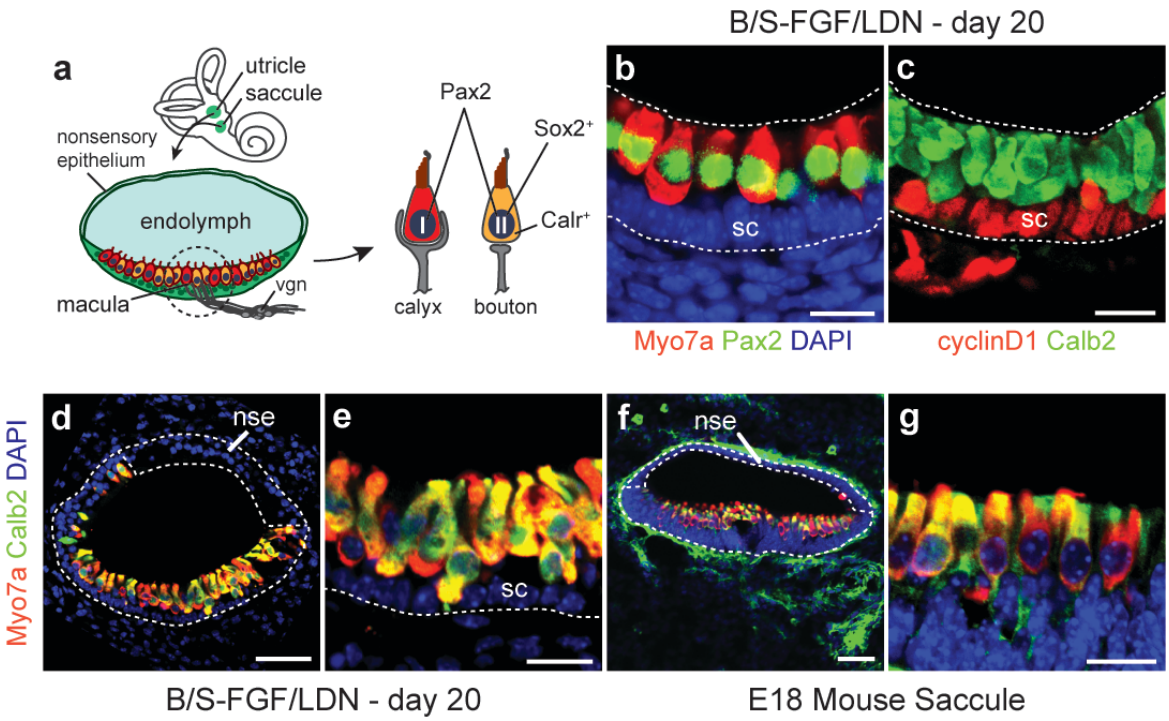

Figure 48: Vestibular characteristics of inner ear organoids.

a, Schematic of vestibular end organs and type I/II vestibular hair cells. vgn, vestibular ganglion neurons. **b**, **c**, Pax2 (**b**) and Calb2 (**c**) are expressed in all Myo7a$^+$ stem-cell-derived hair cells on day 20. CyclinD1 (cD1) is expressed in supporting cells. **d**–**g**, The structural organization of vesicles with Calb2$^+$ Myo7a$^+$ hair cells mimics the E18 mouse saccule (sagittal view) *in vivo.* nse, nonsensory epithelium. Scale bars, 50 mm (**d**, **f**), 25 mm (**b**, **c**, **e**, **g**).

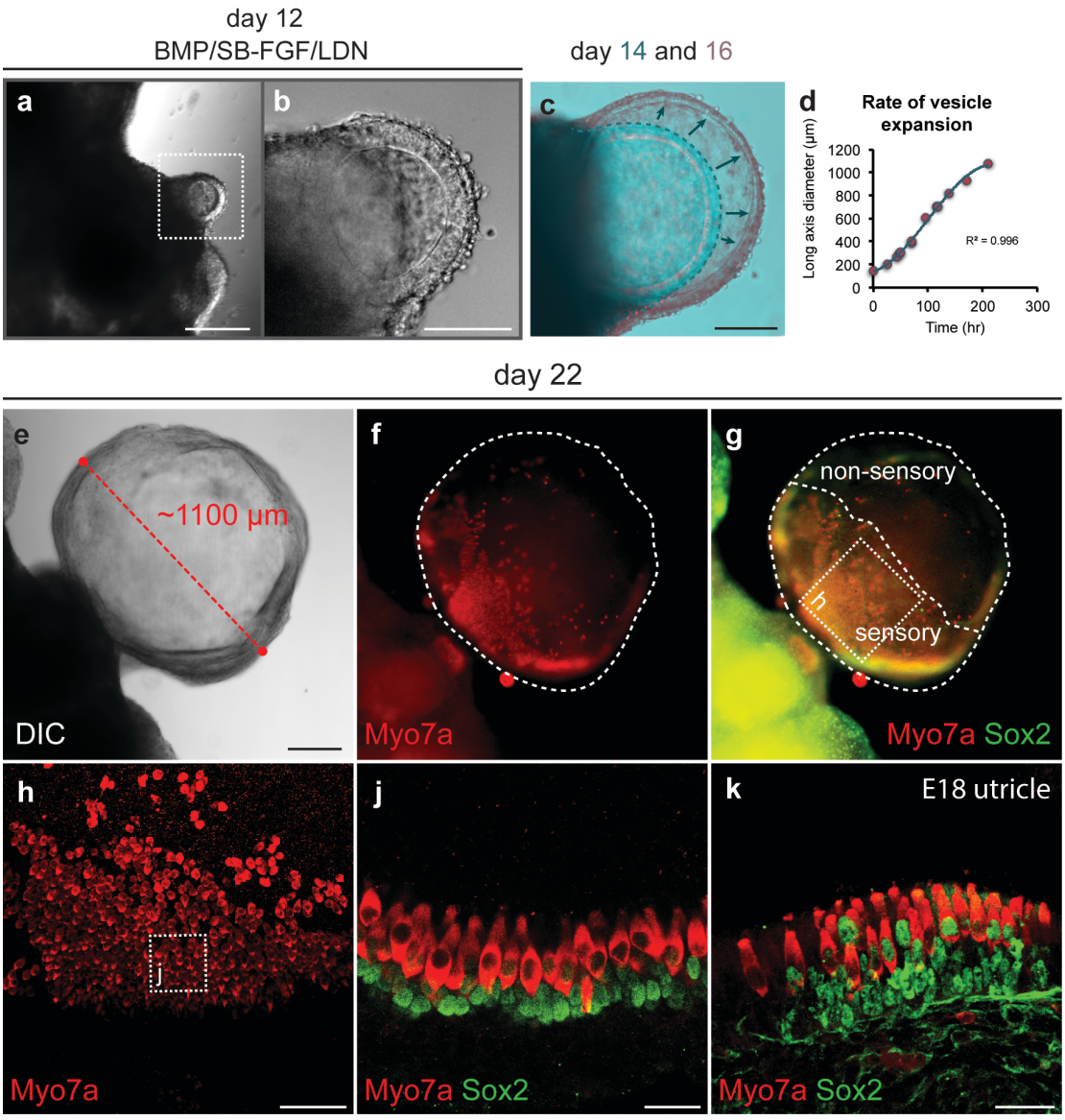

Figure 49: Inner ear organoid expansion and vestibular-like organization.

a, **b**, We tracked the development of a vesicle that erupted on the surface of the aggregate unusually early at day 12. **c-e**, The long-axis diameter of the aggregate grew to be ~1100 μm by day 22, which is on the scale of a typical adult mouse postnatal day 30 utricle (see Li et al. 2008 for comparison). **f-i**, Whole-mount immunohistochemistry showed that a "sensory" region of the vesicle contained an epithelium with $Sox2^+$ supporting cells and a dense population of $Myo7a^+$ $Sox2^+$ hair cells, while a "non-sensory" region contained dispersed clusters of sensory epithelium. **i**, **j**, The regional organization and size of the vesicle is comparable to the E18 utricle (shown in **k**) and saccule (not shown). Scale bars, 250 μm (**a, e-g**), 100 μm (**b, c, h**), 25 μm (**i**, **j**).

increased over time in culture, suggesting a maturation process similar to inner ear hair cells (Figure 50 and 51; Lysakowski et al., 2011). Together, these results indicate that the inner ear organoids in our culture represent immature vestibular end organs, specifically the utricle and/or saccule.

DISCUSSION

In conclusion, the data presented in **Chapters 3**, **4**, and **5** of this dissertation reveal how the sequential transformation of authentic nonneural, preplacodal and inner ear sensory epithelia from pluripotent stem cells can be reconstituted *in vitro* using an approach that combines precisely timed treatments with a series of signaling proteins and a defined 3D culture system. Our findings highlight a binary mechanism of BMP activation and TGFβ inhibition underlying *in vitro* nonneural ectoderm induction. Furthermore, subsequent inhibition of BMP signaling concomitant with activation of FGF signaling are required for preplacodal induction. Notably, the formation of these precursors is sufficient to trigger self-guided induction of inner ear organoids, in which hair cells with structural and functional properties of native mechanosensitive hair cells in the inner ear spontaneously arose in significant numbers (~1,500 hair cells per aggregate). Moreover, microenvironment-derived signals essential for inner ear induction, primarily proteins secreted from the surrounding hindbrain and mesenchyme, are well preserved in the 3D culture system. This new approach cannot only be used as a potent model system to elucidate the mechanisms underlying inner ear

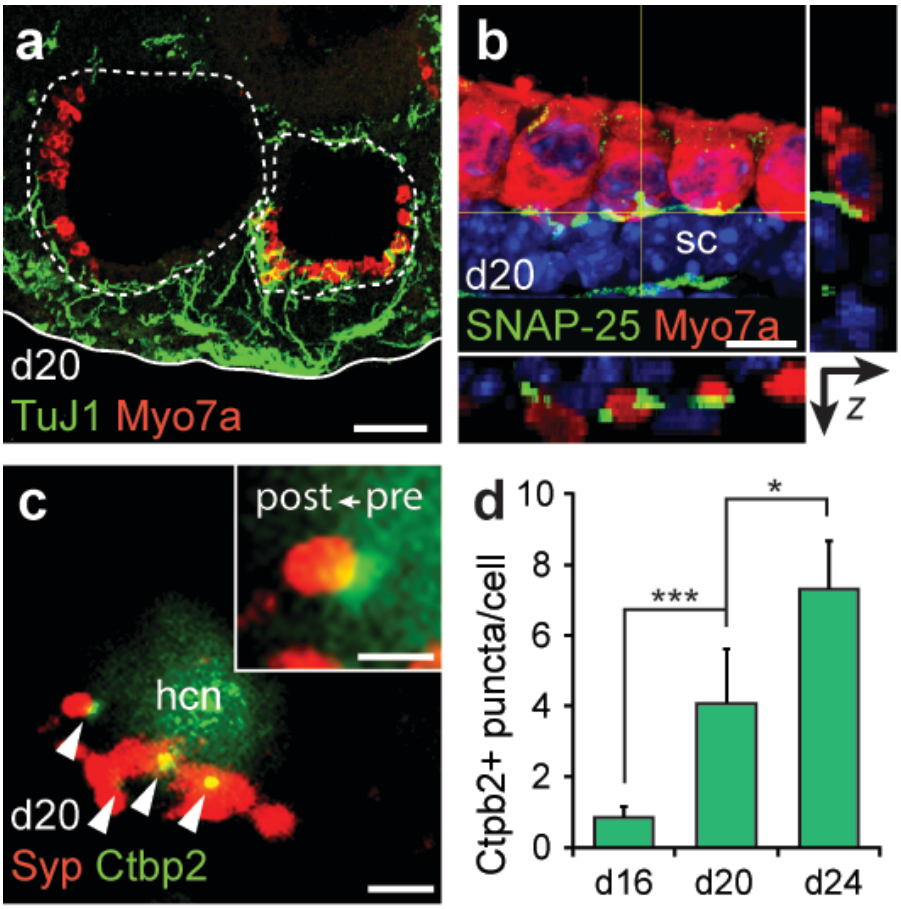

Figure 50: Putative ribbon synapses on hair cells.

a, Tuj1⁺ neurons extending processes to hair cells. **b**, The synaptic protein Snap25 is localized to the basal end of hair cells. **c**, The postsynaptic marker synaptophysin (Syp) co-localizes with Ctbp2 (arrowheads and inset). hcn, hair cell nucleus. **d**, Quantification of synapses on day 16, 20 and 24 hair cells ($n > 100$ cells, $^{*}P < 0.05$, $^{***}P < 0.001$; mean ± s.d.). Scale bars, 50 μm (**a**), 10 μm (**b**), 5 μm (**c**).

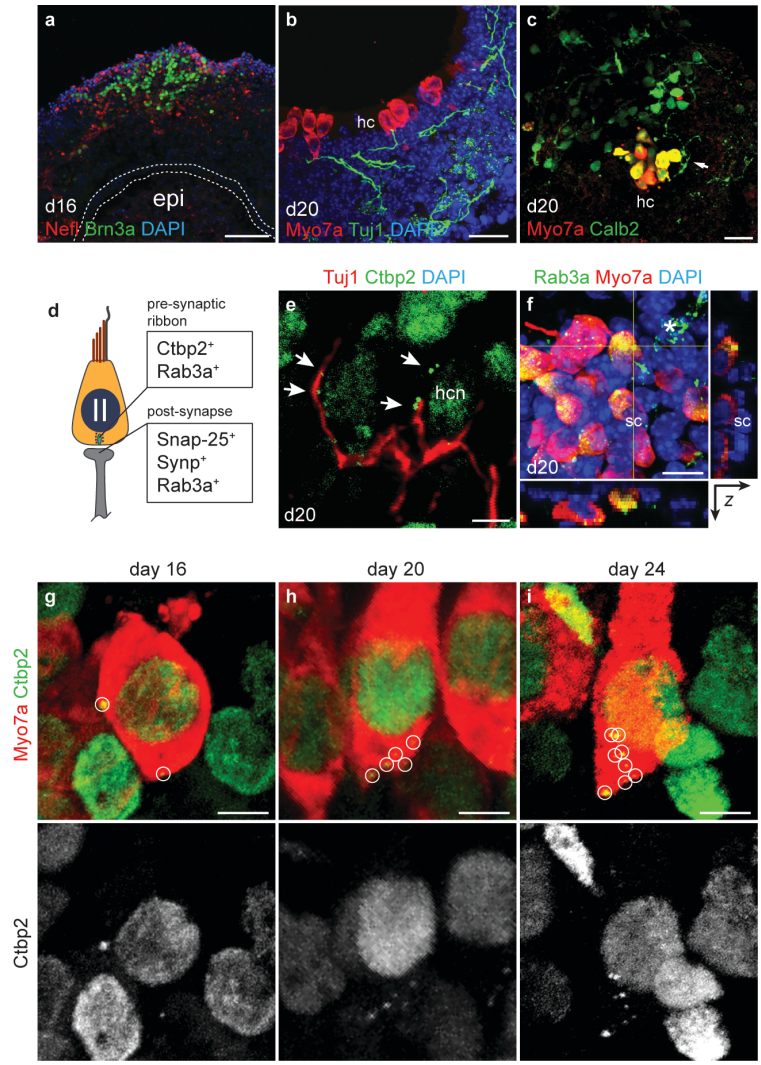

Figure 51: Sensory-like neurons and putative synapses.

Clusters of Nefl+ Brn3a+ (**a**) neurons were found in day 16 aggregates. **b**, Tuj1+ neuronal processes were observed extending toward Myo7a+ hair cells (hc). **c,** Calb2+ neurons extended processes toward and made contact (arrow) with hair cells. Calb2 expression is associated with sensory neurons of the inner ear vestibular and auditory ganglia. **d**, Schematic of Type II vestibular hair cells highlighting several pre- and post-synaptic markers at ribbon synapses. **e**, Tuj1+ neuronal processes are associated with Ctbp2+ puncta in stem cell-derived hair cells. Note that the Ctbp2 antibody labels ribbon synapses and hair cell nuclei (hcn). **f**, Rab3a+puncta were found on the basal end of Myo7a+ hair cells and neuronal process (asterisks). Supporting cells (sc) have been labeled for orientation **g-i**, Representative images showing the increase in Ctbp2+ puncta (white circles) found on hair cells over time in culture (d16, 20 and 24). Note that the quantification of panels **g-i** can be found in Figure 50d. Scale bars, 50 μm (**a**), 25 μm (**b, c**), 10 μm (**f**), 5 μm (**e, g-i**).

development, but will also provide an easily accessible and reproducible means of generating hair cells for *in vitro* disease modeling, drug discovery or cellular therapy experiments.

This chapter was modified from work previously published in Nature and a manuscript in revision

Koehler, K. R., Mikosz, A. M., Molosh, A. I., Patel, D. & Hashino, E. Generation of inner ear sensory epithelia from pluripotent stem cells in 3D culture. *Nature* **500,** 217–221 (2013).

CHAPTER 6: GENERAL DISCUSSION

In the preceding chapters I delineated a novel 3D ES cell culture system that accurately models many aspects of inner ear develop. By leading the experimental elaboration of this system I directly addressed my initial research questions and advanced our general knowledge of how to guide organogenesis *in vitro.* Below I will discuss some of the key findings in regard to my initial research questions:

1. Can precisely timed activation of BMP signaling induce nonneural cells in a three-dimensional mouse embryonic stem cell culture?

We found that a combined BMP4 and TGFβ inhibitor treatment on day 3 of differentiation produced an authentic nonneural epithelium without producing an overabundance of mesoderm-like cells. Previous attempts to direct the development of nonneural cells via BMP4 treatment have been plagued by the issue of mesoderm induction, most likely due to improper timing of treatment (Harvey et al., 2010; Suga et al., 2011). Recall that BMP4 treatment can induce mesoderm from ES cells. Moreover, most previous attempts to derive nonneural ectoderm were targeted at deriving an epidermal monolayer. Thus, our incorporation of the TGFβ inhibitor provides a novel and controlled approach to nonneural induction in 3D culture (Koehler et al., 2013). These findings are important for future attempts to control the *in vitro* development of all nonneural derivatives—both organs (e.g. the skin, cranial ganglia, anterior pituitary gland, olfactory epithelium, lens and inner ear) and mini-organs (e.g. hair follicles and teeth). Of note, mini-organs like hair follicles

and teeth require epithelia-mesenchyme interactions to initiate development (Sasai, 2013b; Schneider et al., 2009). A fortuitous consequence of BMP/SB treatment was the induction of disparate germ layers on the outside (i.e. the outer-epithelium) and inside (i.e. mesoderm-like cells) of the aggregates. This organization might make our culture system ideal for studying mini-organ development *in vitro*.

2. Can subsequent inhibition of BMP signaling and FGF signaling activation promote the induction of preplacode-like cells from nonneural cells?

From embryo studies, we knew that BMP signaling—although necessary for nonneural induction—needed to be attenuated for preplacodal induction (Grocott et al., 2012; Kwon et al., 2010; Schlosser, 2006). By our estimation, 24-48 hours elapses between nonneural and preplacodal induction in the mouse embryo. Consequently, we added a BMP inhibitor, LDN, to the medium between days 4 and 5 of culture (i.e. 24-48 hours after BMP/SB treatment). FGF signaling, however, is also important for preplacodal induction. When we performed a combined treatment of FGF2 and LDN (FGF/LDN), the outer-epithelium developed a placode-like morphology and expressed several marker genes of the preplacodal ectoderm. These findings are, to my knowledge, completely new to the stem cell field and highlight the need to tightly control BMP signaling to achieve preplacodal induction. Of note, in a study published concurrently with ours, Leung and colleagues demonstrated that BMP inhibition was an effective method to generate preplacodal cells from human ES cells—validating our approach (Leung et al., 2013).

Furthermore, recent embryonic work has reiterated the importance of complete BMP inhibition for the induction of preplacodal ectoderm (Reichert et al., 2013).

By contrast, my understanding of the role of FGF signaling in the culture model remains less certain. For instance, is FGF2 necessary for induction of a generic preplacodal epithelium or is BMP inhibition sufficient? Perhaps supplemental FGF2 is only necessary for OEPD and otic placode induction, but not other placodes. The data presented in Figure 20 seem to suggest that there is an endogenous source of FGFs. Moreover, on day 8 we occasionally observed $Pax8^{+}$ epithelium in BMP/SB-LDN treated aggregates (see Figure 30). We did not, however, directly investigate whether endogenous FGFs were sufficient for preplacodal induction by examining the potential of BMP/SB-LDN aggregates to give rise to other placodal tissues besides otic tissue. We only examined the affect of FGF inhibition on epithelium thickness. Although, BMP/SB-LDN treated aggregates did not appear to produce otic tissue, it will be interesting to see whether endogenous FGFs are sufficient to generate other cranial placodes without additional FGF2. Perhaps the outer-epithelium of BMP/SB-LDN treated aggregates express markers for other regions of the PPR (i.e. Pax6 or Pax3; see Figure 31) and can produce more anterior tissues such as anterior pituitary gland, olfactory epithelium and lens. Most critically, we did not confirm whether epibanchial placodes developed, which also express Pax8/Ecad during development. Epibranchial placodes can be distinguished from the otic placode by expression of Sox3 and Pax2, respectively. For future characterization it will be necessary to do more thorough immunostaining with antibodies for Sox3, Pax2 and Pax8 to reveal epibranchial development.

3. If nonneural and preplacodal induction are accurately reproduced in three-dimensional culture, will inner ear tissues arise spontaneously via self-organization?

We were surprised to find patches of $Pax8^+$ cells in the outer epithelium of preplacode-induced aggregates—a sign of OEPD development. This level of specificity was unexpected because BMP inhibition and FGF signaling are necessary for development of the entire PPR not just the OEPD (Grocott et al., 2012). One explanation may be that FGF2 and the insulin found in the knockout serum replacement have a synergistic caudalizing effect on the tissue. For instance, FGF2 and Insulin were previously shown to caudalize brain tissue developing in 3D culture (Muguruma et al., 2010). The recent discovery that mouse retinas can develop spontaneously in a minimal culture medium prompted us to place the OEPD-induced aggregates in the same medium to see if OEPD epithelium spontaneously developed into otic vesicles (Eiraku et al., 2011). Under these conditions, the OEPD epithelium gave rise to vesicles containing $Pax2^+$ $Pax8^+$ $Sox2^+$ and $Jag1^+$ cells, a hallmark of prosensory cells in the embryonic otic vesicle. In stem cell-derivation studies, the more markers that can be co-localized to a given tissue or cell type the more certain the characterization. Our ability to co-localize four or more marker proteins to an individual vesicle by analyzing serial sections was unprecedented for the inner ear field (see Table 2). In previous attempts to derive inner prosensory cells it was impossible to co-localize the expression of more than

two marker proteins due to the limitations of a heterogeneous monolayer culture (Chen et al., 2012; Oshima et al., 2010; Ouji et al., 2012).

To understand why otic vesicles developed, we treated aggregates with a potent Wnt inhibitor based on the knowledge that Wnt signaling is critical for otic vesicle production *in vivo*. The significant deficit in otic vesicle production following treatment highlights the importance of endogenous Wnt signaling. With no additional treatments, aside from medium changes, cells in the epithelia of otic vesicles developed into hair cells and supporting cells. Remarkably, the derived hair cells expressed Myo7a, Brn3c, Calb2, Sox2, and Pax2, denoting a vestibular Type II hair cell identity. The presence of vestibular-like stereocilia bundles and kinocilia corroborated this conclusion. Another interesting observation was that the hair cells were spatially organized into clusters as in the vestibular end organs, rather than in rows as in the organ of Corti in the cochlea. For these reasons we decided to designate the structures as 'inner ear organoids.' Remarkably, quantitative analysis revealed that ~1500 hair cells developed in each cell aggregate by day 20 of differentiation. For perspective, the mouse vestibular organs contain ~15,000 hair cells combined; therefore, ~10 aggregates can produce an amount of hair cells equivalent to one set of vestibular end organs. In regard to percentage of the total population, ~1500 hair cells accounts for approximately 1-2% of the cells in the aggregate. Due to differences in quantification methods, it is difficult to compare the efficiency of our approach to previous methods. Oshima et al. (2010) reported that ~1% of cells in their cultures were Atoh1-GFP^{+}; however, they did not quantify the number of cells confirmed to be hair cells using other markers (Oshima et al., 2010).

We also reported the development of sensory neuron-like cells that developed in discrete groups alongside the organoids. Neuronal processes could be seen extending toward hair cells and analysis of synaptic proteins suggests the presence of putative synapses on the basal end of hair cells. Punctate expression of Ctbp2 indicated the development of ribbon synapses in hair cells. Moreover, the mean number of synapses found on hair cells increased over time in culture. These findings are remarkable because they mark the first evidence that a peripheral sensory circuit could be reconstituted *in vitro* from PS cells. We do not yet know, however, if all of the neurons making contact with hair cells are sensory neurons. Moreover, we do not know whether all or any of the sensory-like neurons are authentic inner ear neurons.

How faithful is inner ear organoid development to normal development?

Altogether, our findings provide significant insight into how to derive inner ear tissue *in vitro* and in many ways the system accurately models normal development. A strength of our approach, versus previous attempts to derive inner ear cells, was our ability to characterize the tissue with antibodies for multiple proteins (Table 2). Thus, we were able to definitively show the presence of each cellular intermediary leading to an inner ear fate. For comparison, Figure 52 contains an overview of inner ear organoid culture with a timeline of *in vivo* and *in vitro* development.

Table 2: Inner ear differentiation strategies including the current study

Year	Group	Cell Type Used	Culture Method Used	Nonneural Cells	Preplacodal Cells	Otic Progenitor Cells	Cell Types Derived	Citation
2003	Heller	mESC	3D/2D, SFM[a], +EGF, +IGF1 +FGF2	N/A	N/A	Pax2+	Hair cell-like cells	Li et al., 2003
2010	Heller	mESC miPSC	3D/2D, SM[b], +IGF1, SIS3[c], Dkk1 +FGF2, Chick utricle cell co-culture	N/A	N/A	Pax2/Pax8/ Dlx5+ En1-	Hair cells-like cells	Oshima et al., 2010
2012	Rivolta	hESC	2D, SFM, +FGF3, FGF10	N/A	N/A	Pax8/Sox2+ Pax8/FoxG1+ Pax8/Nestin+	Hair cell-like and sensory neuron-like cells	Chen et al., 2012
2012	Yoshikawa	mESC	3D/2D, Stromal cell Medium	N/A	N/A	N/A	Hair cell-like cells	Ouji et al., 2012
2013	Hashino	mESC	3D, SFM, +BMP4, SB[d] +FGF2, LDN[e]	AP2/E-cad+ N-cad-	Pax8/E-cad/ GATA3/Six1/ AP2+	Pax8/Pax2/ Sox2/Jag1/ Myo7a/Ecad+	Hair cells and sensory neurons	Koehler et al., 2013

a, SFM, serum-free medium; *b*, SM, serum-containing medium; *c*, SIS3, selective inhibitor of smad3; *d*, TGFβ inhibitor, SB-431452; *e*, BMP inhibitor, LDN-193189.

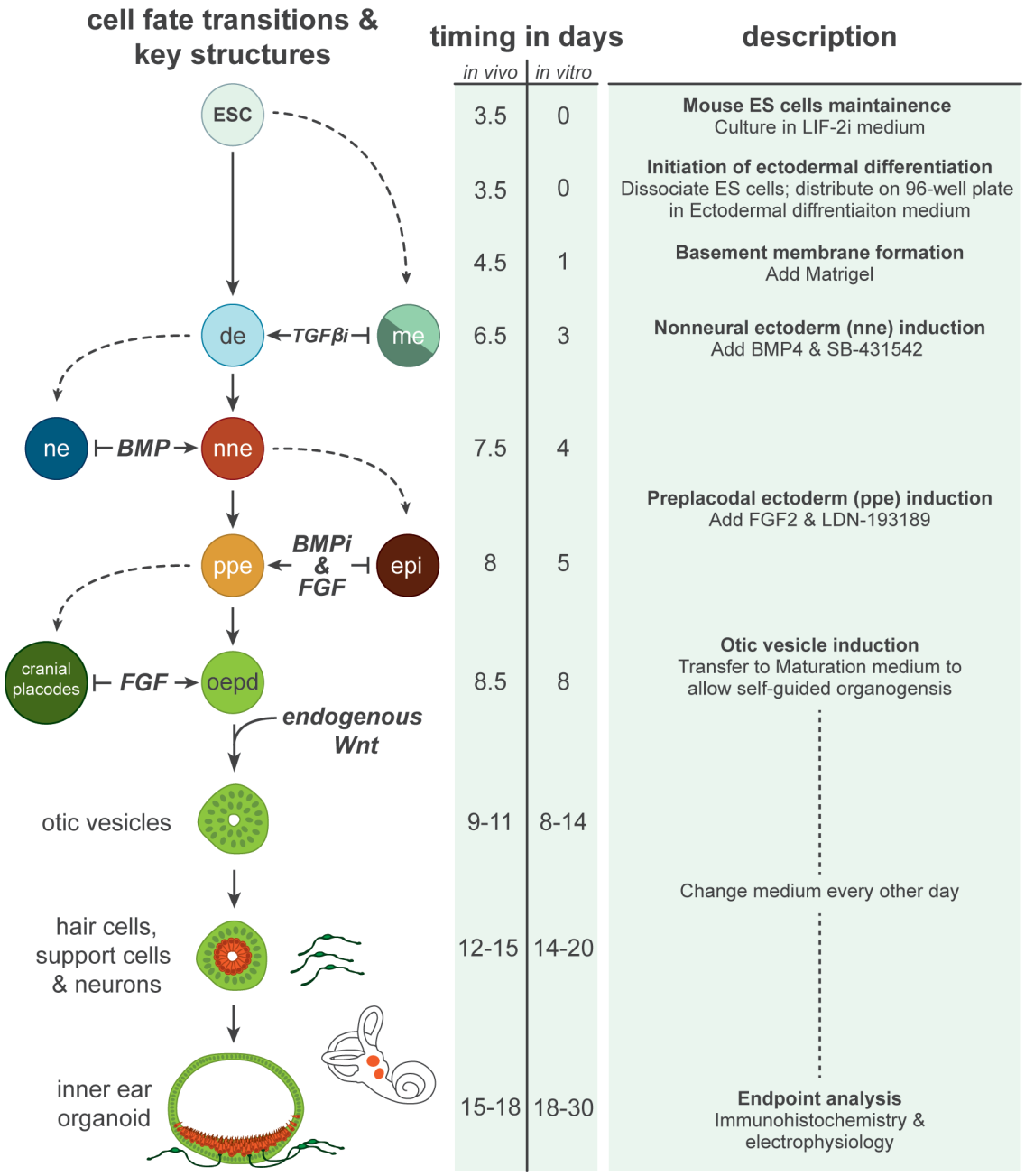

Figure 52: Overview of the inner ear organoid culture system.

A comparison of the various cell fate and morphological transitions that take place during *in vivo* and *in vitro* inner ear development. The descriptions describe the developmental process being modeled and technical manipulation employed. ESC, embryonic stem cells; de, definitive ectoderm; nne, nonneural ectoderm; ne, neural ectoderm; me, mesendoderm; ppe, preplacodal ectoderm; epi, epidermis; oepd, otic-epibranchial placode domain.

One critical component of our study was the incorporation of 1-2% Matrigel into the serum-free medium used to culture PS cell aggregates. Laminin and entactin proteins in the Matrigel have been shown to promote the development of a basement membrane in 3D culture, which helps instructing PS cells to self-organize into epithelia (Eiraku et al., 2011; Fujiwara et al., 2007; Nasu et al., 2012; Sato et al., 2009). In this way, the cells in the *in vitro* epithelia share a nearly identical morphology to the equivalent cells developing *in vivo*. Being able to analyze the morphological changes was advantageous for optimizing the timing and concentration of each treatment. In future iterations of organoid culture, we may be able to draw on recent and future investigations into the impact of the extracellular matrix on cell fate decisions to improve our control over epithelium development and organoid formation (Ivanovitch et al., 2013; Nasu et al., 2012; Watt and Huck, 2013).

Unlike previous inner ear derivation studies, our study was the first to demonstrate the guidance of PS cells through each of the epithelial cell fates representing the definitive ectoderm, nonneural ectoderm, preplacodal ectoderm, and otic placode. Being able to track the precursor of each tissue based on physical location makes this culture system a powerful tool for investigating the underlying molecular mechanisms of inner ear induction. By tracking the occurrence of each cell fate, we learned that developmental timing was well preserved in inner ear organoid culture. For example, we found that the timescale on which each cell type emerged during the first 7 days of *in vitro* differentiation closely followed *in vivo*

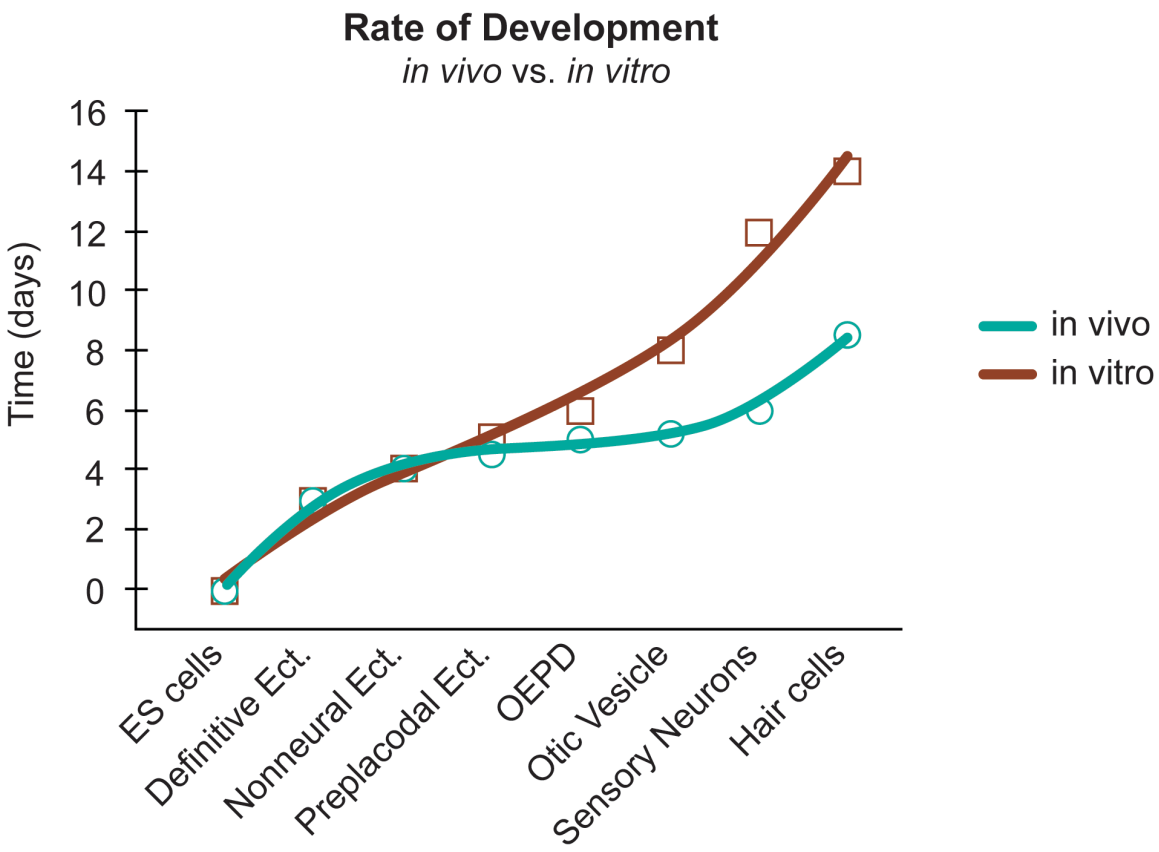

Figure 53: The rate of development *in vivo* and *in vitro*.

This graph compares the time that inner ear precursors and fully differentiated tissues emerge in the embryo (green) and in inner ear organoid culture (red). Note that there is a numerical difference of 3.5 days between *in vivo* and *in vitro* timing; thus, I have adjusted the *in vivo* timescale (green) based on the assumption that developmental timing is fixed. For example, E3.5 is equivalent to undifferentiated ES cells or day 0 of the culture; therefore, we can subtract 3.5 from each known *in vivo* value to arrive at a theoretical *in vitro* value. In other words, a perfectly conceived *in vitro* culture system development will progress at the same rate as *in vivo* development—the lines should overlap completely. In reality, the divergence of the lines indicates that the rate of developmental timing is slower *in vitro* following the development of OEPD (i.e. $Pax8^{+}$ $Ecad^{+}$ epithelium) tissue. In contrast, definitive, nonneural and preplacodal ectoderm induction *in vitro* follows a nearly identical timeline to *in vivo* development. Please note that the values used are approximate and indicate the earliest appearance of each tissue type.

inner ear development (Figure 53). Notably, this is the period of the culture in which we provided exogenous signaling cues to direct differentiation. During the subsequent period of self-guided differentiation the temporal progression seemed to slow down relative to *in vivo* development (Figure 53). The decline in developmental speed may reflect the stochastic nature of the signaling mechanisms underlying the production of otic prosensory vesicles during the later stage of the culture. In accordance with *in vivo* mechanisms, we identified that endogenous Wnt signaling is critical for otic induction *in vitro*; however, further study is needed to fully understand what triggers Wnt signaling and how it can be controlled to yield more otic tissue. For instance, we may find that endogenous Wnt signaling is suboptimal and treatment with a Wnt agonist can induce more otic tissue earlier in the culture.

Fascinatingly, a subset of organoids grew to be as large as 1 mm in the diameter (~5-10% of aggregates produce organoids >500 μm in diameter). In support of our conclusion that these organoids are vestibular in nature, they strongly resemble utricle cysts that have been shown to develop when newborn rat utricle explants are cultured with Matrigel (Gaboyard et al., 2005). Moreover, each organoid epithelium contained defined regions with (sensory) and without (non-sensory) hair cells. A notable feature of vestibular end organs missing from inner ear organoids was a layer of otoconia on the apical surface of regions containing hair cells. Moreover, further investigation will be needed to determine the identity of the nonsensory cells. We do not yet know if all nonsensory cells are supporting cells (i.e. $Sox2^{+}$) or if other inner ear epithelial cells develop, such as vestibular dark

cells. Vestibular dark cells can be identified by high expression of the Na-K-Cl co-transporter NKCC1 and the voltage-gated potassium channel KCNQ1. *In vivo*, these cells are responsible for establishing and maintaining the elevated potassium concentration in the endolymphatic fluid. The composition of the fluid within the organoids is unknown at this time, so it will be interesting to see if this fluid has a similar ionic composition to the inner ear endolymph.

Our functional assessment of the stem cell-derived hair cells determined that they produced voltage-dependent outwardly rectifying potassium currents and took up FM1-43 dye. The uptake of FM1-43 dye has become a general test for presence of mechanosensitive channels in the stereocilia of hair cells (Meyers et al., 2003). Notably, the FM1-43 assay has gained popularity as a benchmark for stem cell or otic progenitor derived hair cells (Hu and Corwin, 2007; Ouji et al., 2012; 2013). Hair cells with compromised or under-developed stereocilia bundles will not take up FM1-43 dye; thus, the assay is a good measure of functional maturity. FM1-43 dye uptake through mechanosensory channels is rapid—typically 5-15 seconds. In our assay we were forced to use a longer incubation (1 min) because of the nature of the tissue. With shorter incubations we could not be certain that enough dye was diffusing through the puncture hole in the organoid wall. Consequently, our method was rather crude and unquantifiable. However, the selective uptake of FM1-43 dye in hair cells, not supporting cells, suggests that FM1-43 was not entering the cells through other mechanisms (e.g. endocytosis). Further experimentation could determine if the kinetics of FM1-43 uptake are congruent with native hair cells;

perhaps using the flattened preparation used for electrophysiological recordings would be more appropriate for this analysis.

The range of outward rectifying currents (194 pA to 3,612 pA) we observed is consistent with values obtained from developing vestibular hair cells in the mouse utricle. In a 2004 study, Géléoc and colleagues demonstrated that outward potassium currents in vestibular hair cells increased from ~300 pA at E14 to ~4,000 pA at E19 using a similar voltage-step paradigm to one we used (Géléoc et al., 2004). Thus, the average outward potassium currents can be used as an indication of functional maturity. Since we saw a range of current responses, the average being 1,003 ± 527 pA, this may be an indication that hair cells representing different stages of maturity are present in organoids at day 24. Interestingly, there are two waves of hair cell production in the mouse utricle at E12 and E15, leading to a mosaic of more and less mature hair cells (Géléoc et al., 2004). It will be fascinating to see if biphasic hair cell production is preserved in organoid culture.

Our functional analysis suggests that organoid hair cells have the potential to function like native hair cells; however, we have not definitively proven that they are mechanosensitive. The gold standard for displaying mechanosensitivity is to simultaneously record currents from hair cells while mechanically stimulating the stereocilia bundles (Gillespie and Müller, 2009). Due to time and equipment restraints we were not able to conduct these experiments; however, future studies will need to incorporate this analysis to fully characterize organoid hair cells.

Limitations of the model system

Heterogeneity is both an advantage and a limitation of our 3D culture system. Unlike a monolayer format, cells in an aggregate receive varying signaling cues depending on their spatial location within the aggregate (Sykova and Nicholson, 2008; Van Winkle et al., 2012). This often leads to unsynchronized differentiation of cells located at different depths of the aggregate; the surface layer of cells differentiates faster than the core. In our model, BMP4 signaling induces a nonneural ectoderm surface layer as well as brachyury$^+$ mesendodermal cells in the central core of the aggregate. BMP4 is known to induce mesendodermal cells from PS cells. Cells in the central core express the pluripotency gene Nanog through day 3 of differentiation; thus, BMP4 likely diffuses through the surface layer of the aggregates to act on these pluripotent cells. The brachyury$^+$ cell layer produces mesenchyme-like cells that eventually cover the surface of the aggregates and give rise to muscle, cartilage and adipose. Additionally, a layer of epidermis lines the core of each aggregate. Consequently, the organization of the tissues is inverted compared to the embryo. In adult mice, an epidermial surface layer, a layer of adipose, craniofacial muscles and the temporal bone surround the fully developed inner ear. Although we have never detected the presence of bone, with further characterization, we may find that inner ear organoid culture is a model of the entire temporal region of the head. Interestingly, the presence of these cell types does not appear to encumber, and may play an essential role in, otic induction. Indeed, the periotic mesenchyme *in vivo* is an integral component of inner ear morphogenesis (Trowe et al., 2010). Due to heterogeneity, however, inner ear

organoid culture would benefit from the use of fluorescent reporter PS cell lines to help identify key phenotypic changes. Specifically, pluripotent stem cells containing fluorescently tagged marker genes for otic prosensory cells, hair cells, supporting cells and inner ear neurons would be highly amenable to this method. Fluorescent reporters would also be important for *in toto* imaging of the aggregates. Organoids develop in random coordinates around the aggregate core, making it difficult to make comparisons between aggregates. *In toto* imaging (i.e. using confocal, multiphoton or light-sheet microscopy), rather than serial analysis of cyrosections, would allow more accurate quantification of organoid attributes—number, size, hair cells per organoid, hair cell organization, etc.—and facilitate time-lapse experiments tracking the development of organoids (Keller, 2013; Sasai, 2013a). Likewise, recent advances in tissue clearing technology will aid the imaging of entire aggregates (Chung and Deisseroth, 2013; Chung et al., 2013; Ertürk et al., 2012a; 2012b).

FUTURE DIRECTIONS

Investigating the signaling mechanisms and gene regulatory networks underlying nonneural, preplacodal and inner ear induction in mouse embryos is challenging; mouse embryos are inaccessible *in vivo* and can not be cultured *ex vivo*. For obvious ethical reasons, similar analysis is impossible in human embryos. Moreover, it is difficult to collect the large amount of embryonic tissue needed to perform biochemical analyses such as chromatin immunoprecipitation. The described 3D culture system addresses these issues because it is both accessible, scalable, and the derived tissues are highly representative of their embryonic

counterparts. Besides studying early inductive events, the culture system can be used to evaluate hair cell and inner ear sensory neuron development, as well as hair cell-sensory neuron synaptogenesis. Additionally, recent advances in gene targeting technology may also be applied to create knockout and knock-in PS cells to study inner ear phenotypes (Ding et al., 2013a; 2013b). The 20-30 day, all *in vitro,* format is a quick and cost effective alternative to generating an entire mouse line if inner ear analysis is all that is desired. The 3D culture system may also be amenable to high-throughput drug screening to uncover novel compounds with regenerative or toxic affects on inner ear sensory epithelia. With these potential applications in mind I will briefly examine several interesting questions that should guide future investigations into inner ear organoid culture.

Characterizing sensory neurons: Are they authentic inner ear neurons?

Perhaps the most unexpected feature of our 3D culture system is that sensory-like neurons develop alongside inner ear organoids. These neurons extend processes toward and make what appear to be synaptic contacts with hair cells, based on expression of several synaptic markers. Subsets of neurons were characterized by expression of Calb2, Brn3a and Islet1, which are indicative of rather generic populations of sensory neurons. In the inner ear this marker profile is similar to that of Type I SGNs in the cochlear or vestibular ganglion neurons that form calyces on Type I hair cells. Further investigation will be needed to truly identify whether these sensory-like neurons are authentic inner ear neurons. Some neural ectoderm tissue develops in the core of the aggregates (see Figure 29), so it is unclear whether neurons derived from this population contribute to the sensory-

like neuron population observed in our study (Koehler et al., 2013). One approach to address this would be to examine whether neuroblasts delaminate from the otic vesicles at an earlier time point (day 12-15; i.e. prior to synapse formation). At the time of delamination *in vivo* neuroblasts are closely associated with the otic vesicle. Therefore, if the same process is mirrored in organoid culture it will be easier to establish a link between newly born neurons and otic vesicles. Because each aggregate develops differently, however, it will be a significant challenge to track neuroblasts derived from otic vesicles over time to determine that they (1) develop into sensory neurons and (2) innervate organoid epithelia. The imaging and tissue clearing modalities mention previously will certainly facilitate these future experiments.

The structure and function of the putative synapses will also need to be investigated in more detail. From our initial analysis, we cannot tell whether the individual Ctbp2+ puncta represent synapses with multiple neurons or multiple pre-synaptic structures interacting with one post-synaptic neuron. This is an important distinction with regard to comparing the model system to the *in vivo* situation. Vestibular Type II and inner cochlear hair cells both generate synapses with multiple sensory neurons (~10-20 in adult mice). Vestibular Type I and outer cochlear hair cells typically generate multiple pre-synaptic ribbons for one or a few sensory neurons, respectively. Examining this issue in more detail or investigating whether synapse formation can be manipulated in organoid culture may lead to novel insights into hair cell synaptogenesis.

Can we induce cochlear organogenesis using the model system?

Inner ear organoids seem to exclusively produce type II vestibular hair cells based on co-expression of Myo7a, Brn3c, Pax2, and Calb2, stereocilia bundle architecture, voltage-gated outward rectifying potassium currents, FM1-43 dye uptake and their organization into clusters rather than rows (Koehler et al., 2013). Previous attempts to derive hair cells have not led to a level of characterization suitable to make claims about the identity of the hair cells. Although not mentioned explicitly by the authors, the hair cells derived by Oshima and colleagues had a stereocilia bundle morphology that closely resembled that of native vestibular hair cells (i.e. type I or II) and the hair cells derived in our study. Notably, the cell and bundle morphology is difficult to discern in Ouji et al. and Chen et al. studies. Could the vestibular hair cell fate be a "default" hair cell fate? Lending credence to this notion, evolutionary studies into the inner ear have concluded that the vestibular organs develop in vertebrates prior to hearing apparatuses such as the basilar papilla and the cochlea (Fritzsch et al., 2013; Manley and Köppl, 1998). A logical extension of this discussion is to ask why cochlear-like hair cells do not develop in the Oshima et al. and our study. One can imagine that in a perfect in vitro system (i.e. containing every signaling cue and mechanical support found *in vivo*) a complete inner ear could develop in 3D culture. Most likely there are signaling cues missing in our model that contribute to cochlear specification. The literature points to sonic hedgehog signaling as a critical inducer of cochlear tissue, but whether this mechanism translates to *in vitro* differentiation remains to be seen (Bok et al., 2007; Riccomagno et al., 2002). Future studies could use Shh inhibitors or agonists to

investigate Shh's role in our 3D culture model. Likewise the balance of BMP and Wnt signaling may need to be fine tuned to yield cochlear tissue.

What are the hurdles to generating human inner ear organoids?

The mouse culture model provides a suitable blueprint for generating human inner ear cells, yet several issues may arise while translating the method. First, the timing of human development differs substantially from mouse development. If the current protocol produces hair cells in 14 days, it may take as long as 30-40 days for hair cells to emerge in human ES cell culture. An apt example can be found in the difference between mouse and human SFEBq cultures that produce retinal cups (Eiraku et al., 2011). In mouse ES cell culture, retinal cups develop by day 7 and in human ES cell culture they develop by day 26 (Nakano et al., 2012). Consequently, the timing of each treatment needs to be adjusted in our culture model. In addition, the size of the aggregates likely needs to be increased (i.e. by seeding more ES cells at the beginning of the culture); thus, proper nutrient exposure and oxygenation become major issues. A recent report demonstrated how culturing human ES cell aggregates in a bioreactor enhances the variety of tissue types the cells can self-organize into, the overall aggregate size and the health of the tissue (Lancaster et al., 2013; Sasai et al., 2012; Van Winkle et al., 2012). Notably, the researchers were able to generate aggregates 2-4 mm in diameter that contained most tissue types of the human brain—designated "cerebral organoids" (Lancaster et al., 2013). Combining the lessons learned from these studies and the work described in this dissertation should aid in the development of a human inner ear organoid culture system. It will be exciting to see whether translation of our approach to human ES cells or iPS cells

opens the door to novel cell therapies, *in vitro* disease models, or drug discovery platforms.

CONCLUSIONS

Decades of vertebrate embryo studies have culminated in our detailed understanding of the molecular and biochemical mechanisms underlying inner ear organogenesis. In this dissertation I have tested and reconfirmed much of this knowledge by successfully recreating the process *in vitro* using PS cells. Importantly, my colleagues and I demonstrated that by focusing on early cell fate transitions—nonneural and preplacode induction—tissue maintained in 3D culture can be coaxed to self-organize into elaborate inner ear organoids. The resulting model system can now be used to investigate unforeseen aspects of inner ear development and the etiology of inner ear disorders.

Portions of this discussion were modified from a forthcoming book chapter in the 4th edition of Development of Auditory and Vestibular Systems

Koehler KR, Malone A, Hashino E. Recapitulating inner ear development with pluripotent stem cells: biology and translation. Development of Auditory and Vestibular Systems 4 edition. Copyright Elseiver 2014.

REFERENCES

A J Hudspeth, R.S.L. (1988). A model for electrical resonance and frequency tuning in saccular hair cells of the bull-frog, Rana catesbeiana. The Journal of Physiology *400*, 275.

Abranches, E., Silva, M., Pradier, L., Schulz, H., Hummel, O., Henrique, D., and Bekman, E. (2009). Neural differentiation of embryonic stem cells in vitro: a road map to neurogenesis in the embryo. PLoS ONE *4*, e6286.

Aburto, M.R., Magariños, M., Leon, Y., Varela-Nieto, I., and Sanchez-Calderon, H. (2012). AKT signaling mediates IGF-I survival actions on otic neural progenitors. PLoS ONE *7*, e30790.

Ahrens, K., and Schlosser, G. (2005). Tissues and signals involved in the induction of placodal Six1 expression in Xenopus laevis. Developmental Biology *288*, 40–59.

Appler, J.M., and Goodrich, L.V. (2011). Connecting the ear to the brain: Molecular mechanisms of auditory circuit assembly. Progress in Neurobiology *93*, 488–508.

Appler, J.M., Lu, C.C., Druckenbrod, N.R., Yu, W.-M., Koundakjian, E.J., and Goodrich, L.V. (2013). Gata3 is a critical regulator of cochlear wiring. Journal of Neuroscience *33*, 3679–3691.

Azuara, V., Perry, P., Sauer, S., Spivakov, M., Jørgensen, H.F., John, R.M., Gouti, M., Casanova, M., Warnes, G., Merkenschlager, M., et al. (2006). Chromatin signatures of pluripotent cell lines. Nature Cell Biology *8*, 532–538.

Bao, H., Wong, W.H., Goldberg, J.M., and Eatock, R.A. (2003). Voltage-gated calcium channel currents in type I and type II hair cells isolated from the rat crista. Journal of Neurophysiology *90*, 155–164.

Barth, K.A., Kishimoto, Y., Rohr, K.B., Seydler, C., Schulte-Merker, S., and Wilson, S.W. (1999). Bmp activity establishes a gradient of positional information throughout the entire neural plate. Development (Cambridge, England) *126*, 4977–4987.

Bermingham-McDonogh, O., and Reh, T.A. (2011). Regulated reprogramming in the regeneration of sensory receptor cells. Neuron *71*, 389–405.

Bernardo, A.S., Faial, T., Gardner, L., Niakan, K.K., Ortmann, D., Senner, C.E., Callery, E.M., Trotter, M.W., Hemberger, M., Smith, J.C., et al. (2011). BRACHYURY and CDX2 mediate BMP-induced differentiation of human and mouse pluripotent stem cells into embryonic and extraembryonic lineages. Cell Stem Cell *9*, 144–155.

Bernstein, B.E., Mikkelsen, T.S., Xie, X., Kamal, M., Huebert, D.J., Cuff, J., Fry, B., Meissner, A., Wernig, M., Plath, K., et al. (2006). A bivalent chromatin structure marks key developmental genes in embryonic stem cells. Cell *125*, 315–326.

Boëda, B., Weil, D., and Petit, C. (2001). A specific promoter of the sensory cells of the inner ear defined by transgenesis. Human Molecular Genetics *10*, 1581–1589.

Bok, J., Dolson, D.K., Hill, P., Rüther, U., Epstein, D.J., and Wu, D.K. (2007). Opposing gradients of Gli repressor and activators mediate Shh signaling along the dorsoventral axis of the inner ear. Development (Cambridge, England) *134*, 1713–1722.

Brennand, K.J., Simone, A., Jou, J., Gelboin-Burkhart, C., Tran, N., Sangar, S., Li, Y., Mu, Y., Chen, G., Yu, D., et al. (2011). Modelling schizophrenia using human induced pluripotent stem cells. Nature *473*, 221–225.

Brigande, J.V., and Heller, S. (2009). Quo vadis, hair cell regeneration? Nature Neuroscience *12*, 679–685.

Brugmann, S.A., Pandur, P.D., Kenyon, K.L., Pignoni, F., and Moody, S.A. (2004). Six1 promotes a placodal fate within the lateral neurogenic ectoderm by functioning as both a transcriptional activator and repressor. Development (Cambridge, England) *131*, 5871–5881.

Carey, B.W., Markoulaki, S., Hanna, J.H., Faddah, D.A., Buganim, Y., Kim, J., Ganz, K., Steine, E.J., Cassady, J.P., Creyghton, M.P., et al. (2011). Reprogramming Factor Stoichiometry Influences the Epigenetic State and Biological Properties of Induced Pluripotent Stem Cells. Cell Stem Cell *9*, 588–598.

Chambers, S.M., Fasano, C.A., Papapetrou, E.P., Tomishima, M., Sadelain, M., and Studer, L. (2009). Highly efficient neural conversion of human ES and iPS cells by dual inhibition of SMAD signaling. Nature Biotechnology *27*, 275–280.

Chambers, S.M., Qi, Y., Mica, Y., Lee, G., Zhang, X.-J., Niu, L., Bilsland, J., Cao, L., Stevens, E., Whiting, P., et al. (2012). Combined small-molecule inhibition accelerates developmental timing and converts human pluripotent stem cells into nociceptors. Nature Biotechnology *30*, 715–720.

Chen, W., Johnson, S.L., Marcotti, W., Andrews, P.W., Moore, H.D., and Rivolta, M.N. (2009). Human fetal auditory stem cells can be expanded in vitro and differentiate into functional auditory neurons and hair cell-like cells. Stem Cells *27*, 1196–1204.

Chen, W., Jongkamonwiwat, N., Abbas, L., Eshtan, S.J., Johnson, S.L., Kuhn, S., Milo, M., Thurlow, J.K., Andrews, P.W., Marcotti, W., et al. (2012). Restoration of auditory evoked responses by human ES-cell-derived otic progenitors. Nature *490*, 278–282.

Chin, M.H., Pellegrini, M., Plath, K., and Lowry, W.E. (2010). Molecular Analyses of Human Induced Pluripotent Stem Cells and Embryonic Stem Cells. Stem Cell *7*, 263–269.

Chung, K., and Deisseroth, K. (2013). CLARITY for mapping the nervous system. Nature Methods *10*, 508–513.

Chung, K., Wallace, J., Kim, S.-Y., Kalyanasundaram, S., Andalman, A.S., Davidson, T.J., Mirzabekov, J.J., Zalocusky, K.A., Mattis, J., Denisin, A.K., et al. (2013). Structural and molecular interrogation of intact biological systems. Nature.

Coate, T.M., Raft, S., Zhao, X., Ryan, A.K., Crenshaw, E.B., III, and Kelley, M.W. (2012). Otic Mesenchyme Cells Regulate Spiral Ganglion Axon Fasciculation through a Pou3f4/EphA4 Signaling Pathway. Neuron *73*, 49–63.

Coraux, C., Hilmi, C., Rouleau, M., Spadafora, A., Hinnrasky, J., Ortonne, J.-P., Dani, C., and Aberdam, D. (2003). Reconstituted skin from murine embryonic stem cells. Current Biology : CB *13*, 849–853.

Corrales, C.E., Pan, L., Li, H., Liberman, M.C., Heller, S., and Edge, A.S.B. (2006). Engraftment and differentiation of embryonic stem cell-derived neural progenitor cells in the cochlear nerve trunk: growth of processes into the organ of Corti. Journal of Neurobiology *66*, 1489–1500.

Danjo, T., Eiraku, M., Muguruma, K., Watanabe, K., Kawada, M., Yanagawa, Y., Rubenstein, J.L.R., and Sasai, Y. (2011). Subregional specification of embryonic stem cell-derived ventral telencephalic tissues by timed and combinatory treatment with extrinsic signals. The Journal of Neuroscience : the Official Journal of the Society for Neuroscience *31*, 1919–1933.

Daudet, N., Ariza-McNaughton, L., and Lewis, J. (2007). Notch signalling is needed to maintain, but not to initiate, the formation of prosensory patches in the chick inner ear. Development (Cambridge, England) *134*, 2369–2378.

Davidovics, N.S., Rahman, M.A., Dai, C., Ahn, J., Fridman, G.Y., and Santina, Della, C.C. (2013). Multichannel vestibular prosthesis employing modulation of pulse rate and current with alignment precompensation elicits improved VOR performance in monkeys. Journal of the Association for Research in Otolaryngology : JARO *14*, 233–248.

De Robertis, E.M., and Kuroda, H. (2004). Dorsal-ventral patterning and neural induction in Xenopus embryos. Annual Review of Cell and Developmental Biology *20*, 285–308.

De Silva, M.G., Hildebrand, M.S., Christopoulos, H., Newman, M.R., Bell, K., Ritchie, M., Smyth, G.K., and Dahl, H.H. (2006). Gene expression changes during step-wise differentiation of embryonic stem cells along the inner ear hair cell pathway. Acta Oto-Laryngologica *126*, 1148–1157.

Desai, S.S., Zeh, C., and Lysakowski, A. (2005). Comparative morphology of rodent vestibular periphery. I. Saccular and utricular maculae. Journal of Neurophysiology *93*, 251–266.

Di Giorgio, F.P., Boulting, G.L., Bobrowicz, S., and Eggan, K.C. (2008). Human embryonic stem cell-derived motor neurons are sensitive to the toxic effect of glial cells carrying an ALS-causing mutation. Cell Stem Cell *3*, 637–648.

Dimos, J.T., Rodolfa, K.T., Niakan, K.K., Weisenthal, L.M., Mitsumoto, H., Chung, W., Croft, G.F., Saphier, G., Leibel, R., Goland, R., et al. (2008). Induced pluripotent stem cells generated from patients with ALS can be differentiated into motor neurons. Science *321*, 1218–1221.

Ding, Q., Lee, Y.-K., Schaefer, E.A.K., Peters, D.T., Veres, A., Kim, K., Kuperwasser, N., Motola, D.L., Meissner, T.B., Hendriks, W.T., et al. (2013a). A TALEN genome-editing system for generating human stem cell-based disease models. Cell Stem Cell *12*, 238–251.

Ding, Q., Regan, S.N., Xia, Y., Oostrom, L.A., Cowan, C.A., and Musunuru, K. (2013b). Enhanced Efficiency of Human Pluripotent Stem Cell Genome Editing through Replacing TALENs with CRISPRs. Cell Stem Cell *12*, 393–394.

Dolmetsch, R., and Geschwind, D.H. (2011). The Human Brain in a Dish: The Promise of iPSC-Derived Neurons. Cell *145*, 831–834.

Eiraku, M., and Sasai, Y. (2012). Mouse embryonic stem cell culture for generation of three-dimensional retinal and cortical tissues. Nature Protocols *7*, 69–79.

Eiraku, M., Takata, N., Ishibashi, H., Kawada, M., Sakakura, E., Okuda, S., Sekiguchi, K., Adachi, T., and Sasai, Y. (2011). Self-organizing optic-cup morphogenesis in three-dimensional culture. Nature *472*, 51–56.

Eiraku, M., Watanabe, K., Matsuo-Takasaki, M., Kawada, M., Yonemura, S., Matsumura, M., Wataya, T., Nishiyama, A., Muguruma, K., and Sasai, Y. (2008). Self-organized formation of polarized cortical tissues from ESCs and its active manipulation by extrinsic signals. Cell Stem Cell *3*, 519–532.

Ernfors, P., Kucera, J., Lee, K.F., Loring, J., and Jaenisch, R. (1995). Studies on the physiological role of brain-derived neurotrophic factor and neurotrophin-3 in knockout mice. The International Journal of Developmental Biology *39*, 799–807.

Ertürk, A., Becker, K., Jährling, N., Mauch, C.P., Hojer, C.D., Egen, J.G., Hellal, F., Bradke, F., Sheng, M., and Dodt, H.-U. (2012a). Three-dimensional imaging of solvent-cleared organs using 3DISCO. Nature Protocols *7*, 1983–1995.

Ertürk, A., Mauch, C.P., Hellal, F., Förstner, F., Keck, T., Becker, K., Jährling, N., Steffens, H., Richter, M., Hübener, M., et al. (2012b). Three-dimensional imaging of the unsectioned adult spinal cord to assess axon regeneration and glial responses after injury. Nature Medicine *18*, 166–171.

Evans, A.J., Thompson, B.C., Wallace, G.G., Millard, R., O'Leary, S.J., Clark, G.M., Shepherd, R.K., and Richardson, R.T. (2009). Promoting neurite outgrowth from spiral ganglion neuron explants using polypyrrole/BDNF-coated electrodes. Journal of Biomedical Materials Research Part A *91A*, 241–250.

Fariñas, I., Jones, K.R., Tessarollo, L., Vigers, A.J., Huang, E., Kirstein, M., de Caprona, D.C., Coppola, V., Backus, C., Reichardt, L.F., et al. (2001). Spatial shaping of cochlear innervation by temporally regulated neurotrophin expression. The Journal of Neuroscience : the Official Journal of the Society for Neuroscience *21*, 6170–6180.

Freter, S., Muta, Y., Mak, S.-S., Rinkwitz, S., and Ladher, R.K. (2008). Progressive restriction of otic fate: the role of FGF and Wnt in resolving inner ear potential. Development (Cambridge, England) *135*, 3415–3424.

Fritzsch, B., Matei, V.A., Nichols, D.H., Bermingham, N., Jones, K., Beisel, K.W., and Wang, V.Y. (2005). Atoh1 null mice show directed afferent fiber growth to undifferentiated ear sensory epithelia followed by incomplete fiber retention. Developmental Dynamics : an Official Publication of the American Association of Anatomists *233*, 570–583.

Fritzsch, B. (2003). Development of inner ear afferent connections: forming primary neurons and connecting them to the developing sensory epithelia. Brain Research Bulletin *60*, 423–433.

Fritzsch, B., Eberl, D.F., and Beisel, K.W. (2010). The role of bHLH genes in ear development and evolution: revisiting a 10-year-old hypothesis. Cellular and Molecular Life Sciences : CMLS *67*, 3089–3099.

Fritzsch, B., Pan, N., Jahan, I., Duncan, J.S., Kopecky, B.J., Elliott, K.L., Kersigo, J., and Yang, T. (2013). Evolution and development of the tetrapod auditory system: an organ of Corti-centric perspective. Evolution & Development *15*, 63–79.

Fujiwara, H., Hayashi, Y., Sanzen, N., Kobayashi, R., Weber, C.N., Emoto, T., Futaki, S., Niwa, H., Murray, P., Edgar, D., et al. (2007). Regulation of mesodermal differentiation of mouse embryonic stem cells by basement membranes. The Journal of Biological Chemistry *282*, 29701–29711.

Gaboyard, S., Chabbert, C., Travo, C., Bancel, F., Lehouelleur, J., Yamauchi, D., Marcus, D.C., and Sans, A. (2005). Three-dimensional culture of newborn rat utricle using an extracellular matrix promotes formation of a cyst. Neuroscience *133*, 253–265.

Gale, J.E., Marcotti, W., Kennedy, H.J., Kros, C.J., and Richardson, G.P. (2001). FM1-43 dye behaves as a permeant blocker of the hair-cell mechanotransducer channel. Journal of Neuroscience *21*, 7013–7025.

Géléoc, G.S.G., and Holt, J.R. (2003). Developmental acquisition of sensory transduction in hair cells of the mouse inner ear. Nature Neuroscience *6*, 1019–1020.

Géléoc, G.S.G., Risner, J.R., and Holt, J.R. (2004). Developmental acquisition of voltage-dependent conductances and sensory signaling in hair cells of the embryonic mouse inner ear. Journal of Neuroscience *24*, 11148–11159.

Gillespie, P.G., and Müller, U. (2009). Mechanotransduction by hair cells: models, molecules, and mechanisms. Cell *139*, 33–44.

Glavic, A., Maris Honoré, S., Gloria Feijóo, C., Bastidas, F., Allende, M.L., and Mayor, R. (2004). Role of BMP signaling and the homeoprotein Iroquois in the specification of the cranial placodal field. Developmental Biology *272*, 89–103.

Gonzalez-Cordero, A., West, E.L., Pearson, R.A., Duran, Y., Carvalho, L.S., Chu, C.J., Naeem, A., Blackford, S.J.I., Georgiadis, A., Lakowski, J., et al. (2013). Photoreceptor precursors derived from three-dimensional embryonic stem cell cultures integrate and mature within adult degenerate retina. Nature Biotechnology *31*, 741–747.

Gore, A., Li, Z., Fung, H.-L., Young, J.E., Agarwal, S., Antosiewicz-Bourget, J., Canto, I., Giorgetti, A., Israel, M.A., Kiskinis, E., et al. (2011). Somatic coding mutations in human induced pluripotent stem cells. Nature *471*, 63–67.

Green, H., Easley, K., and Iuchi, S. (2003). Marker succession during the development of keratinocytes from cultured human embryonic stem cells. Proceedings of the National Academy of Sciences of the United States of America *100*, 15625–15630.

Grocott, T., Tambalo, M., and Streit, A. (2012). The peripheral sensory nervous system in the vertebrate head: A gene regulatory perspective. Developmental Biology *370*, 3–23.

Groves, A.K., and Fekete, D.M. (2011). Shaping sound in space: the regulation of inner ear patterning. Development (Cambridge, England) *139*, 245–257.

Groves, A.K. (2010). The challenge of hair cell regeneration. Experimental Biology and Medicine (Maywood, N.J.) *235*, 434–446.

Guenther, M.G., Frampton, G.M., Soldner, F., Hockemeyer, D., Mitalipova, M., Jaenisch, R., and Young, R.A. (2010). Chromatin structure and gene expression programs of human embryonic and induced pluripotent stem cells. Cell Stem Cell *7*, 249–257.

Hama, H., Kurokawa, H., Kawano, H., Ando, R., Shimogori, T., Noda, H., Fukami, K., Sakaue-Sawano, A., and Miyawaki, A. (2011). Scale: a chemical approach for fluorescence imaging and reconstruction of transparent mouse brain. Nature Neuroscience *14*, 1481–1488.

Han, S.S.W., Williams, L.A., and Eggan, K.C. (2011). Constructing and Deconstructing Stem Cell Models of Neurological Disease. Neuron *70*, 626–644.

Hanna, J.H., Saha, K., and Jaenisch, R. (2010). Pluripotency and cellular reprogramming: facts, hypotheses, unresolved issues. Cell *143*, 508–525.

Hansen, D.V., Rubenstein, J.L.R., and Kriegstein, A.R. (2011). Deriving Excitatory Neurons of the Neocortex from Pluripotent Stem Cells. Neuron *70*, 645–660.

Hartman, B.H., Reh, T.A., and Bermingham-McDonogh, O. (2010). Notch signaling specifies prosensory domains via lateral induction in the developing mammalian inner ear. Proceedings of the National Academy of Sciences of the United States of America *107*, 15792–15797.

Harvey, N.T., Hughes, J.N., Lonic, A., Yap, C., Long, C., Rathjen, P.D., and Rathjen, J. (2010). Response to BMP4 signalling during ES cell differentiation defines intermediates of the ectoderm lineage. Journal of Cell Science *123*, 1796–1804.

Hausdorff, J.M., Rios, D.A., and Edelberg, H.K. (2001). Gait variability and fall risk in community-living older adults: a 1-year prospective study. Archives of Physical Medicine and Rehabilitation *82*, 1050–1056.

Hayashi, K., Ohta, H., Kurimoto, K., Aramaki, S., and Saitou, M. (2011). Reconstitution of the mouse germ cell specification pathway in culture by pluripotent stem cells. Cell *146*, 519–532.

Hegarty, J.L., Kay, A.R., and Green, S.H. (1997). Trophic support of cultured spiral ganglion neurons by depolarization exceeds and is additive with that by neurotrophins or cAMP and requires elevation of [Ca2+]i within a set range. The Journal of Neuroscience : the Official Journal of the Society for Neuroscience *17*, 1959–1970.

Hemmati-Brivanlou, A., and Melton, D. (1997). Vertebrate embryonic cells will become nerve cells unless told otherwise. Cell *88*, 13–17.

Hou, P., Li, Y., Zhang, X., Liu, C., Guan, J., Li, H., Zhao, T., Ye, J., Yang, W., Liu, K., et al. (2013). Pluripotent stem cells induced from mouse somatic cells by small-molecule compounds. Science *341*, 651–654.

Hu, Z., and Corwin, J.T. (2007). Inner ear hair cells produced in vitro by a mesenchymal-to-epithelial transition. Proceedings of the National Academy of Sciences of the United States of America *104*, 16675–16680.

Hu, Z., Andäng, M., Ni, D., and Ulfendahl, M. (2005). Neural cograft stimulates the survival and differentiation of embryonic stem cells in the adult mammalian auditory system. Brain Research *1051*, 137–144.

Hu, Z., Ulfendahl, M., and Olivius, N.P. (2004). Central migration of neuronal tissue and embryonic stem cells following transplantation along the adult auditory nerve. Brain Research *1026*, 68–73.

Huch, M., Dorrell, C., Boj, S.F., van Es, J.H., Li, V.S.W., van de Wetering, M., Sato, T., Hamer, K., Sasaki, N., Finegold, M.J., et al. (2013). In vitro expansion of single Lgr5+ liver stem cells induced by Wnt-driven regeneration. Nature *494*, 247–250.

Ikeda, H., Osakada, F., Watanabe, K., Mizuseki, K., Haraguchi, T., Miyoshi, H., Kamiya, D., Honda, Y., Sasai, N., Yoshimura, N., et al. (2005). Generation of Rx+/Pax6+ neural retinal precursors from embryonic stem cells. Proceedings of the National Academy of Sciences of the United States of America *102*, 11331–11336.

Itoh, M., Kiuru, M., Cairo, M.S., and Christiano, A.M. (2011). Generation of keratinocytes from normal and recessive dystrophic epidermolysis bullosa-induced pluripotent stem cells. Proceedings of the National Academy of Sciences of the United States of America *108*, 8797–8802.

Ivanovitch, K., Cavodeassi, F., and Wilson, S.W. (2013). Precocious Acquisition of Neuroepithelial Character in the Eye Field Underlies the Onset of Eye Morphogenesis. Developmental Cell.

Jegalian, B.G., and De Robertis, E.M. (1992). Homeotic transformations in the mouse induced by overexpression of a human Hox3.3 transgene. Cell *71*, 901–910.

Jeon, S.J., Oshima, K., Heller, S., and Edge, A.S. (2007). Bone marrow mesenchymal stem cells are progenitors in vitro for inner ear hair cells. Molecular and Cellular Neurosciences *34*, 59–68.

Kamiya, D., Banno, S., Sasai, N., Ohgushi, M., Inomata, H., Watanabe, K., Kawada, M., Yakura, R., Kiyonari, H., Nakao, K., et al. (2011). Intrinsic transition of embryonic stem-cell differentiation into neural progenitors. Nature *470*, 503–509.

Keller, P.J. (2013). Imaging Morphogenesis: Technological Advances and Biological Insights. Science (New York, NY) *340*, 1234168–1234168.

Kinney, M.A., Sargent, C.Y., and McDevitt, T.C. (2011). The multiparametric effects of hydrodynamic environments on stem cell culture. Tissue Engineering. Part B, Reviews *17*, 249–262.

Kishimoto, Y., Lee, K.H., Zon, L., Hammerschmidt, M., and Schulte-Merker, S. (1997). The molecular nature of zebrafish swirl: BMP2 function is essential during early dorsoventral patterning. Development (Cambridge, England) *124*, 4457–4466.

Koehler, K.R., Mikosz, A.M., Molosh, A.I., Patel, D., and Hashino, E. (2013). Generation of inner ear sensory epithelia from pluripotent stem cells in 3D culture. Nature *500*, 217–221.

Koehler, K.R., Tropel, P., Theile, J.W., Kondo, T., Cummins, T.R., Viville, S., and Hashino, E. (2011). Extended passaging increases the efficiency of neural differentiation from induced pluripotent stem cells. BMC Neurosci *12*, 82.

Kondo, T., Johnson, S.A., Yoder, M.C., Romand, R., and Hashino, E. (2005). Sonic hedgehog and retinoic acid synergistically promote sensory fate specification from bone marrow-derived pluripotent stem cells. Proceedings of the National Academy of Sciences of the United States of America *102*, 4789–4794.

Kondo, T., Matsuoka, A.J., Shimomura, A., Koehler, K.R., Chan, R.J., Miller, J.M., Srour, E.F., and Hashino, E. (2011). Wnt Signaling Promotes Neuronal Differentiation From Mesenchymal Stem Cells Through Activation of Tlx3 - Kondo - STEM CELLS - Wiley Online Library. Stem Cells *29*, 836–846.

Kondo, T., Sheets, P.L., Zopf, D.A., Aloor, H.L., Cummins, T.R., Chan, R.J., and Hashino, E. (2008). Tlx3 exerts context-dependent transcriptional regulation and promotes neuronal differentiation from embryonic stem cells. Proceedings of the National Academy of Sciences of the United States of America *105*, 5780–5785.

Kondo, T., Asai, M., Tsukita, K., Kutoku, Y., Ohsawa, Y., Sunada, Y., Imamura, K., Egawa, N., Yahata, N., Okita, K., et al. (2013). Modeling Alzheimer's disease with iPSCs reveals stress phenotypes associated with intracellular Aβ and differential drug responsiveness. Cell Stem Cell *12*, 487–496.

Kriks, S., Shim, J.-W., Piao, J., Ganat, Y.M., Wakeman, D.R., Xie, Z., Carrillo-Reid, L., Auyeung, G., Antonacci, C., Buch, A., et al. (2011). Dopamine neurons derived from human ES cells efficiently engraft in animal models of Parkinson's disease. Nature.

Kros, C.J., Ruppersberg, J.P., and Rüsch, A. (1998). Expression of a potassium current in inner hair cells during development of hearing in mice. Nature *394*, 281–284.

Kwon, H.-J., and Riley, B.B. (2009). Mesendodermal signals required for otic induction: Bmp-antagonists cooperate with Fgf and can facilitate formation of ectopic otic tissue. Developmental Dynamics : an Official Publication of the American Association of Anatomists *238*, 1582–1594.

Kwon, H.-J., Bhat, N., Sweet, E.M., Cornell, R.A., and Riley, B.B. (2010). Identification of early requirements for preplacodal ectoderm and sensory organ development. PLoS Genetics *6*.

Ladher, R.K., O'Neill, P., and Begbie, J. (2010). From shared lineage to distinct functions: the development of the inner ear and epibranchial placodes. Development (Cambridge, England) *137*, 1777–1785.

Laine, H., Sulg, M., Kirjavainen, A., and Pirvola, U. (2010). Cell cycle regulation in the inner ear sensory epithelia: role of cyclin D1 and cyclin-dependent kinase inhibitors. Developmental Biology *337*, 134–146.

Lancaster, M.A., Renner, M., Martin, C.-A., Wenzel, D., Bicknell, L.S., Hurles, M.E., Homfray, T., Penninger, J.M., Jackson, A.P., and Knoblich, J.A. (2013). Cerebral organoids model human brain development and microcephaly. Nature –.

Lang, H., Schulte, B.A., and Schmiedt, R.A. (2005). Ouabain induces apoptotic cell death in type I spiral ganglion neurons, but not type II neurons. Journal of the Association for Research in Otolaryngology : JARO *6*, 63–74.

Leung, A.W., Kent Morest, D., and Li, J.Y.H. (2013). Differential BMP signaling controls formation and differentiation of multipotent preplacodal ectoderm progenitors from human embryonic stem cells. Developmental Biology *379*, 208–220.

Li, A., Xue, J., and Peterson, E.H. (2008). Architecture of the mouse utricle: macular organization and hair bundle heights. Journal of Neurophysiology *99*, 718–733.

Li, H., Roblin, G., Liu, H., and Heller, S. (2003). Generation of hair cells by stepwise differentiation of embryonic stem cells. Proceedings of the National Academy of Sciences of the United States of America *100*, 13495–13500.

Li, W., and Ding, S. (2010). Small molecules that modulate embryonic stem cell fate and somatic cell reprogramming. Trends in Pharmacological Sciences *31*, 36–45.

Lim, H.H., Lenarz, M., and Lenarz, T. (2009). Auditory midbrain implant: a review. Trends in Amplification *13*, 149–180.

Litsiou, A., Hanson, S., and Streit, A. (2005). A balance of FGF, BMP and WNT signalling positions the future placode territory in the head. Development (Cambridge, England) *132*, 4051–4062.

Lleras-Forero, L., and Streit, A. (2012). Development of the sensory nervous system in the vertebrate head: the importance of being on time. Current Opinion in Genetics & Development *22*, 315–322.

Lu, C.C., Appler, J.M., Houseman, E.A., and Goodrich, L.V. (2011). Developmental profiling of spiral ganglion neurons reveals insights into auditory circuit assembly. The Journal of Neuroscience : the Official Journal of the Society for Neuroscience *31*, 10903–10918.

Lysakowski, A., Gaboyard-Niay, S., Calin-Jageman, I., Chatlani, S., Price, S.D., and Eatock, R.A. (2011). Molecular microdomains in a sensory terminal, the vestibular calyx ending. Journal of Neuroscience *31*, 10101–10114.

Ma, L., Hu, B., Liu, Y., Vermilyea, S.C., Liu, H., Gao, L., Sun, Y., Zhang, X., and Zhang, S.-C. (2012). Human Embryonic Stem Cell-Derived GABA Neurons Correct Locomotion Deficits in Quinolinic Acid-Lesioned Mice. Cell Stem Cell *10*, 455–464.

Ma, Q., Anderson, D.J., and Fritzsch, B. (2000). Neurogenin 1 null mutant ears develop fewer, morphologically normal hair cells in smaller sensory epithelia devoid of innervation. Journal of the Association for Research in Otolaryngology : JARO *1*, 129–143.

Magarinos, M., Aburto, M.R., Sanchez-Calderon, H., Munoz-Agudo, C., Rapp, U.R., and Varela-Nieto, I. (2010). RAF kinase activity regulates neuroepithelial cell proliferation and neuronal progenitor cell differentiation during early inner ear development. PLoS ONE *5*, e14435.

Manley, G.A., and Köppl, C. (1998). Phylogenetic development of the cochlea and its innervation. Current Opinion in Neurobiology *8*, 468–474.

Marchetto, M.C.N., Carromeu, C., Acab, A., Yu, D., Yeo, G.W., Mu, Y., Chen, G., Gage, F.H., and Muotri, A.R. (2010). A model for neural development and treatment of Rett syndrome using human induced pluripotent stem cells. Cell *143*, 527–539.

Marcotti, W. (2012). Functional assembly of mammalian cochlear hair cells. Experimental Physiology *97*, 438–451.

Martin, K., and Groves, A.K. (2006). Competence of cranial ectoderm to respond to Fgf signaling suggests a two-step model of otic placode induction. Development (Cambridge, England) *133*, 877–887.

Matsuoka, A.J., Kondo, T., Miyamoto, R.T., and Hashino, E. (2006). In vivo and in vitro characterization of bone marrow-derived stem cells in the cochlea. Laryngoscope *116*, 1363–1367.

Matsuoka, A.J., Kondo, T., Miyamoto, R.T., and Hashino, E. (2007). Enhanced survival of bone-marrow-derived pluripotent stem cells in an animal model of auditory neuropathy. Laryngoscope *117*, 1629–1635.

McCarroll, M.N., Lewis, Z.R., Culbertson, M.D., Martin, B.L., Kimelman, D., and Nechiporuk, A.V. (2012). Graded levels of Pax2a and Pax8 regulate cell differentiation during sensory placode formation. Development (Cambridge, England) *139*, 2740–2750.

McCracken, K.W., Howell, J.C., Wells, J.M., and Spence, J.R. (2011). Generating human intestinal tissue from pluripotent stem cells in vitro. Nature Protocols *6*, 1920–1928.

Metallo, C.M., Ji, L., de Pablo, J.J., and Palecek, S.P. (2008). Retinoic acid and bone morphogenetic protein signaling synergize to efficiently direct epithelial differentiation of human embryonic stem cells. Stem Cells *26*, 372–380.

Meyer, J.S., Shearer, R.L., Capowski, E.E., Wright, L.S., Wallace, K.A., McMillan, E.L., Zhang, S.-C., and Gamm, D.M. (2009). Modeling early retinal development with human embryonic and induced pluripotent stem cells. Proceedings of the National Academy of Sciences of the United States of America *106*, 16698–16703.

Meyers, J.R., MacDonald, R.B., Duggan, A., Lenzi, D., Standaert, D.G., Corwin, J.T., and Corey, D.P. (2003). Lighting up the senses: FM1-43 loading of sensory cells through nonselective ion channels. Journal of Neuroscience *23*, 4054–4065.

Millard, R.E., and Shepherd, R.K. (2007). A fully implantable stimulator for use in small laboratory animals. Journal of Neuroscience Methods *166*, 168–177.

Muguruma, K., Nishiyama, A., Ono, Y., Miyawaki, H., Mizuhara, E., Hori, S., Kakizuka, A., Obata, K., Yanagawa, Y., Hirano, T., et al. (2010). Ontogeny-recapitulating generation and tissue integration of ES cell-derived Purkinje cells. Nature Neuroscience *13*, 1171–1180.

Nakano, T., Ando, S., Takata, N., Kawada, M., Muguruma, K., Sekiguchi, K., Saito, K., Yonemura, S., Eiraku, M., and Sasai, Y. (2012). Self-Formation of Optic Cups and Storable Stratified Neural Retina from Human ESCs. Cell Stem Cell *10*, 771–785.

Nasu, M., Takata, N., Danjo, T., Sakaguchi, H., Kadoshima, T., Futaki, S., Sekiguchi, K., Eiraku, M., and Sasai, Y. (2012). Robust Formation and Maintenance of Continuous Stratified Cortical Neuroepithelium by Laminin-Containing Matrix in Mouse ES Cell Culture. PLoS ONE *7*, e53024.

Neave, B., Holder, N., and Patient, R. (1997). A graded response to BMP-4 spatially coordinates patterning of the mesoderm and ectoderm in the zebrafish. Mechanisms of Development *62*, 183–195.

Neves, J., Parada, C., Chamizo, M., and Giraldez, F. (2011). Jagged 1 regulates the restriction of Sox2 expression in the developing chicken inner ear: a mechanism for sensory organ specification. Development (Cambridge, England) *138*, 735–744.

Neves, J., Uchikawa, M., Bigas, A., and Giraldez, F. (2012). The Prosensory Function of Sox2 in the Chicken Inner Ear Relies on the Direct Regulation of Atoh1. PLoS ONE *7*, e30871.

Newman, A.M., and Cooper, J.B. (2010). Lab-specific gene expression signatures in pluripotent stem cells. Cell Stem Cell *7*, 258–262.

Nichols, J., and Smith, A. (2009). Naive and primed pluripotent states. Cell Stem Cell *4*, 487–492.

Oesterle, E.C., Campbell, S., Taylor, R.R., Forge, A., and Hume, C.R. (2007). Sox2 and Jagged1 Expression in Normal and Drug-Damaged Adult Mouse Inner Ear. Journal of the Association for Research in Otolaryngology : JARO *9*, 65–89.

Ohyama, T., Mohamed, O.A., Taketo, M.M., Dufort, D., and Groves, A.K. (2006). Wnt signals mediate a fate decision between otic placode and epidermis. Development (Cambridge, England) *133*, 865–875.

Okano, T., Nakagawa, T., Endo, T., Kim, T.S., Kita, T., Tamura, T., Matsumoto, M., Ohno, T., Sakamoto, T., Iguchi, F., et al. (2005). Engraftment of embryonic stem cell-derived neurons into the cochlear modiolus. NeuroReport *16*, 1919–1922.

Oshima, K., Shin, K., Diensthuber, M., Peng, A.W., Ricci, A.J., and Heller, S. (2010). Mechanosensitive Hair Cell-like Cells from Embryonic and Induced Pluripotent Stem Cells. Cell *141*, 704–716.

Ouji, Y., Ishizaka, S., Nakamura-Uchiyama, F., and Yoshikawa, M. (2012). In vitro differentiation of mouse embryonic stem cells into inner ear hair cell-like cells using stromal cell conditioned medium. Cell Death and Disease *3*, e314.

Ouji, Y., Ishizaka, S., Nakamura-Uchiyama, F., Wanaka, A., and Yoshikawa, M. (2013). Induction of inner ear hair cell-like cells from Math1-transfected mouse ES cells. Cell Death and Disease *4*, e700.

Pankratz, M.T., Li, X.-J., LaVaute, T.M., Lyons, E.A., Chen, X., and Zhang, S.-C. (2007). Directed neural differentiation of human embryonic stem cells via an obligated primitive anterior stage. Stem Cells *25*, 1511–1520.

Park, I.-H., Arora, N., Huo, H., Maherali, N., Ahfeldt, T., Shimamura, A., Lensch, M.W., Cowan, C., Hochedlinger, K., and Daley, G.Q. (2008). Disease-specific induced pluripotent stem cells. Cell *134*, 877–886.

Patthey, C., and Gunhaga, L. (2011). Specification and regionalisation of the neural plate border. The European Journal of Neuroscience *34*, 1516–1528.

Patthey, C., Edlund, T., and Gunhaga, L. (2009). Wnt-regulated temporal control of BMP exposure directs the choice between neural plate border and epidermal fate. Development (Cambridge, England) *136*, 73–83.

Pera, E.M., Wessely, O., Li, S.Y., and De Robertis, E.M. (2001). Neural and head induction by insulin-like growth factor signals. Developmental Cell *1*, 655–665.

Pieper, M., Ahrens, K., Rink, E., Peter, A., and Schlosser, G. (2012). Differential distribution of competence for panplacodal and neural crest induction to non-neural and neural ectoderm. Development (Cambridge, England) *139*, 1175–1187.

Qin, H., Zhao, L.D., Sun, J.H., Ren, L.L., Guo, W.W., Liu, H.Z., Zhai, S.Q., and Yang, S.M. (2011). The differentiation of mesenchymal stem cells into inner ear hair cell-like cells in vitro. Acta Oto-Laryngologica *131*, 1136–1141.

Raft, S., Koundakjian, E.J., Quinones, H., Jayasena, C.S., Goodrich, L.V., Johnson, J.E., Segil, N., and Groves, A.K. (2007). Cross-regulation of Ngn1 and Math1 coordinates the production of neurons and sensory hair cells during inner ear development. Development (Cambridge, England) *134*, 4405–4415.

Regala, C., Duan, M., Zou, J., Salminen, M., and Olivius, P. (2005). Xenografted fetal dorsal root ganglion, embryonic stem cell and adult neural stem cell survival following implantation into the adult vestibulocochlear nerve. Experimental Neurology *193*, 326–333.

Reichert, S., Randall, R.A., and Hill, C.S. (2013). A BMP regulatory network controls ectodermal cell fate decisions at the neural plate border. Development (Cambridge, England) *140*, 4435–4444.

Reversade, B., and De Robertis, E.M. (2005). Regulation of ADMP and BMP2/4/7 at opposite embryonic poles generates a self-regulating morphogenetic field. Cell *123*, 1147–1160.

Reyes, J.H., O'Shea, K.S., Wys, N.L., Velkey, J.M., Prieskorn, D.M., Wesolowski, K., Miller, J.M., and Altschuler, R.A. (2008). Glutamatergic neuronal differentiation of mouse embryonic stem cells after transient expression of neurogenin 1 and treatment with BDNF and GDNF: in vitro and in vivo studies. Journal of Neuroscience *28*, 12622–12631.

Riccomagno, M.M., Martinu, L., Mulheisen, M., Wu, D.K., and Epstein, D.J. (2002). Specification of the mammalian cochlea is dependent on Sonic hedgehog. Genes & Development *16*, 2365–2378.

Sahly, I., El-Amraoui, A., Abitbol, M., Petit, C., and Dufier, J.L. (1997). Expression of myosin VIIA during mouse embryogenesis. Anatomy and Embryology *196*, 159–170.

Sandoe, J., and Eggan, K. (2013). Opportunities and challenges of pluripotent stem cell neurodegenerative disease models. Nature Neuroscience *16*, 780–789.

Sasai, Y. (2013a). Cytosystems dynamics in self-organization of tissue architecture. Nature *493*, 318–326.

Sasai, Y. (2013b). Next-Generation Regenerative Medicine: Organogenesis from Stem Cells in 3D Culture. Cell Stem Cell *12*, 520–530.

Sasai, Y., Eiraku, M., and Suga, H. (2012). In vitro organogenesis in three dimensions: self-organising stem cells. Development (Cambridge, England) *139*, 4111–4121.

Sato, T., Vries, R.G., Snippert, H.J., van de Wetering, M., Barker, N., Stange, D.E., van Es, J.H., Abo, A., Kujala, P., Peters, P.J., et al. (2009). Single Lgr5 stem cells build crypt-villus structures in vitro without a mesenchymal niche. Nature *459*, 262–265.

Schlosser, G. (2006). Induction and specification of cranial placodes. Developmental Biology *294*, 303–351.

Schmiedt, R.A., Okamura, H.-O., Lang, H., and Schulte, B.A. (2002). Ouabain application to the round window of the gerbil cochlea: a model of auditory neuropathy and apoptosis. Journal of the Association for Research in Otolaryngology : JARO *3*, 223–233.

Schneider, M.R., Schmidt-Ullrich, R., and Paus, R. (2009). The hair follicle as a dynamic miniorgan. Current Biology : CB *19*, R132–R142.

Sekiya, T., Holley, M.C., Kojima, K., Matsumoto, M., Helyer, R., and Ito, J. (2007). Transplantation of conditionally immortal auditory neuroblasts to the auditory nerve. The European Journal of Neuroscience *25*, 2307–2318.

Shepherd, R.K., Coco, A., Epp, S.B., and Crook, J.M. (2005). Chronic depolarization enhances the trophic effects of brain-derived neurotrophic factor in rescuing auditory neurons following a sensorineural hearing loss. The Journal of Comparative Neurology *486*, 145–158.

Shi, F., and Edge, A.S.B. (2013). Prospects for replacement of auditory neurons by stem cells. Hearing Research *297*, 106–112.

Silos-Santiago, I., Fagan, A.M., Garber, M., Fritzsch, B., and Barbacid, M. (1997). Severe sensory deficits but normal CNS development in newborn mice lacking TrkB and TrkC tyrosine protein kinase receptors. The European Journal of Neuroscience *9*, 2045–2056.

Spence, J.R., Mayhew, C.N., Rankin, S.A., Kuhar, M.F., Vallance, J.E., Tolle, K., Hoskins, E.E., Kalinichenko, V.V., Wells, S.I., Zorn, A.M., et al. (2010). Directed differentiation of human pluripotent stem cells into intestinal tissue in vitro. Nature *470*, 105–109.

Sprinzl, G.M., and Riechelmann, H. (2010). Current trends in treating hearing loss in elderly people: a review of the technology and treatment options - a mini-review. Gerontology *56*, 351–358.

Stern, C.D. (2005). Neural induction: old problem, new findings, yet more questions. Development (Cambridge, England) *132*, 2007–2021.

Stevens, G., Flaxman, S., Brunskill, E., Mascarenhas, M., Mathers, C.D., and Finucane, M. (2011). Global and regional hearing impairment prevalence: an analysis of 42 studies in 29 countries. European Journal of Public Health *32*, 146–152.

Suga, H., Kadoshima, T., Minaguchi, M., Ohgushi, M., Soen, M., Nakano, T., Takata, N., Wataya, T., Muguruma, K., Miyoshi, H., et al. (2011). Self-formation of functional adenohypophysis in three-dimensional culture. Nature *480*, 57–62.

Sykova, E., and Nicholson, C. (2008). Diffusion in brain extracellular space. Physiological Reviews *88*, 1277–1340.

Takahashi, K., and Yamanaka, S. (2006). Induction of pluripotent stem cells from mouse embryonic and adult fibroblast cultures by defined factors. Cell *126*, 663–676.

Tritsch, N.X., and Bergles, D.E. (2010). Developmental Regulation of Spontaneous Activity in the Mammalian Cochlea. The Journal of Neuroscience : the Official Journal of the Society for Neuroscience *30*, 1539–1550.

Tritsch, N.X., Rodríguez-Contreras, A., Crins, T.T.H., Wang, H.C., Borst, J.G.G., and Bergles, D.E. (2010). Calcium action potentials in hair cells pattern auditory neuron activity before hearing onset. Nature Neuroscience *13*, 1050–1052.

Trowe, M.-O., Shah, S., Petry, M., Airik, R., Schuster-Gossler, K., Kist, R., and Kispert, A. (2010). Loss of Sox9 in the periotic mesenchyme affects mesenchymal expansion and differentiation, and epithelial morphogenesis during cochlea development in the mouse. Developmental Biology *342*, 51–62.

Van Winkle, A.P., Gates, I.D., and Kallos, M.S. (2012). Mass transfer limitations in embryoid bodies during human embryonic stem cell differentiation. Cells Tissues Organs (Print) *196*, 34–47.

Warchol, M.E., and Richardson, G.P. (2009). Expression of the Pax2 transcription factor is associated with vestibular phenotype in the avian inner ear. Developmental Neurobiology *69*, 191–202.

Watanabe, K., Kamiya, D., Nishiyama, A., Katayama, T., Nozaki, S., Kawasaki, H., Watanabe, Y., Mizuseki, K., and Sasai, Y. (2005). Directed differentiation of telencephalic precursors from embryonic stem cells. Nature Neuroscience *8*, 288–296.

Watt, F.M., and Huck, W.T.S. (2013). Role of the extracellular matrix in regulating stem cell fate. Nature Reviews Molecular Cell Biology *14*, 467–473.

White, P.M., Stone, J.S., Groves, A.K., and Segil, N. (2012). EGFR signaling is required for regenerative proliferation in the cochlea: conservation in birds and mammals. Developmental Biology *363*, 191–200.

Williams, L.A., Davis-Dusenbery, B.N., and Eggan, K.C. (2012). SnapShot: directed differentiation of pluripotent stem cells. Cell *149*, 1174–1174.e1.

Wilson, P.A., and Hemmati-Brivanlou, A. (1995). Induction of epidermis and inhibition of neural fate by Bmp-4. Nature *376*, 331–333.

Wilson, P.A., Lagna, G., Suzuki, A., and Hemmati-Brivanlou, A. (1997). Concentration-dependent patterning of the Xenopus ectoderm by BMP4 and its signal transducer Smad1. Development (Cambridge, England) *124*, 3177–3184.

Wray, J., Kalkan, T., Gomez-Lopez, S., Eckardt, D., Cook, A., Kemler, R., and Smith, A. (2011). Inhibition of glycogen synthase kinase-3 alleviates Tcf3 repression of the pluripotency network and increases embryonic stem cell resistance to differentiation. Nature Cell Biology *13*, 838–845.

Yamanaka, S. (2009). A fresh look at iPS cells. Cell *137*, 13–17.

Yamanaka, S. (2012). Induced Pluripotent Stem Cells: Past, Present, and Future. Cell Stem Cell *10*, 678–684.

Yang, C., Yang, Y., Brennan, L., Bouhassira, E.E., Kantorow, M., and Cvekl, A. (2010). Efficient generation of lens progenitor cells and lentoid bodies from human embryonic stem cells in chemically defined conditions. The FASEB Journal *24*, 3274–3283.

Yang, T., Kersigo, J., Jahan, I., Pan, N., and Fritzsch, B. (2011). The molecular basis of making spiral ganglion neurons and connecting them to hair cells of the organ of Corti. Hearing Research *278*, 21–33.

Yardley, N., and García-Castro, M.I. (2012). FGF signaling transforms non-neural ectoderm into neural crest. Developmental Biology *372*, 166–177.

Ying, Q.-L., Stavridis, M., Griffiths, D., Li, M., and Smith, A. (2003). Conversion of embryonic stem cells into neuroectodermal precursors in adherent monoculture.

Ying, Q.-L., Wray, J., Nichols, J., Batlle-Morera, L., Doble, B., Woodgett, J., Cohen, P., and Smith, A. (2008). The ground state of embryonic stem cell self-renewal. Nature *453*, 519–523.

Young, R.A. (2011). Control of the embryonic stem cell state. Cell *144*, 940–954.

Yu, J., Vodyanik, M.A., Smuga-Otto, K., Antosiewicz-Bourget, J., Frane, J.L., Tian, S., Nie, J., Jonsdottir, G.A., Ruotti, V., Stewart, R., et al. (2007). Induced pluripotent stem cell lines derived from human somatic cells. Science (New York, NY) *318*, 1917–1920.

Zhang, S.C., Wernig, M., Duncan, I.D., Brüstle, O., and Thomson, J.A. (2001). In vitro differentiation of transplantable neural precursors from human embryonic stem cells. Nature Biotechnology *19*, 1129–1133.

CURRICULUM VITAE

KARL RUSSELL KOEHLER

Education

2004-2008	Undergraduate studies, DePauw University, Greencastle, IN, B.A. in Biology Advisor: **Dr. Vanessa Fox**
2008-2014	Graduate studies, Indiana University School of Medicine, Indianapolis, IN, Ph.D. in Medical Neuroscience Advisor: **Dr. Eri Hashino**

Honors

2004-2008	DePauw University Merit Scholarship
2004-2008	DePauw University Science Research Fellowship
2004-2008	DePauw University Information Technology Associates Program Fellowship
2008-2010	Indiana University School of Medicine University Fellowship
2009-2010	Paul and Carole Stark Neuroscience Research Fellowship
2010	Keystone Symposia Scholarship
2010-2012	Indiana CTSI Career Development Award
2011	Indiana University Educational Enhancement Grant
2013-2014	Larry Kays Fellowship

Peer-Reviewed Research Publications

1. Kondo T, Matsuoka AJ, Shimomura A, Koehler KR, Chan RJ, Miller JM, Srour EF, Hashino E (2011) Wnt signaling promotes neuronal specification from mesenchymal stem cells through activation of Tlx3. Stem Cells 29:836-846

2. Koehler KR, Tropel P, Theile JW, Kondo T, Cummins TR, Viville S, Hashino E (2011) Extended passaging increases the efficiency of neural differentiation of induced pluripotent stem cells. BMC Neuroscience 12:82

3. Krishnan S, Mali RS, Koehler KR, Vemula S, Chatterjee A, Ghosh J, Ramdas B, Ma P, Hashino E, Kapur R (2012) Class IA PI3Kinase regulatory subunit, p85α, mediates mast cell development through regulation of growth and survival related genes. PLoS ONE 7:e28979

4. Vemula S, Shi J, Mali R, Ma P, Hanneman P, Koehler KR, Wei L, Hashino E, Kapur R (2012) ROCK1 functions as a critical regulator of stress erythropoiesis and survival by regulating p53. Blood (*in press*)

5. **Koehler KR**, Mikosz AM, Molosh AI, Patel D, Hashino E (2013) Generation of inner ear sensory epithelia from pluripotent stem cells in 3D culture. Nature 500(7461):217-221

6. **Koehler KR**, Hashino E (2013) Three-dimensional mouse embryonic stem cell culture for generating inner ear organoids. Nature Protocols (*submitted*)

Other Publications

Book Chapters

1. **Koehler KR**, Malone A, Hashino E (2013) Recapitulating inner ear development with pluripotent stem cells: biology and translation. Development of Auditory and Vestibular Systems 4 edition. (*in press*)

Presentations

Invited Talks

1. **Koehler KR** (2013) Modeling inner ear development using pluripotent stem cells in 3D culture. Dr. Pascal Dolle's Laboratory, Institut de Génétique et de Biologie Moléculaire et Cellulaire, Illkirch, France.

Abstracts / Poster Presentations

1. **Koehler KR**, Kondo T, Tropel P, Viville S, Hashino E (2010) Quantitative comparative analysis of iPS and ES cells directed to differentiate into neurons. Abstract for poster presentation, Keystone Symposium on Stem Cell Differentiation and Dedifferentiation. Keystone, CO.

2. **Koehler KR**, Tropel P, Kondo T, Cummins TR, Viville S, Hashino E (2010) Gene and protein profiling reveals delayed, but robust differentiation of neurons from induced pluripotent stem cells. Abstract for poster presentation, International Society for Stem Cell Research, 8th Annual Meeting, San Francisco, CA.

3. Matsuoka AJ, Fritsch MH, **Koehler KR**, Hashino E (2010) Assessment of migration and engraftment of stem cells in the cochlea using a high-resolution microscopic-endoscope. Abstract for poster and short-talk presentation, The Triological Society Combined Meeting, Orlando, FL.

4. Matsuoka AJ, Fritsch MH, **Koehler KR**, Hashino E (2011) Monitoring migration and engraftment of mesenchymal stem cells in the cochlea using a high-resolution microscopic-endoscope and MRI. Abstract for poster and short-talk presentation, Association for Research in Otolaryngology, 34th Annual Meeting, Baltimore, MD.

5. Miller DM, **Koehler KR**, Kondo T, Hashino E (2011) Ectopic expression of Nex1 on murine embryonic stem cells undergoing neural

differentiation. Abstract for poster presentation, Association for Research in Otolaryngology, 34th Annual Meeting, Baltimore, MD.

6. **Koehler KR**, Beans EE, Hashino E (2011) A stem cell-based approach to replacing degenerated auditory neurons for the treatment of sensorineural hearing loss. Abstract for poster presentation, National Predoctoral Clinical Research Training Program Meeting. St. Louis, MO.

7. **Koehler KR**, Tropel P, Thiele JW, Kondo T, Cummins TR, Viville S, Hashino E (2011) The derivation of functional neurons from mouse induced pluripotent stem cells is enhanced by extended passaging. Abstract for poster presentation, International Society for Stem Cell Research, 9th Annual Meeting, Toronto, Canada.

8. Piron C, **Koehler KR**, Matsuoka A, Fritsch M, Hashino E (2012) High-resolution MRI of stem cell engraftment in the human temporal bone using superparamagnetic iron-oxide nanoparticles. Abstract for poster presentation, Association for Research in Otolaryngology, 35th Annual Meeting, San Diego, CA.

9. **Koehler KR**, Mikosz AM, Hashino E (2012) Modeling inner ear development using pluripotent stem cells. Abstract for poster presentation, National Predoctoral Clinical Research Training Program Meeting. Mayo Clinic, Rochester, MN.

10. **Koehler KR**, Mikosz AM, Molosh AI, Patel D, Hashino E (2013) Modeling inner ear organogenesis using mouse embryonic stem cells. Abstract for poster presentation, International Society for Stem Cell Research, Regional Forum. Florence, Italy.

Patent Applications

1. Koehler KR, Oxford G, Hashino E. Method for generating inner ear and other cranial placode-derived tissues using pluripotent stem cells. PCT application, filed 6 May 2013.

Membership in Professional Societies:

2009-present	Student Member, International Society for Stem Cell Research (ISSCR)
2010-present	Student Member, The American Association for the Advancement of Science
2011-present	Student Member, The Society for Neuroscience

Teaching Experience

Student supervision

2009-present	Supervisor for 1st year biomedicine graduate student rotation projects and 2nd year medical student summer research projects (11 students, 8 weeks each) Indiana University School of Medicine, IN.
2011-present	Supervisor for undergraduate work/study student (1 student, 2 academic years) Indiana University and Purdue University Indianapolis, IN.

Classroom Lecturing

2012	Guest Lecturer (1 class, fall semester) *Fundamental Neuroscience VI: Developmental Neurobiology (N616)*, Medical Neuroscience Graduate Program, Indiana University School of Medicine, IN. Host: **Drs. Wei-Hua Lee and Eri Hashino**

Research Support

Indiana University School of Medicine University Fellowship (2008-2010):
Indiana University School of Medicine
This fellowship is awarded to incoming graduate students in the Indiana University School of Medicine Biomedical Gateway Program based on their undergraduate performance. I used this fellowship to present my work at the International Society for Stem Cell Research (ISSCR) 8th annual meeting in San Francisco.

Paul and Carole Stark Neuroscience Research Fellowship (2009-2010):
Stark Neurosciences Research Institute
This 1-year fellowship is awarded each year to 1-2 graduate students in the Medical Neuroscience Graduate Program. Recipients are selected based on their performance and accomplishments during the first year of graduate study.

Keystone Symposia Scholarship (2010):
Keystone Symposia
This award allowed me to present a poster at the Keystone Symposium on "Stem cell differentiation and dedifferentiation". Recipients were selected by the program coordinators Drs. Shinya Yamanaka and Fiona Watt and were funded through the Eunice Kennedy Shriver National Institute of Child Health & Human Development Grant (R13HD063192-01).

Indiana CTSI Career Development Award (2010-2012):
Indiana Clinical and Translational Sciences Institute (CTSI)
This competitive 1-2 year training grant is awarded to graduate students studying biomedicine at Indiana University, Purdue University and Notre Dame University. As part of the fellowship, awardees attended a yearly CTSA meeting to present their work and took part in a multi-institutional course on translational research. My project proposal, titled "Induced pluripotent stem cells for inner ear therapy", was granted a 2nd year of funding during a renewal process.

Indiana University Educational Enhancement Grant (2011):
IU Graduate and Professional Student Government
I used this grant to attend and present my work at the 9th annual meeting of the ISSCR in Toronto, Canada.

Larry Kays Fellowship (2013-2014):
Indiana University School of Medicine Medical Neuroscience Program
This fellowship is awarded each year to two PhD candidates in the Medical Neuroscience program. Recipients are selected based on their credentials and a recommendation from their mentor.